Hierarchical self-assembly of novel *para*-aryltriazole helical foldamers

Dissertation presented in partial fulfilment of the requirements for the degree

of PhD of Polymer Science

By Rueben Pfukwa

Supervisor: Prof Bert Klumperman

Co-supervisor: Prof Alan E. Rowan

Stellenbosch University

Department of Chemistry and Polymer Science

Faculty of Science

March 2012

Declaration

By Submitting this dissertation electronically, I declare that the entirety of the work contained therein is my own, original work, that I am the sole author thereof (save to the extent explicitly otherwise stated), that reproduction and publication thereof by Stellenbosch University will not infringe any third party rights and that I have not previously in its entirety or in part submitted it for obtaining any qualification.

Rueben Pfukwa

Stellenbosch, February 2012

Abstract

Hierarchical information transfer is investigated as a tool to prepare well-defined nanostructures with high aspect ratios, via the self-assembly of helically folding poly(*para*-aryltriazole) (P(*p*-AT)) foldamers.

A novel 'helicity codon' based on the 1,4-linkage geometry in 1,4-aryl-disubstituted-1,2,3-triazoles is developed. Helical folding is induced exclusively by directing all triazole moieties into a *cisoid* configuration. By linking the triazole rings in a *para* fashion about the aryl moiety, this helicity codon codes for a helix with a large internal cavity of ~ 3 nm. One turn of the putative helical conformation requires 14 repeat units and the helical pitch is ~ 0.38 nm. The aryltriazole backbone is appended with amphiphilic oligo(ethylene glycol) (oEG) units which have the dual roles of imparting solubility as well as instigating a solvophobic helical folding in solvents which poorly solvate the hydrophobic arytriazole backbone but, solvate the side chains fully. The helix interior is hydrophobic and the exterior is amphiphilic.

A true polymer synthesis approach to the foldamer synthesis, based on the copper catalysed azide-alkyne cycloaddition (CuAAC) AB step growth polymerization system, is developed. This is preceded by a facile synthetic protocol for the AB monomers. The subsequent P(*p*-AT)s have high molecular weights ensuring several turns in the helical foldamer. A DMF/H_2O good solvent/bad solvent system is established. Twist sense bias in the helical foldamers is successfully imparted by installing enantiopure chiral oEG side chains. Spectroscopic signatures for the solvent dependent coil to helix transition are established enabling the tracking of the conformational transitions from primary to secondary and finally tertiary structure. Conclusive evidence for the formation of stable, long stacked helical columns, in the solution state, is provided via cryo-TEM. The helical stacks are several microns long, but of random lengths and do not intertwine but rather run parallel to each other. The helical stacks, however, have indeterminate lengths.

Control over the length and chirality of the self-assembled helical stacks is successfully imparted by using a template which mimics the role of ribonucleic acid (RNA) in tobacco mosaic virus (TMV). The template used is the hydrophobic α-helical polypeptide poly(γ-benzyl-L-glutamate) (PBLG). Self-assembly is driven by solvophobicity in a DMF/H_2O system,

the PBLG template being encapsulated inside the hydrophobic cavities of the stacked/self-assembled helical foldamers. Information from the template, *i.e*. length and chirality, is used to control the length and the chirality of the stacked/self-assembled construct.

The templated self-assembly process is solvent dependent. When carried out in the solvent regime at the coil to helix transition mid-point of the foldamer host, system operates under a dynamic equilibrium. Under these conditions, the self-assembly process is shown to take place between two distinct states, the foldamer helices and the helical template, the template threading through the foldamer helices. The resulting self-assembled construct has a pseudo-rotaxane architecture.

Under dynamic equilibrium conditions, temperature induced dis-assembly of the templated assembled construct, is shown to be a cooperative process, whilst re-assembly is characterized by a large hysteresis. By increasing the volume fraction of water, the solvophobic character of the system is increased and template assembled construct is better stabilised. The assembly system, however, loses its dynamic equilibrium character and falls into kinetic traps. Temperature induced de-threading, of the foldamer helices, becomes less favourable and loses its cooperative character although the hysteresis loop is reduced.

Opsomming

Hiërargiese inligtingsoordrag is bestudeer as ‘n hulpmiddel om goed gedefinieerde nanostrukture met ‘n goeie beeldverhouding voor te berei. Die nanostrukture word voorberei deur middel van self-samestelling van heliese vouing van poli(para-arieltriasool) (P(*p*-AT)) ‘foldamers’.

‘n Nuwe heliese-kodon gebaseer op die 1,4 koppelingsgeometrie in 1,4 ariel-digesubstitueerde-1,2,3-triasool is ontwikkel. Heliese vouing word uitsluitlik geïnduseer as al die triasole in die sis konfigurasie is. Deur die triasole in ‘n para konfigurasie te bind, kodeer die heliese kodon vir ‘n heliks met ‘n groot interne kanaal van ~ 3 nm. Een draai van die heliks benodig 14 herhalende eenhede en die heliese gradiënt ~ 0.38 nm. Amfifiliese oligo(etileen glikol) (oEG) eenhede is aan die arieltriasoolruggraat aangeheg. Hierdie aanhegting van oEG eenhede bevorder oplosbaarheid en dit induseer ‘n solvofobiese heliese vouing in oplosmiddels wat nie die hidrofobiese arieltriasoolruggraat oplos nie, maar wel die sy-kettings volledig oplos. Die binnekant van die heliks is hidrofobies en die buitekant is amfifilies.

‘n Polimeersintese benadering tot die ‘foldamer’ sintese (gebaseer op die koper gekataliseerde siklo-addisie reaksie tussen ‘n asied en ‘n alkyn) AB stapsgewyse groei polimerisasiestelsel, is ontwikkel. Dit is voorafgegaan deur ‘n geskikte sintetiese protokol vir die AB monomere. Die daaropvolgende P(*p*-AT) het ‘n hoë molekulêre massa wat verseker dat daar ‘n hele paar draaie in die heliese ‘foldamer’ is. ‘n DMF/H_2O goeie oplosmiddel/ swak oplosmiddel sisteem is vasgestel. Draaiing van die heliks na ‘n spesifieke kant alleenlik is suksesvol geïnduseer deur die toevoeging van suiwer enantiomere van die chirale oEG sy-kettings. Spektroskopiese handtekeninge van die oplosmiddel-afhanklike ketting tot heliks transformasie word vasgestel sodat die oorgangstoestande gevolg kan word vanaf primêre tot sekondêre en uiteindelik tesiêre struktuur. Beslissende bewyse vir die formasie van stabiele, lang gestapelde heliese kolomme in die opgeloste toestand is bewys met cryo-TEM. Die heliese stapels is verskeie mikron lank, maar het verskillende lengtes. Die heliese stapels is parallel aan mekaar en oorvleuel nie. Die lengte van die heliese stapels is egter onbepaalbaar.

Beheer oor die lengte en chiraliteit van die self-samestellende heliese stapels is verkry deur gebruik te maak van ‘n templaat wat die rol van ribonukleïensuur (RNS) in die tabakmosaïekvirus (TMV) naboots. Hidrofobiese α-heliese polipeptied poli(γ-bensiel-L-glutamaat) (PBLG) is gebruik as die templaat. Self-samestelling word gedryf deur solvofobisiteit in ‘n DMF/H_2O stelsel, met die PBLG templaat wat dan geënkapsuleer word binne die hidrofobiese holtes van die gestapelde/ self-saamgestelde heliese ‘foldamers’. Die lengte en die chiraliteit van die templaat word gebruik om die lengte en chiraliteit van die gestapelde helikse te beheer.

Die templaatbemiddelde self-samestellende proses is afhanklik van die oplosmiddel. Die stelsel is by ‘n dinamiese ewewig wanneer, uitgevoer in ‘n oplosmiddel, die ketting na heliks oorgang die middelpunt van die ‘foldamer’ gasheer bereik het. By hierdie omstandighede vind die self-samestellende proses plaas tussen twee afsonderlike toestande nl. die ‘foldamer’ helikse en die heliese templaat, en die templaat wat vleg deur die ‘foldamer’ helikse vleg. Die gevolglike struktuur het ‘n pseudo-rotaxane argitektuur.

By dinamiese ewewigstoestande veroorsaak temperatuur dat die self-samestellende templaatstrukture weer disintegreer. Hierdie is ‘n koöperatiewe proses terwyl die her-samestelling gekarakteriseer word deur ‘n sloerende proses. Deur die waterfraksie te vermeerder, word die solvofobiese karakter van die sisteem verhoog en die templaat self-samestellende struktuur beter gestabiliseer. Die samestellingsproses verloor egter sy dinamiese ewewigkarakter en val in kinetiese slaggate. Temperatuur geïnduseerde disintegrasie van die foldamer helikse word minder gunstig en dit verloor die koöperatiewe karakter alhoewel die sloering verminder is.

Acknowledgements

I owe a lot of gratitude to many people who helped me in my research, each in their different ways. Firstly my promoter Bert Klumperman for availing the opportunity to join his research group way back in 2006, for the guidance and advice he offered and for his willingness to help. My co-promoter Alan Rowan is gratefully acknowledged for availing the opportunity to work in his research group in Nijmegen and for the advice, the many hints and pointers he gave. Paul Kouwer is gratefully acknowledged for his advice and for reading this thesis. I am eternally grateful for the funding I received right from the MSc days until the completion of my PhD study. For that I thank the following from the bottom of my heart: Stellenbosch University, the National Research Fund, the Postgraduate Merit Bursary and the Harry Crossely Foundation. I also deeply thank the Marie Curie Foundation for the fellowship I received in my stay at Radboud University.

To the many colleagues, mentors and friends from Stellenbosch University, past and present, I owe my thanks: Eric (Mdara, maita basa) for being a good friend, Gwen, Howard, Austin, Niels, Zaskia, Lebohang, Lilian, Estella and Alvira. Welmarie van Schalkwyk, Freda Meltz, Jaco Jacobs and Neliswa Mama are gratefully acknowledged for their contributions to the synthetic work. Colleagues and friends in the Klumperman group: Khotso, Welmarie, Paul, Freda, Nelly, Sandile, Nathalie, Walid, Njabu, Ahmed, Mpoh, Osama, William, Hamilton, Lizl and Celeste. Staff members at the Polymer Science staff building: Prof. Ron Sanderson, Prof. Harald Pasch, Prof. Peter Mallon, Prof. Albert van Reenen, Dr Wolfgang Weber, Erinda Cooper, Deon Koen, Jim Motshweni, Calvin Maart, Aneli Fourie and Maggie Hurndall.

Colleagues and friends at Radboud University Nijmegen are gratefully acknowledged; Niels and Zaskia Akeroyd for kindly offering the hospitality of your home in my early days in Nijmegen and showing me around; in the Rowan group and the IMM cluster: Pjotr Michels for the work he carried out in the lab, Niels, Zaskia, Eeegle, Sudip, Giorgio, Denis, Alex, Jialiang, Eli, Jan (the bicycle was much appreciated), Tahoora, Riccardo, Rob, Very, Paula, Theo, Paul Schlebos, Vincent, Kathleen, Kerstin, Hans, Roy, Femke, Monique, Sophie, Petri, Arend, Onno, Luuk, Tim, Maarten, Daniel, Daniela, and Chris.

Colleagues for who assisted in analysis work: Gozde Tuzcu, Martin Fijten, Elsa Malherbe, Jaco Brand, Paul Schlebos, Heidi Assumption, Susanne Causemann, Marietjie Stander, Meryl Adonis, Fletcher Hiten, Rinske Knoop, Paul Boumans, Mohammed Jafta and Madhu Chauhan.

On a more personal level, I deeply thank the support and encouragement of my family, immediate and extended, and my in-laws. Saving the best for last, of course, I am eternally grateful to the support and encouragement of my wife, Helen, you are God sent my dear; this is as much yours as it is mine. *Ndatenda, siyabonga, maita basa, baie dankie!*

List of figures

List of schemes

List of abbreviations

ACN	acetonitrile
BTP	2,6-bis(1,2,3-triazol-4-yl)pyridines
CD	circular dichroism
cryo-TEM	cryogenic transmission electron microscopy
CuAAC	copper catalysed azide-alkyne cycloaddition
DMF	dimethylformamide
DMSO	dimethyl sulfoxide
DNA	deoxyribonucleic acid
DMAP	4-dimethylamino pyridine
DLS	dynamic light scattering
EG	ethylene glycol
h-EG	hexa-ethylene glycol
HFIP	1,1,1,3,3,3-hexafluoro-2-propanol
HPLC	high performance liquid chromatography
LDTE	length dependent templating effect
*m*PE	oligo(*m*-phenylene ethynylene)
NMR	nuclear magnetic resonance
oEG	oligo(ethylene glycol)
PMDETA	N,N,N',N'',N''-pentamethyldiethylenetriamine
P(*p*-AT)	poly(*para*-aryltriazole)
PBLG	poly(γ-benzyl-L-glutamate)
PPh_3	triphenylphosphine
RNA	ribonucleic acid
ROESY	rotating frame Overhauser effect spectroscopy
SEC	size exclusion chromatography

S-(+)-MTPA-Cl	(*S*)-(+)-a-methoxy-α-trifluoromethylphenylacetyl chloride
TgOH	tetraethylene glycol mono methyl ether
THF	tetrahydrofuran
TMSA	trimethylsilyl acetylene
TEM	transmission electron microscopy
TMV	tobacco mosaic virus
UV-vis	ultraviolet-visible
VT	variable temperature

Chapter 1. Hierarchical information programing

Introduction

In order to advance abiotic self-assembly to the levels of control and complexity, seamlessly attained by nature, it is paramount to understand the driving forces behind biological self-assembly and the different levels of organization involved. Parameters used to control biological self-assembly include molecular size, stereochemistry, polarity, shape and topology. This information is then used at the different hierarchical levels of biological self-assembly, i.e. at the molecular, macromolecular and supramolecular levels. Nature uses a small set of building blocks (for example just 4 nucleoside bases and just 20 amino acids) and an even fewer recurring structural motifs (the beta sheet and the helix) to construct a massive array of functional biological assemblies which work in unison to sustain life. The helix is an ubiquitous structural motif in nature. It is the basis of numerous complex architectures in proteins and in genetic materials. It is not surprising therefore, that the design, synthesis and manipulation of helical molecules is a very active area of research with paramount fundamental and commercial significance.

Whilst a number of studies have been dedicated towards developing helically folding backbones,[1-3] significant attention is yet to be paid to the use of this structural motif to generate higher order structures, using the principles of molecular recognition, self-assembly and self-organization, which is now being addressed.[4,5] An added incentive to this emerging research angle is that synthetic helices offer “easier to manipulate” models with which to understand biological self-assembly.[5,6] This brings this discussion to some of the key areas of abiotic self-assembly, i.e. introducing asymmetry and controlling the lengths of long one dimensional self-assembled constructs. The asymmetric control and mechanistic understanding of the self-assembly of discotic[7,8] and dendritic[9] molecules into helical superstructures is well documented. Asymmetric control in the self-assembly of synthetic helices, into one dimensional stacks is now being tackled successfully.[10] Most of the studies present spectroscopic evidence indicating the formation of higher order structures. Definite evidence of the formation of the higher order structures in the solution state, however, is

limited. In addition, relatively little effort has gone towards controlling the size/length of the self-assembled helical supramolecules.[11,12]

Aim of this work

The helical structural motif provides a basis for this work. A novel helical foldamer, based on a poly(*para*-aryltriazole) [P-(*p*-AT)] backbone, is presented. The coil to helix transitions are readily controlled by solvophobic forces. The exterior of the helix is amphiphilic whist the interior is hydrophobic. The helix possesses a well-defined cylindrical hollow which is hydrophobic and readily amenable for use in host guest chemistry. The self-assembly of the subsequent helices into helical stacks of indeterminate lengths, as a function of solvent quality, is demonstrated and evidence for the formation of higher order structures given. Asymmetric and assembly length control of the self-assembled one dimensional helical stacks of helical P(*p*-AT) polymers is then demonstrated, mimicking the processes found in nature for the tobacco mosaic virus (TMV).

Organization of the thesis

Chapter 2 gives a literature overview of the particular class of helical polymers known as foldamers, to which the P(*p*-AT)s introduced in this work belong. The discussion then focuses on the use of the copper catalysed azide-alkyne cycloaddition (CuAAC) reaction in step growth polymerization systems, since this polymerization technique is used to synthesize the P(*p*-AT)s. Helical *meta*-polytriazoles are also discussed. The chapter concludes by looking at reported examples of the formation of higher order structures by helical foldamers.

In chapter 3 the basic tenets for “curling up” (folding) of a *para*-aryl triazole system and its driving force are presented. A solvent system to induce the coil to helix conformational transition is developed. Relevant spectroscopic signatures for tracking this conformational transition are identified. Preliminary evidence for the formation of helical stacks in the solid state is also presented.

In chapter 4, clear and definite evidence for the formation of long one-dimensional helical stacks is presented. Assembly length and asymmetric control of the helical stacks, mediated

by a polypeptide template, is demonstrated. Finally in Chapter 5 a mechanistic investigation, into the template controlled self-assembly, of these unique foldamers is presented.

References

(1) Nakano, T.; Okamoto, Y. *Chem. Rev.* **2001**, *101*, 4013.

(2) Yashima, E.; Maeda, K.; Iida, H.; Furusho, Y.; Nagai, K. *Chem. Rev.* **2009**, *109*, 6102.

(3) Hill, D. J.; Mio, M. J.; Prince, R. B.; Hughes, T. S.; Moore, J. S. *Chem. Rev.* **2001**, *101*, 3893.

(4) Guichard, G.; Huc, I. *Chem. Commun.* **2011**.

(5) Cheng, R. P.; Gellman, S. H.; DeGrado, W. F. *Chem. Rev.* **2001**, *101*, 3219.

(6) Horne, W. S.; Price, J. L.; Keck, J. L.; Gellman, S. H. *J. Am. Chem. Soc.* **2007**, *129*, 4178.

(7) Jonkheijm, P.; van der Schoot, P.; Schenning, A. P. H. J.; Meijer, E. W. *Science* **2006**, *313*, 80.

(8) Greef, T. F. A. D.; Smulders, M. M. J.; Wolffs, M.; Schenning, A. P. H. J.; Sijbesma, R. P.; Meijer, E. W. *Chem. Rev.* **2009**.

(9) Rudick, J. G.; Percec, V. *Acc. Chem. Res.* **2008**, *41*, 1641.

(10) Brunsveld, L.; Meijer, E. W.; Prince, R. B.; Moore, J. S. *J. Am. Chem. Soc.* **2001**, *123*, 7978.

(11) Lortie, F.; Boileau, S.; Bouteiller, L.; Chassenieux, C.; Lauprêtre, F. *Macromolecules* **2005**, *38*, 5283.

(12) Besenius, P.; Portale, G.; Bomans, P. H. H.; Janssen, H. M.; Palmans, A. R. A.; Meijer, E. W. *Proc. Natl. Acad. Sci.* **2010**, *107*, 17888.

Chapter 2. Helical foldamers, a general introduction

Introduction

In nature, the specific folding of polymers leads to a massive array of well-defined biological molecules with specific functions. Out of only 20 genetically encoded amino acids, a vast array of proteins with very specific instructions is assembled. Proteins function as hormones, biocatalysts, transport agents, components of immune systems and as components of structural systems.[1] A constant theme is "structure for function" i.e. the chemical and physical structures of proteins are directly related to the specific protein's function.[2] For example, the secondary structure of the fibrous protein collagen consists of three α-helices wound around each other to form a triple helix. The triple helices then associate/assemble into microfibrils held together by disulfide bonds. This confers rigidity and strength needed in this structural protein which is a component of muscle tissue and tendons.[1,2]

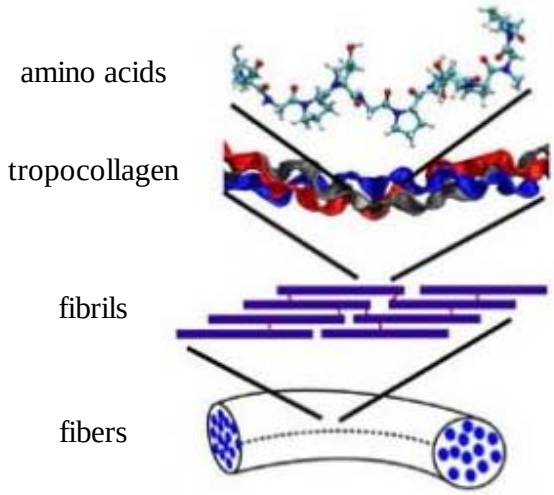

Figure 2.1: Hierarchical assembly of collagen microfibrils from polypeptides.[3]

To attain these high levels of organization nature programmes the final architectural plan into the smallest building block. This information is in the form of chirality, hydrophobicity/hydrophilicity, steric constraints, hydrogen bonding ability, metal ion

coordinating ability, and electrostatic potential.[4] For example the rigidity of amide bonds, hydrophobic interactions, the formation of intra-molecular hydrogen bonds in combination with the exclusive use of L-α-amino acids, in higher animals, results in the formation of peptide sequences which form right-handed helices.[1,2] It is therefore not surprising that synthetic chemists have been trying to mimic nature by deliberately designing molecules that can also fold into well-defined structures. The motivation for this effort is that this could lead to a better understanding of how biological systems operate, i.e. how nature has managed to build such a massive and complex array of nano-sized biological machines with specific and precise functions like enzymes.

The helical structural motif

The helix is an interesting structural motif. Helical biopolymers, like the DNA double helix has inspired many synthetic chemists. Synthetic helical polymers have a number of applications such as ferroelectric liquid crystals, nonlinear optical materials and as chiral stationary phases in High Performance Liquid Chromatography (HPLC) in the separation of enantiomers.[5]

Historically nature's monopoly on making stereoregular polymers with a helical conformation was ended in 1955, when Natta discovered that highly isotactic polypropylene, synthesized by the Ziegler-Natta catalyst, had a helical conformation in the solid state.[6] It was found that the X-ray of fibers drawn from the polypropylene had an extremely regular chain structure (highly isotactic) and this was only possible if the main chain spiralized. Upon dissolution, however, the isotactic PP lost its helical conformation and formed a random polymer.

Helical polymers can be grouped into static and dynamic helical polymers with the differentiation between them being entirely dependent on the magnitude of the helical inversion barrier. Static helical polymers are rigid helices with a high helix inversion barrier and have an excess of one screw sense, which is stable in solution, when prepared by asymmetric polymerization.[4] A good example is that of poly(triphenylmethylmethacrylate).[7] During the polymerization, each monomer gets sterically locked into its conformation, thereby inducing a screw sense. The helical conformation is formed under kinetic conditions as the stiffness of

these pendant groups prevents the helical conformation from unraveling.[5,8] The polymers are fully isotactic and the specific rotation increases with molecular weight. Their helicity is the only source of their optical activity.[7] The optical activity is caused by the steric restrictions imposed by bulky substitutions. The helical sense can be predetermined by polymerizing asymmetrically using chiral catalysts.[8]

Dynamic helical polymers have a low helix inversion barrier and are characterized by right and left-handed helical conformations, which are punctuated by helical reversals that move along the backbone.[5] A chiral bias can be induced into the main chain by copolymerization of achiral monomers with small amounts of chiral ones to give a polymer with an excess screw sense. This concept, introduced by Green, was termed the "Soldiers and Sergeants effect".[9] An excess helical screw sense can also be induced in dynamic helical polymers through non-covalent interaction with chiral guests.[5,10] Non-covalent interactions between the pendant functionalities in polyphenylacetylenes and chiral, nonracemic molecules with complementary functionalities induce the polymer to fold into an excess of one screw sense. This is confirmed by the resulting induction of a Circular Dichroism (CD) activity which reflects the stereochemistry of the organic molecules in organic solvents.[5,10]

Foldamer based helical polymers

The term foldamer was initially used by Gellman to define "polymers with a strong tendency to adopt specific compact conformations".[11] The definition was later adjusted to define oligomers/polymers which fold into well-defined conformations in solution.[12,13] Foldamers have been noted to bear the closest resemblance to natural helical systems like the alpha helix in proteins.[14,15] The folding is brought about by interplay of specific structural and conformational features built into the monomers. The folding is driven by noncovalent interactions such as hydrogen bonds,[11,14-16] π-π stacking[17-19] and solvophobic forces.[20,21] In helicates it is induced by metal coordination,[13] whilst in some systems, the helically folded conformation is stabilized by charge transfer interactions.[22,23] These driving forces help to reduce the entropic penalty that must be paid in order to adopt a defined helically folded conformation.

Foldamer design

Steps to foldamer design involve designing a backbone capable of folding, devising efficient synthetic methods and incooperation of chemical function.[11,15] Figure 2.2 shows an array of some reported helical foldamers.

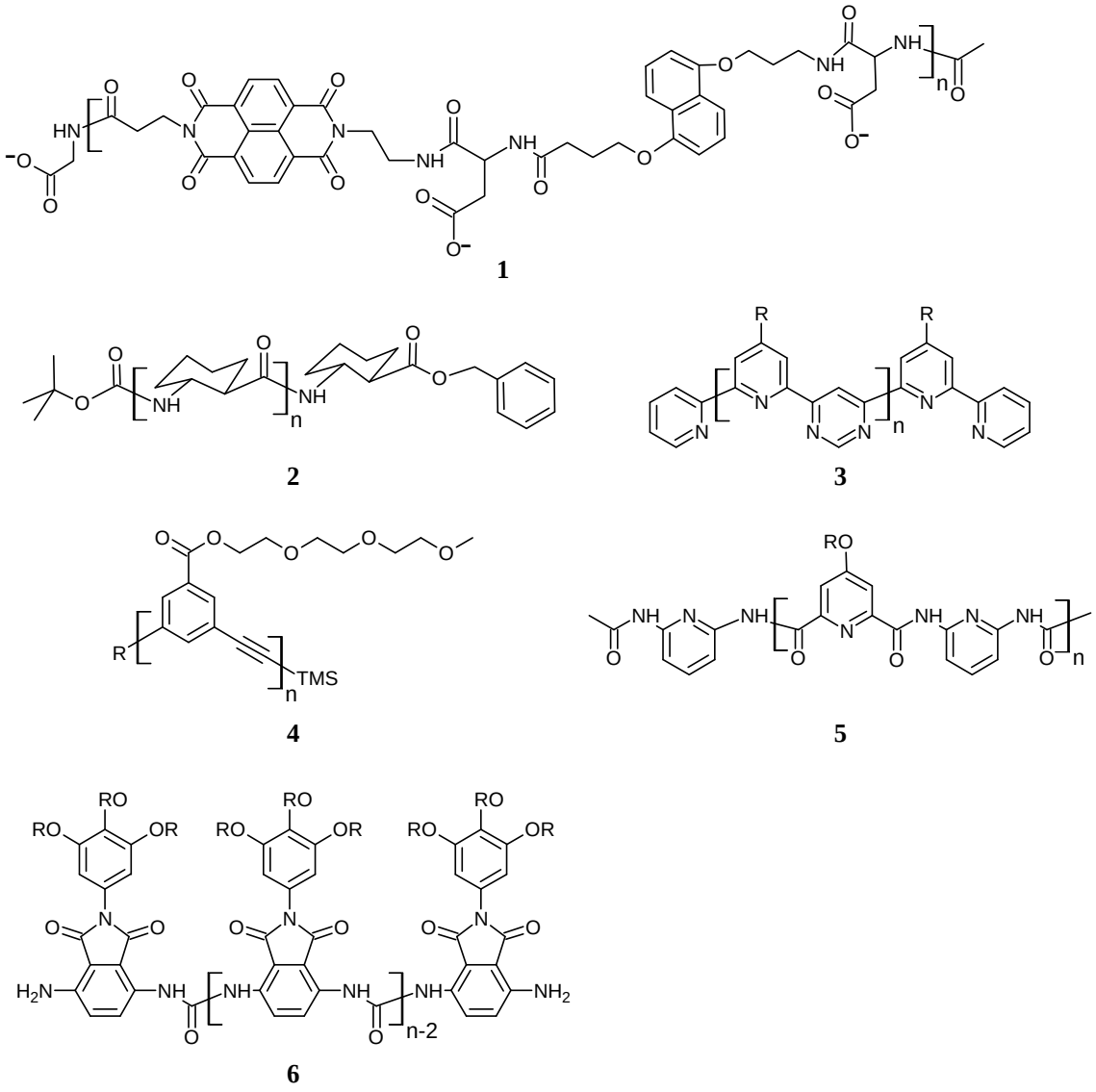

Figure 2.2: Some reported helix forming foldamers: aedamer oligomers (1);[24] oligo(β-peptides) (2);[11] oligo(pyridine-pyrimidines) (3);[17] oligo(*m*-pheylene ethynylenes) (4);[21] oligo(pyridine dicaboxyamides) (5);[25] oligo(ureidophthalimides) (6).[14]

Nature is able to precisely place monomers with specific functionalities in their correct sequences and this is vital for accurate folding into stable three-dimensional structures. In synthetic systems, helical winding is induced by rigidity of the monomer units, specific linkage of repeat units at appropriate positions and conformational preferences at the single bonds linking the repeat units.[26,27] Extra stability is added to this secondary structure by interactions of stacked aromatic rings in the helices, hydrogen bonding and solvophobicity.[26] These strategies are always put together to work in concert. For example with oligo(*m*-phenyleneethynylene) (*m*PEs), solvophobic interactions are aided by π-π stacking interactions once a turn is completed[21] or by hydrogen bonds.[28]

An interesting approach utilized in this thesis involves the use of an aromatic backbone, which is rigid and apolar, tethered with flexible amphiphilic oligo(ethylene glycol) (oEG) side chains. *m*PEs foldamers, pioneered by Moore have a similar structure.[13,20,21] A large degree of conformational freedom exists about the ethynylene linkers, enabling them to freely rotate between the *cisoid* and *transoid* torsional states (Scheme 2.1). Cisoid geometry between adjoining phenyl rings is characteristic of the helical folded geometry.[13] In a "good" solvent, like chloroform, the whole oligomer structure is effectively solvated and the *m*PEs exist in random chain form. However, polar, "bad" solvents, such as acetonitrile, induce a solvophobic folding of the oligomer into a helical conformation. Cooperative π-stacking interactions and favorable interactions between the polar side chains and the solvent aid this folding process, while unfavorable interactions between the hydrophobic backbone and the polar solvent are minimized.[13]

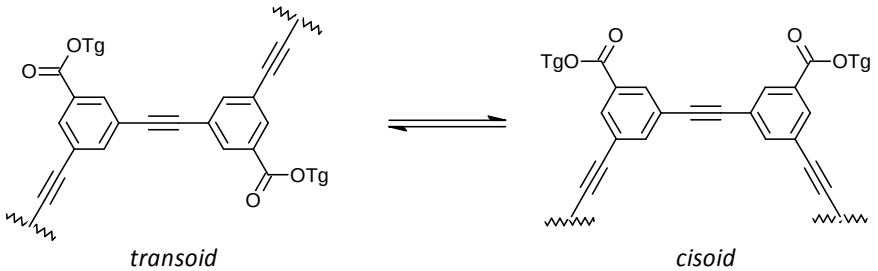

Scheme 2.1: The cisoid-transoid equilibrium in *m*PEs.

The stability of the helical conformation as well as the cooperative nature of the folding process increase linearly with chain length.[29]

Analysis of the helical folded state

An accurate structural model of the helically folded oligomers can be provided by X-ray crystallography, however it is difficult to obtain crystalline synthetic helical polymers, even from discrete oligomers prepared in a stepwise fashion such as *m*PEs.[21] Therefore, a combination of spectroscopic techniques like UV-vis, fluorescence, circular dichroism (CD) and NMR are frequently used to infer a helical conformation as these techniques give indirect evidence of folding.[30] With UV-vis spectroscopy, hypochromicity associated to folding of the oligomers into a helical conformation is observed, whilst with fluorescence spectroscopy, excimer-like emission, associated with aromatic stacking, is observed upon folding. Frequently, the absorption spectral pattern or the emission spectral pattern is monitored as a function of solvent composition.[29,31] The folded and unfolded oligomers give different spectroscopic signals. For systems that undergo cooperative conformational transitions, the solvent titration curves generated have a characteristic sigmoidal shape, a clear experimental signature for cooperative processes.[32] In ^{1}H NMR spectroscopy analysis, helicity induction is characterized by upfield shifting of aromatic protons, indicating overlap of the aromatic protons in the folded conformation.[19,33] Conformational analysis may also be accomplished with ^{1}H-^{1}H-ROESY NMR spectroscopy experiments, which gives through space connectivities.[34] Chiral helical oligomers with an excess screw sense can be characterized by CD spectroscopy.

Chirality in helical foldamers

Helices are intrinsically chiral structures due to their conformational asymmetry even if they do not have a chiral building block in the polymeric structure. If a helical polymer with one screw sense is synthesized, or if one screw sense is induced into a macromolecule, the helical polymer will be optically active, even if it does not have chiral side chains or chiral components in the main chain. If the barrier of rotation, between two screw senses is low, they racemise and exist as enantiomers, where the left (M) and right (P) handed helices will be in equilibrium with the same free energies. If, however, configurationally chiral components are introduced into the

molecular structure, then helices become diastereomers with different free energies.[4,35,36] In foldamers, chiral groups can be inserted in the main chain[37] or side chains[28,38] resulting in an excess screw sense which can monitored by CD spectroscopy.

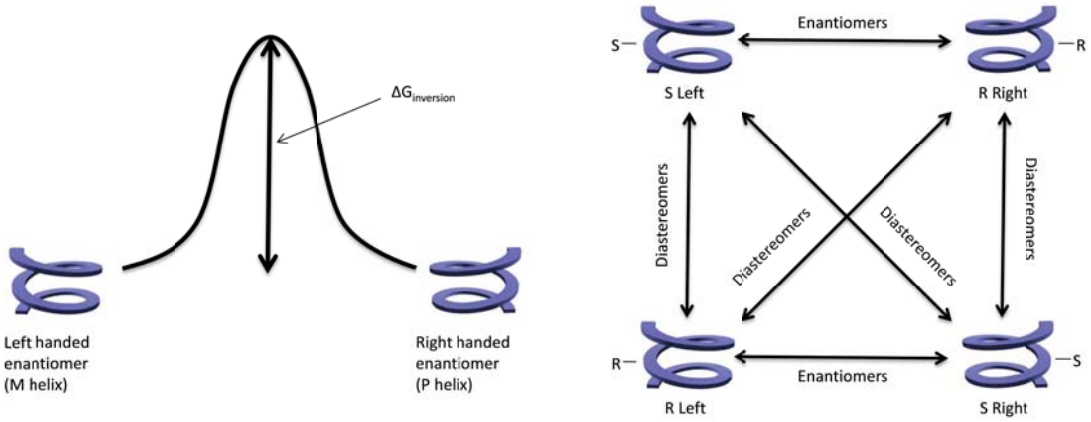

Figure 2.3: Schematic illustration of (left) the equilibrium between M and P helices made from achiral monomers and (right) that between helices with configurationally chiral components.[4]

Uses of aryl foldamers

It still remains a challenge to find practical applications for aromatic helical foldamers. However, a number of potential applications have been reported in literature, most utilizing the hollow cavity for molecular recognition. For example, the ability of oligohydrazides[39] and *m*-ethynylpyridines oligomers[40-43] to recognize saccharides has been reported. Amphiphilic helically ordered *m*PE oligomers have also been shown to provide a prototype for designing synthetic receptors.[44-48] *m*PE foldamers functionalized with 4-dimethylamino pyridine (DMAP) rings in the centre (of the helix) displayed significant increases in the methylation of the pyridine nitrogen by iodomethane.[49] It was observed that methylation rates increased with the chain length of the substrate's alkyl chain and it could be shown that the shape of the substrate, more so than size, was important in determining reactivity.[50,51]

The reversible nature of the folding reaction renders it dynamic, thereby making the foldamers potentially useful as responsive materials. In light of that, Hecht and co-workers demonstrated

that the helix-coil transition in *m*PEs could be made photoswitchable by inserting the photoisomerizable *trans*-azobenzene motif into the oligomer structure.[52]

Meijer and coworkers used a helical ureidophthalimide-based foldamer (**7**) as a scaffold for the chiral alignment of oligo(*p*-phenylenevinylene) (**8**) (OPV).[53]

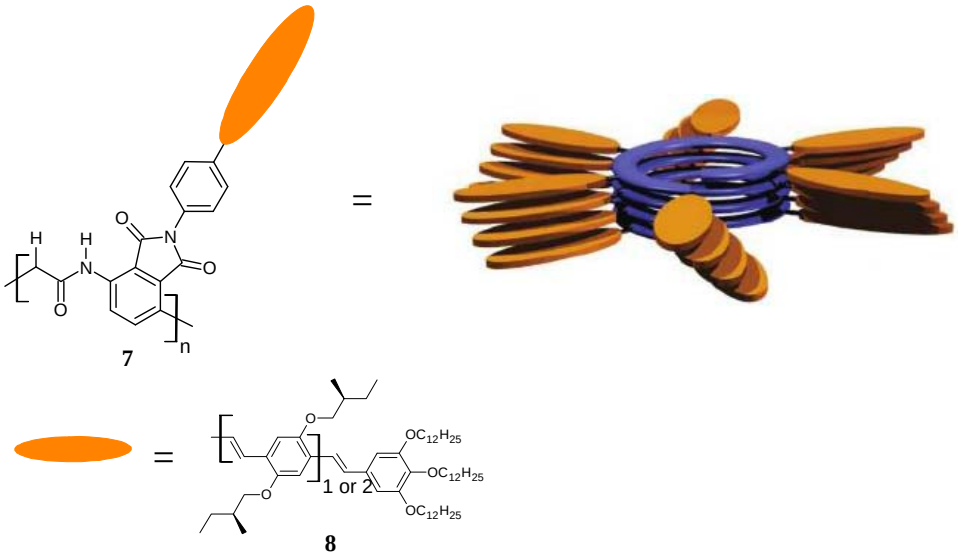

Figure 2.4: Meijer's oligo(ureidophthalimides) with OPV side chains.

Whilst the more frequent uses of aromatic foldamers, involve regular helices with a consistent cylindrical hollow, Huc and co-workers prepared an aromatic oligoamide foldamer with reduced diameter at both ends. They then showed that the resulting foldamer was egg shaped, using X-ray diffraction and also showed, by NMR spectroscopy that it could partially unfold and encapsulate a guest.[54,55]

1,2,3-Triazole-based polymer systems

Since the theme of this thesis is focused on helical 1,2,3-triazole foldamers, it is appropriate to give a general overview of the mechanistic aspects of the copper-catalyzed azide-alkyne reaction and a brief survey of literature on triazole-based polymers, where the triazole unit is part of the repeating backbone main chain.

1,2,3-Triazoles are formed by the Huisgen 1,3-dipolar cycloaddition reaction between organic azides and terminal alkynes.[56]

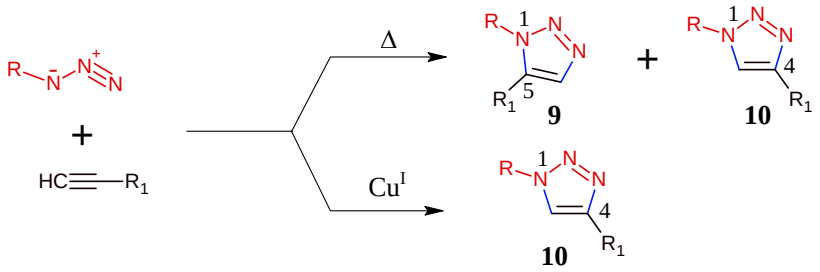

Scheme 2.2: Thermal and Cu^I catalysed [3 + 2] cycloaddition reactions between terminal alkynes and organic azides.

Uncatalyzed reactions between simple organic azides and terminal alkynes tend to be very sluggish due to the high activation energy of the cycloaddition.[57] High temperatures, long reaction times,[57] and high pressures[58] are required to increase the rate of reaction. With elevated temperatures, a mixture of the 1,4 and 1,5 disubstituted regioisomers (**9** and **10** respectively) can be obtained. Besides, substantial decomposition of the azide moiety occurs at elevated temperatures. Good regioselectivity for the uncatalyzed reaction can be achieved by using alkynes attached to highly electron deficient functionalities like carbonyls,[59] perfluoroalkyls[57] or strained alkynes.[60,61] In 2002, Meldal[62] and Sharpless[63] independently discovered the Cu^I-catalyzed variant which yields only the 1,4-disubstituted 1,2,3-triazole regioisomer (**10**). Thus, this 3+2 cycloaddition reaction was transformed from a sluggish, non-regioselective reaction, requiring special precautions and reagents, to one that meets the "click chemistry" criteria, i.e. robust, orthogonal and general.[64] The click chemistry concept, introduced by Sharpless and co-workers in 2002, defines reactions that are modular, high yielding, wide in scope, stereospecific and easy to perform under relatively undemanding conditions.[64]

Mechanism of the Cu^I-catalyzed azide-alkyne cycloaddition (CuAAC)

The mechanism of the copper-catalyzed pathway is still subject to considerable debate.[65] The initial mechanism put forward suggested a stepwise process catalyzed by one Cu^I ion which is

coordinated in an end-on fashion to the alkyne.[66] As pointed out by Meldal, ligand (alkyne) complexation to Cu^{I} is a very complicated affair,[67] making it hard to provide precise and detailed transition state complexes involved in the Cu^{I} catalyzed reaction. It has been argued therefore, that this early assertion was probably incorrect. Kinetic studies showing the reaction to be second order with respect to Cu^{I}, supported this argument.[68] This has also been further supported by computational studies, which showed that polynuclear copper(I) μ-acetylide complexes were key intermediates in the copper-catalyzed pathway.[69] A thorough discussion on this complicated mechanism can be found in the excellent reviews by Meldal,[67,70] here only a brief description will be given. The proposed mechanism is outlined in Scheme 2.3.

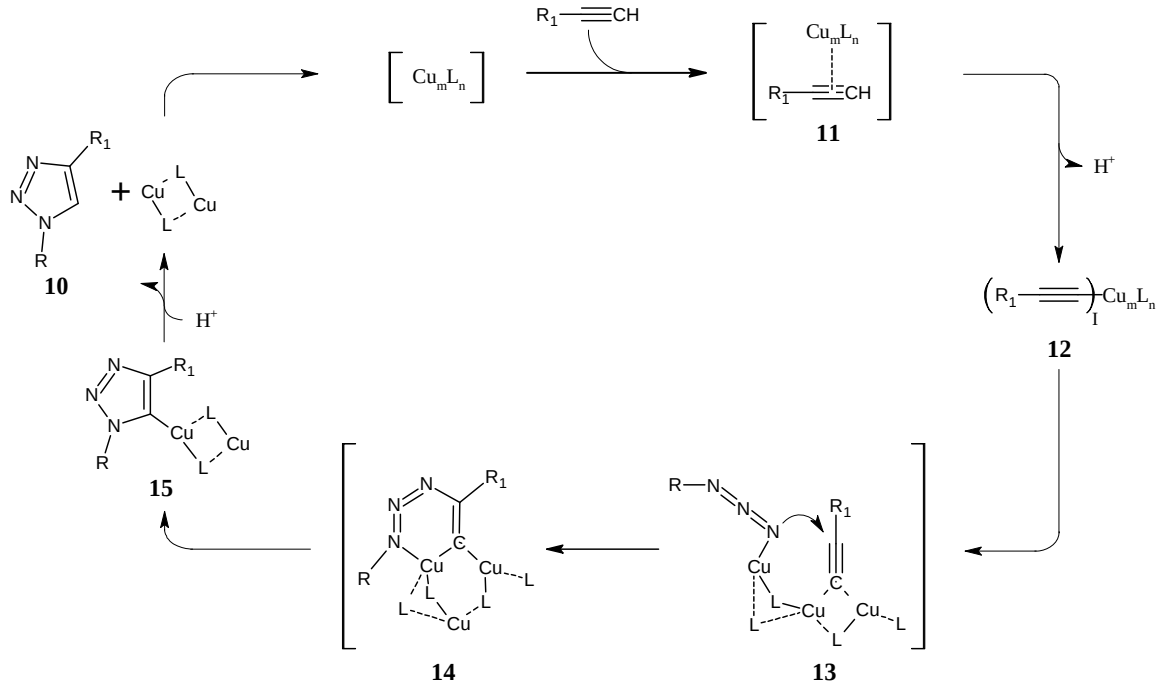

Scheme 2.3: Outline of proposed mechanism for the CuAAC (L = copper ligand).[70]

Firstly, the copper acetylide species (**12**) is formed via the formation of a π-complex. The azide then displaces one of the ligands bound to copper, forming a copper acetylide-azide complex (**13**) making the azide active for a nucleophilic attack on the acetylide.[57] Subsequent contraction gives the copper triazole derivative **15**, which is protonated, to generate the triazole product (**10**) completing the stepwise catalytic cycle. Recently, Straub isolated a stable copper triazolide by reacting sterically hindered Cu^{I} acetylides and sterically hindered organo azides at room

temperature.[71] This suggested that dinuclear copper complexes were not compulsory in this mechanism. The sterically burdened environment around the copper center perhaps stabilized the complex.[71]

Step growth polymerization by CuAAC

The azide functionality can be introduced into organic molecules under a variety of conditions[72,73] and remain relatively inert under many conditions in biological[74,75] as well as organic synthetic reaction conditions, until it is presented with a good dipolarophile.[63] As a matter of fact, the Cu^{I}-catalyzed azide-alkyne cycloaddition (CuAAC) reaction is the pre-eminent click reaction as evidenced by the vast amount and diversity of work reported in the last decade utilizing this reaction.[57,67,70,76-85]

Of more interest to us is the application of the CuAAC methodology in polymer and materials synthesis by the step growth polymerization technique. Step growth polymerizations proceed with the formation of an inter-unit linking group as below.[86] Depending on monomer type, step growth polymerizations can be classified as AA/BB or AB step growth polymerization. The former entails the use of bifunctional monomers, with two similar functional groups in each molecule, whilst the latter entails the use of polyfunctional monomers with two different functional groups in the same molecule.[87] Hyperbranched polymers can also be prepared in a stepwise fashion using AB_2 monomers.

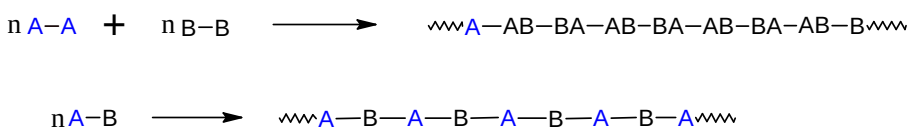

Scheme 2.4: Illustration of a AA/BB and AB step growth polymerization systems.

A successful step growth polymerization demands very high conversions (> 98 %) and a strict intolerance for side reactions so as to achieve an efficient co-reaction between the complimentary A and B functional groups and subsequently attain maximum molecular weights.[86] This immediately restricts the window of "useful" reactions for this polymerization technique. The CuAAC reaction is ideal for the polymer synthesis as it proceeds to high

conversions, is robust, orthogonal, and has a very high fidelity. Also the requisite azide and alkyne functional groups are easy to install onto the potential building blocks.[70,85] The triazole unit is also chemically inert to a range of harsh conditions.[88] As such a number of reports have appeared which entail the use of the CuAAc reaction to make linear polymers/oligomers in a step growth fashion.[85,89] A few examples will be discussed here. Other practical considerations for a successful step growth polymerization will be discussed in Chapter 3.

Figure 2.5 shows structures of some reported polytriazoles. The list is by no means exhaustive; however, this illustrates the emergence of this type of polymer system in which a triazole functionality is incooperated in the main chain. Materials based on poly(1,2,3-triazoles) have good potential for use as high performance metal coatings and as adhesives (**16**).[90,91] Compared to the 1,2,4-triazole analogues, widely used as corrosion inhibitors and adhesion promoters, on copper based materials, the 1,2,3-triazole analogues offer the added advantage of being more chemically stable.[90] Zhu *et al*. prepared fluoro-functional polytriazoles (**18**) with good thermal stability and melting fluidity.[92] Matyjaszewski showed that the CuAAC technique can be used to grow azide-alkyne end-functional oligomers into longer functional polymers (**17**).[93,94] Recently Schmidt synthesized poly(dimethylsiloxane) (PDMS) copolymers from siloxane based copolymers (**20**).[95] Ye *et al*. recently reported the synthesis of polytriazole/clay nanocomposites by an in situ CuAAC polymerization in the presence of alkyne functionalized clay.[96] It has also been shown in several studies that the incooporation of the triazole functionality into the main chain has resulted in an increase in thermal stability.[97-99] Binauld *et al*. suggested that the increase in T_g was due to inter-chain hydrogen bonding emanating from the triazole ring.[97] Studies have shown 1,3-disubstituted-1,2,3-triazole oligomers to be effective mimics of peptide β-strands as they adopted a zigzag conformation reminiscent of peptide β-strands, in polar solvents, which appeared to be stabilized by dipole-dipole interactions between neighbouring triazole rings.[100] Liskamp and coworkers polymerized an azide-alkyne functional dipeptide to yield high molecular weight biopolymers (e.g. **19**),[101,102] obtained by microwave heating rather than by conventional heating. The polymerization could be tuned to obtain mainly short and cyclic oligomers, (low monomer concentrations) or long linear chains (high monomer concentrations).

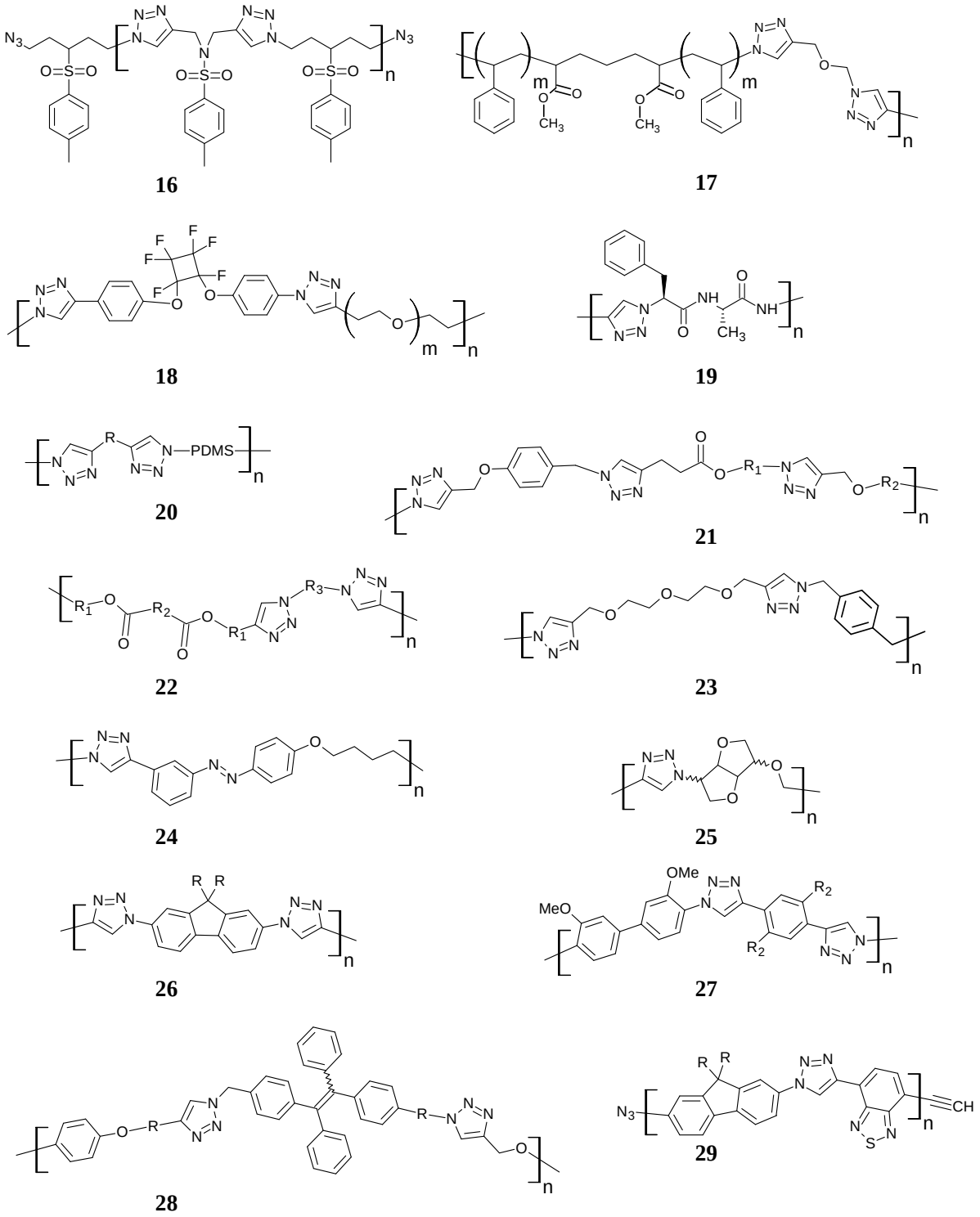

Figure 2.5: Some reported triazole oligomers and polymers prepared by step growth polymerization.

The CuAAC step growth polymerization has also been used to prepare conjugated polymers (**26** and **27**).[103,104] It was suggested that the monomers used led to polymers with localized HOMO and LUMO.[104] Qin *et al*. prepared a polytriazole (**28**) which emitted efficiently in its aggregated form, and demonstrated that the polytriazole was potentially useful as a chemosensor in the detection of explosives.[105] Fluorene-functional polytriazoles (e.g. **29**) have also been used as quasi solid state electrolytes in dye-sensitized solar cells, opening another potential avenue for applications of conjugated polytriazoles.[98,99]

Problems with the CuAAC step growth polymerization

Whilst the CuAAC is the pre-eminent click reaction judging by the number, and diversity, of publications using this technique, its main problem is the removal of the copper catalyst after the polymerization. This is further complicated by the ability of the triazoles to bind to copper. The presence of the metal impurities is detrimental for conjugated poytriazoles as the metal traps can quench light emission, reducing the efficiency of the materials.[106] Extensive purification procedures have to be employed to remove copper.[103]

Another problem associated with the CuAAC step growth polymerizations is the loss of orthogonality associated with the use of $Cu(PPh_3)_3Br$ as a catalyst. Triphenylphosphine (PPh_3) (**31**) from the catalyst reduces azido groups to amine groups in a Staudinger reaction (Scheme 2.5).[107]

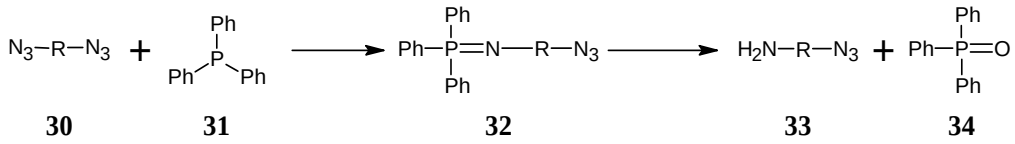

Scheme 2.5: Reduction of azido group by the Staudinger reaction.

This side reaction lowers the efficiency of the step growth polymerization as it alters the stoichiometry, dramatically lowering molecular weights.[107] This problem, however, can be solved by simply switching to other Cu^{I} catalysts that do not possess PPh_3 ligands. A Glaser coupling of terminal alkynes is another possible side reaction, however it can be curtailed by running the reaction under an inert atmosphere.[108]

Lastly another problem is the low solubility of the polymers formed by the CuAAC step growth polymerization technique which leads to vitrification of the reaction media.[97,101-103,108,109] The formation of cyclic species is also an attendant problem.[93,94,101,102,107] However this can be curtailed by carrying out the experiments at high concentrations.[102]

Polytriazole foldamers

It has been shown that aryl-triazoles can be programmed to fold into well-defined conformations. Hecht used 2,6-bis(1,2,3-triazol-4-yl)pyridines (BTPs) and showed that they can fold into helical foldamers.[110] The helical programming made use of the strong preference for a kinked *anti-anti* conformation, by the BTP scaffold (**36**),[111,112] as well as use of meta-phenylene linkages, which imparted a natural inclination, in the molecule, to fold. The extended *syn-syn* conformation (**35**) is disfavoured due to the lone pair repulsions among the nitrogen lone pairs. Further stability to the helical folded conformation was conferred by π-π interactions, as well as solvophobic forces which rendered the molecule amphiphilic.

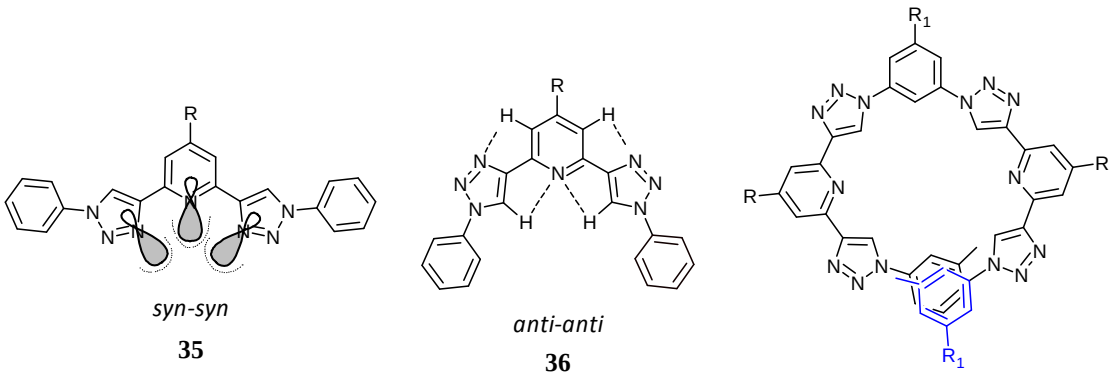

Figure 2.6: Illustration of the *syn-syn* and *anti-anti* BTP scaffold and *meta*-linked polytriazole foldamer 37.

A helical conformation was confirmed by CD spectroscopy. The CD spectra exhibited an intense bisignate signal in which chirality was transferred from the chiral side chains to the backbone. The *syn-syn* conformation, however, has coordinative ability. Addition of transition metal ions to a solution of the polytriazole led to coordinative crosslinking and gel formation.[110]

Later, Hecht showed that the oligo(aryl-triazole) foldamer undergoes a helix inversion upon the addition of halide ions.[113] This was remarkable in that the "clean" helicity inversion was induced by an achiral guest. At about the same time, it was shown that the 3_4[triazolophanes] (**38**, Scheme 2.6) can bind selectively to halide anions.[114,115]

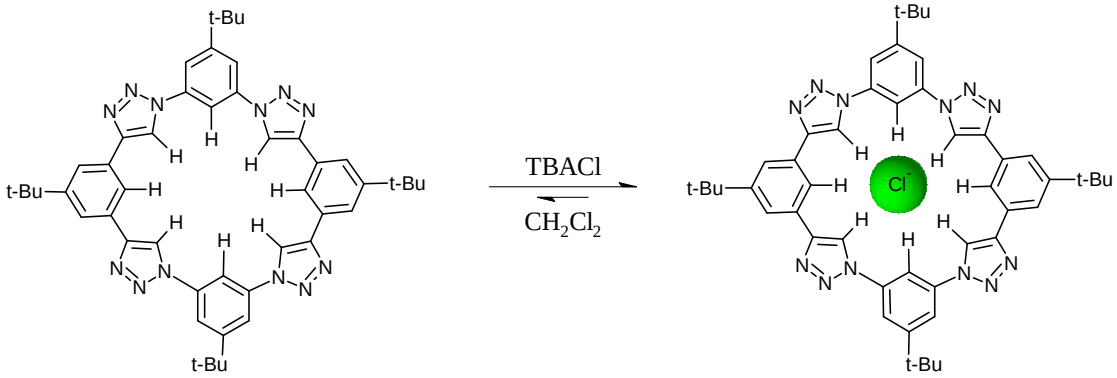

38 **39**

Scheme 2.6: Halide anion binding by 3_4[triazolophanes] 38.

The anion binding was brought about by the strong hydrogen bond donating ability of the triazole. This is because the CH bond, of the triazole ring, is highly polarized owing to the three electronegative nitrogens. Also a large positive dipole is directed towards the hydrogen atom, by the nitrogens lone pairs.[116] When a ring-opened version of the aryl-triazole tetramer was presented with chloride anions, it wrapped around the halide anion into a helical conformation with a pseudocircular electropositive cavity (**42**, Figure 2.7), like the one in macrocycle **39**.[114] ^{1}H NMR analysis showed that the halide anion formed primary hydrogen bonds with the triazole protons enabling the phenylene protons to form weaker hydrogen bonds, driving the helical folding process.[114] The interactions between the triazole and the halide anions were shown to be directional and guided the folding process in both solution and solid state. The strength of the interactions increased with increasing generation or the oligo(aryl-triazole).[117] Craig showed that this increase was not due to tighter interactions as the strength of the individual interactions actually reduced, but it was due to the longer foldamer having more electropositive CH donors, resulting in an increased binding constant. In the same report Craig

also showed anion binding decreased, with a few exceptions, with increasing size of the anion.[118]

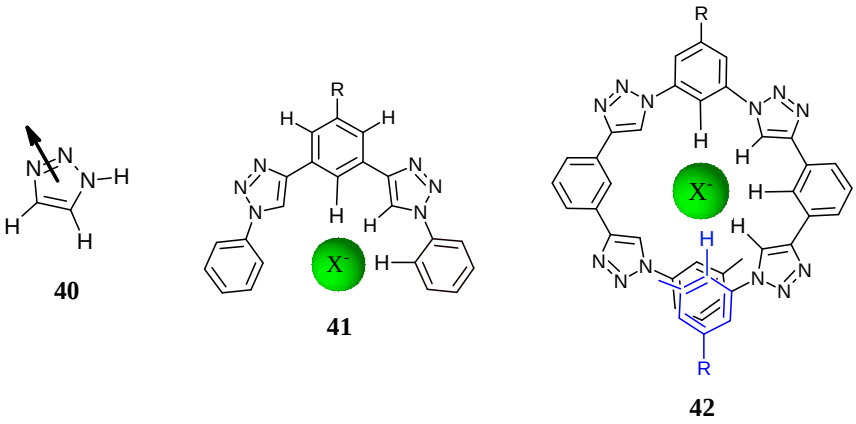

Figure 2.7: Illustration of the dipole polarizability of a 1,2,3-triazole (40) with the arrow pointing towards the negative end[116] and halide anion binding in oligo(aryl triazoles) (41 and 42).[118]

Anion binding was also shown to be subject to solvent effects. Use of solvents with an increased ability to accept electron density through electrostatic interactions, like hydrogen bonding, led to weaker binding.[118] Recently Wang *et al*. have shown that the binding affinity of the oligo(aryl-triazole) foldamers can be controlled by light through insertion of an azobenzene moiety into the oligomer structure.[119]

Jiang and coworkers also synthesized similar meta-linked oligo(aryl-triazoles) with cationic side chains and a different asymmetric sequence, since the oligomers defined an AB step growth polymer prepared by a divergent/convergent synthesis.[120] These oligomers existed in a random chain conformation in methanol, but folded into a helical conformation in aqueous solutions driven by solvophobic forces, without need for chloride anions to drive the folding process. In higher concentrations the foldamers also aggregated in water to form superstructures. As a matter of fact, the presence of chloride ions served to prevent the aggregation of the cationic oligo(aryl-triazoles). The authors attributed this to electrostatic repulsions between chloride anions binding to the foldamers.[120] Yashima's group prepared meta-linked aryl-triazole polymers (**44**) with chiral side chains which exhibited an apparent CD in DMF and DMSO. Upon the addition of poor solvents, however, the CD spectra intensity increased. A concomitant red

shift and a fluorescence color change was also observed. This was attributed to the formation of chiral aggregates, upon addition of poor solvents, an assertion that was backed up by DLS measurements, which showed an increase in the hydrodynamic diameter of the polymer in the presence of the poor solvent.[121]

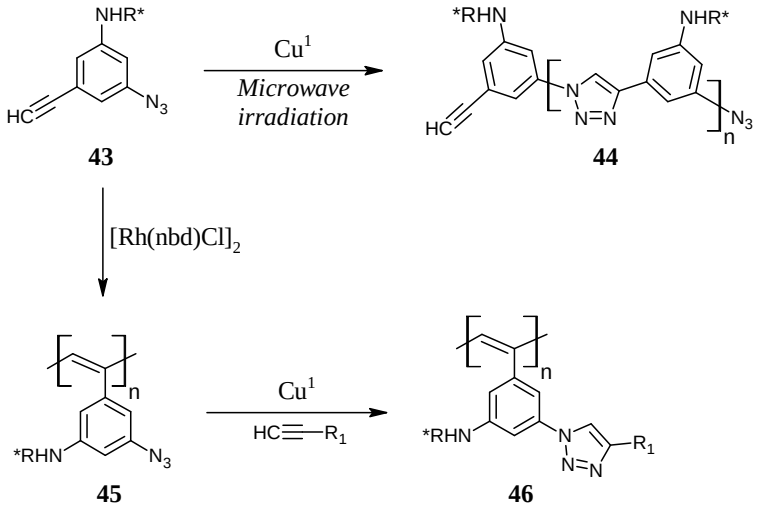

Scheme 2.7: Click and rhodium-catalyzed polymerizations of optically active phenylacetylene.

Interestingly, the same monomer could also be polymerized by a ruthenium-catalyzed chain polymerization to form helical poly(phenylacteylenes) (PPAs, **45**), which could be further modified by clicking on the pendant azide functionalities. [121]

Foldamers in higher order structures

Most of the applications of reported synthetic foldamers relate to their use in molecular recognition, by making use of the well-defined cavity.[122] A wide variety of abiotic foldamer systems can now be routinely accessed. The level of architectural complexity frequently only goes as far as the secondary structure, *i.e*. the helically folded state. In nature, isolated secondary structures do not realize any function. There is a need to pursue higher order structures and bring foldamer research closer to the levels of complexity realised in nature. Nature provides direction on how to go about this. The first step is to construct primary sequences with information to fold into defined secondary structures. The subsequent secondary structures are then assembled into higher order structures using weak non-covalent

interactions, like van de Waals interactions, hydrophobic interactions and hydrogen bonding.[123] Use of weak (and reversible) non-covalent interactions allows for dynamic self-assembly, enabling the assembly systems to equilibrate into preferred positions and to self-check. On the face of it, it appears that abiotic aryl-based helical foldamers present "easier to manipulate" determinants of tertiary and quaternary structures. This is because folded conformations of abiotic aryl-based foldamers are easy to program and their folding tendencies are predictable. Examples with higher order structures based on aryl abiotic foldamers are, however, still few.

To date there are only a few examples describing higher order structures realized from abiotic aryl foldamers. Lehn and co-workers showed that helical pyridine-pyridazine foldamers (**50**) self-assemble into supramolecular stacks which subsequently assembled into extended and entangled fiber-like structures with helical substructures (Figure 2.8).[124]

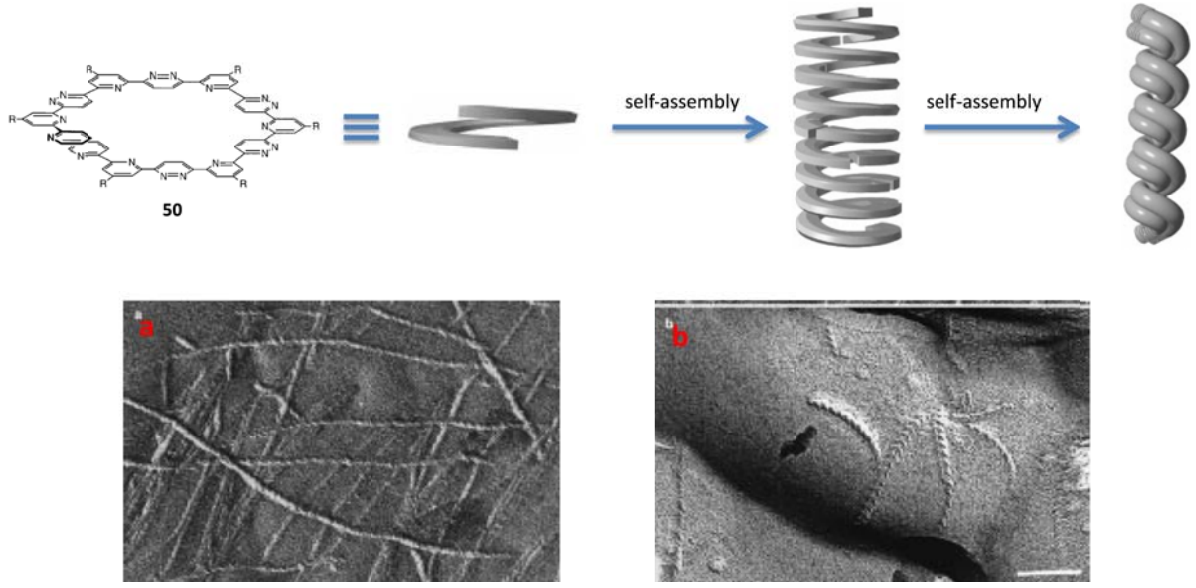

Figure 2.8: Self-assembly pathway of Lehn's pyridine-pyridazine helical foldamer first into supramolecular stacks and subsequently into fiber-like structure (top); and freeze fracture electron microscopy images of 50 in dichloromethane (a) and in pyridine (b) (bottom).[124]

The remarkable freeze fracture micrographs showed fibers with uniform diameters, which was attributed to coiled-coil bundles of 2 or 3 supramolecular stacks of **50**. The fibers were chiral, implying that helices of the same twist sense were interacting.[124] Parallels were drawn between

the heterocylic sequence and connectivity (in **50**) which predisposed the oligomer to helical folding and subsequently self-assembly, to the primary amino acid sequences in polypeptides with information for protein folding and assembly.

Moore and Meijer demonstrated the self-assembly of helical *m*PE foldamers, in aqueous acetronitrile solutions. Intermolecular chirality transfer was demonstrated via the so called "soldiers and sergeants" experiment. Mixtures of chiral and achiral helical fodamers displayed a positive non-linear relationship between mole chiral percent oligomers and CD signal response indicating intermolecular chirality transfer.[125] *Meta*-linked aryltriazole oligomers, tethered with cationic side chains, were also shown to assemble into helical stacks.[120]

Delsuc *et al*. connected helical aryl oligoamides via metal complexes into structures with defined orientations reminiscent of turn structures in proteins.[126] When a tetrahedral Cu^{I} ion was used, two helices were linked in fairly perpendicular manner, whilst an octahedral Fe^{II} ion resulted in an almost parallel linkage (Figure 2.9a). Recently, the same workers designed a system in which a pair of helical oligo arylamide foldamers was joined in the middle by a short ethylene glycol spacer, holding the two helices in close proximity (Figure 2.9b).

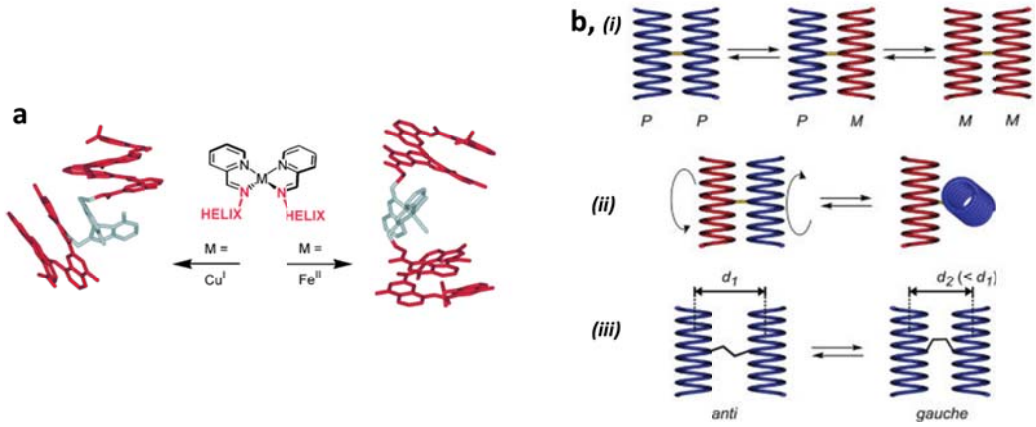

Figure 2.9: Schematic illustration of synthetic helical turns (a) and the allowed degrees of freedom; helix screw sense inversion (*i*), relative helix orientations (*ii*) and inter-helix distances adjusted by the conformation of the spacer which results (*iii*) in branched aryl oligoamide foldamers (b).

The helices could adopt similar and/or different screw senses, the distances between them could be subtly adjusted by the adoption of gauche/anti conformations by the spacer and they

could also orient their axes parallel or perpendicular to each other. Inter-helix communication, manifested in the form of helix-helix handedness, was shown to be mediated by the side chains which interdigitated, impeding free rotation between the spacers. Solvent was also speculated to have a role in inter-helix communication.[127]

It has also been shown that helical aryl oligoamides can undergo dimerization into double stranded helices.[128,129] Extensive face-to-face aromatic stacking interactions promoted the inter-strand association. The isolated helices were only able to make one to one-and-a-half turns and therefore were incapable of forming extensive aromatic stacking interaction. The stacking interactions resulted in extra stabilization from van der Waals forces. Inter-strand hydrogen bonds were minimal, occurring only between repeat units at the ends of the dimerized chains.

Lehn and coworkers further demonstrated the self-assembly of helical foldamers promoted by small cations and by "stringed" cations.[130,131] In the latter example, oligo ammonium cationic substrates were used to regulate the self-assembly of the helical foldamers. Information transfer in the form of assembly length and chirality was demonstrated. This system was likened to rotaxane-like architectures, except that macrocyclic rings in the conventional rotaxanes were replaced with helical subunits.[131]

Our proposal

The work detailed in earlier sections considers folding oligo(aryl-triazole) architectures based on meta linkages between the benzene and triazole rings as the helicity codon.[113] However, the 1,4-disubsitution pattern about the triazole unit also defines an angle < 180^{o}. We postulated that this alone would be sufficient to induce a crescent resulting in a helical conformation, in oligomers long enough, in an all *para*-aryl di-substituted system. This will be the subject of the following chapter.

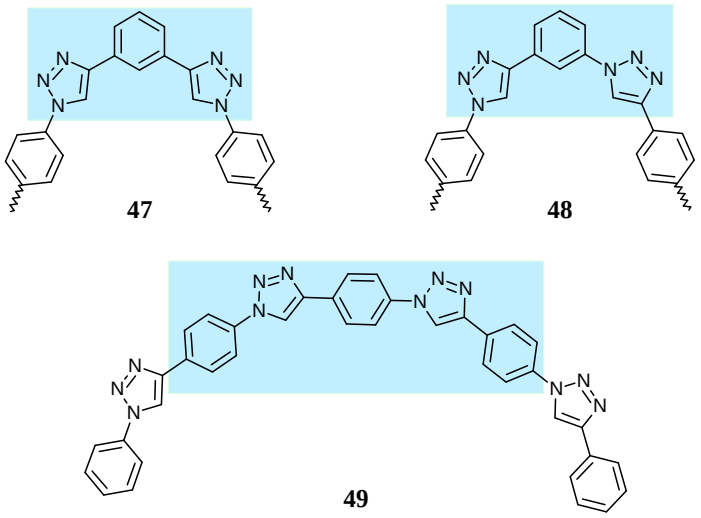

Figure 2.10: *meta* aryl-triazole helicity codon (47, 48) and *para*-aryl triazole helicity codon (49).

In subsequent chapters, the dynamic self-assembly of helical P(*p*-AT) foldamers into higher order structures will be demonstrated. The putative P(*p*-AT) helix possesses a well-defined cylindrical cavity, and its folding is driven by solvophobic forces. The exterior of the folded conformation is amphiphilic and the interior is hydrophobic. The coil to helix conformational transitions of the foldamer can be controlled by variation of the volume fraction of good to bad solvent. It will be shown that increasing the strength of the solvophobic driving forces induces stable P(*p*-AT) helical foldamers to assemble into supramolecular stacks. Template length control will also be demonstrated.

References

(1) Stryer, L. *Biochemistry*; Fourth ed.; Freeman: New York, 1995.

(2) Steed, J. W.; Atwood, J. L. *Supramolecular Chemistry*; Wiley, 2000.

(3) Buehler, M. J. *Proc. Natl. Acad. Sci.* **2006**, *103*, 12285.

(4) Cornelissen, J. J. L. M.; Rowan, A. E.; Nolte, R. J. M.; Sommerdijk, N. A. J. M. *Chem. Rev.* **2001**, *101*, 4039.

(5) Yashima, E.; Maeda, K.; Iida, H.; Furusho, Y.; Nagai, K. *Chem. Rev.* **2009**, *109*, 6102.

(6) Natta, G.; Pino, P.; Corradini, P.; Danusso, F.; Mantica, E.; Mazzanti, G.; Moraglio, G. *J. Am. Chem. Soc.* **1955**, *77*, 1708.

(7) Okamoto, Y.; Suzuki, K.; Ohta, K.; Hatada, K.; Yuki, H. *J. Am. Chem. Soc.* **1979**, *101*, 4763.

(8) Nakano, T.; Okamoto, Y. *Chem. Rev.* **2001**, *101*, 4013.

(9) Green, M. M.; Reidy, M. P.; Johnson, R. D.; Darling, G.; O'Leary, D. J.; Willson, G. *J. Am. Chem. Soc.* **1989**, *111*, 6452.

(10) Yashima, E.; Maeda, K. *Macromolecules* **2007**, *41*, 3.

(11) Gellman, S. H. *Acc. Chem. Res.* **1998**, *31*, 173.

(12) Hoogboom, J.; Elemans, J. A. A. W.; Rowan, A. E.; Rasing, T. H. M.; Nolte, R. J. M. *Phil. Trans. R. Soc. A* **2007**, *365*, 1553.

(13) Hill, D. J.; Mio, M. J.; Prince, R. B.; Hughes, T. S.; Moore, J. S. *Chem. Rev.* **2001**, *101*, 3893.

(14) van Gorp, J. J.; Vekemans, J. A. J. M.; Meijer, E. W. *Chem. Commun.* **2004**, 60.

(15) Appella, D. H.; Christianson, L. A.; Karle, I. L.; Powell, D. R.; Gellman, S. H. *J. Am. Chem. Soc.* **1996**, *118*, 13071.

(16) Hamuro, Y.; Geib, S. J.; Hamilton, A. D. *J. Am. Chem. Soc.* **1996**, *118*, 7529.

(17) Bassani, D. M.; Lehn, J.-M.; Baum, G.; Fenske, D. *Angew. Chem. Int. Ed. Engl.* **1997**, *36*, 1845.

(18) Gardinier, K. M.; Khoury, R. G.; Lehn, J.-M. *Chem. Eur. J.* **2000**, *6*, 4124.

(19) Ohkita, M.; Lehn, J.-M.; Baum, G.; Fenske, D. *Chem. Eur. J.* **1999**, *5*, 3471.

(20) Nelson, J. C.; Saven, J. G.; Moore, J. S.; Wolynes, P. G. *Science* **1997**, *277*, 1793.

(21) Ray, C. R.; Moore, J. S. *Adv. Polym. Sci.* **2005**, *177*, 91.

(22) Ghosh, S.; Ramakrishnan, S. *Macromolecules* **2005**, *38*, 676.

(23) Ramkumar, S. G.; Ramakrishnan, S. *Macromolecules* **2010**, *43*, 2307.

(24) Lokey, R. S.; Iverson, B. L. *Nature* **1995**, *375*, 303.

(25) Huc, I.; Maurizot, V.; Gornitzka, H.; Léger, J.-M. *Chem. Commun.* **2002**, 578.

(26) Kirshenbaum, K.; Zuckermannl, R. N.; Dill, K. A. *Curr. Opin. Struct. Biol.* **1999**, *9*, 530.

(27) Hanan, G. S.; Lehn, J.-M.; Kyritsakas, N.; Fischer, J. *J. Chem. Soc., Chem. Commun.* **1995**, 765.

(28) Liu, R.; Shiotsuki, M.; Masuda, T.; Sanda, F. *Macromolecules* **2009**, *42*, 6115.

(29) Prince, R. B.; Saven, J. G.; Wolynes, P. G.; Moore, J. S. *J. Am. Chem. Soc.* **1999**, *121*, 3114.

(30) Pace, C. N.; Scholtz, J. M. In *Protein Structure: A Practical Approach*; Second ed.; Creighton, T. E., Ed.; IRL Press: Oxford, 1997, p 299.

(31) Pan, X.; Zhao, Y. *Org. Lett.* **2009**, *11*, 69.

(32) Chan, H. S.; Bromberg, S.; Dill, K. A. *Phil. Trans. R. Soc. Lond. B* **1995**, *348*, 61.

(33) Jones, T. V.; Slutsky, M. M.; Laos, R.; de Greef, T. F. A.; Tew, G. N. *J. Am. Chem. Soc.* **2005**, *127*, 17235.

(34) Christel, D.; Axelle, G.; Michel, L.; Hua, J.; Victor, M.; Ivan, H. *Chem. Eur. J.* **2005**, *11*, 6135.

(35) Ute, K.; Hirose, K.; Kashimoto, H.; Hatada, K.; Vogl, O. *J. Am. Chem. Soc.* **1991**, *113*, 6305.

(36) Ute, K.; Hirose, K.; Kashimoto, H.; Nakayama, H.; Hatada, K.; Vogl, O. *Polym. J.* **1993**, *25*, 1175.

(37) Gin, M. S.; Yokozawa, T.; Prince, R. B.; Moore, J. S. *J. Am. Chem. Soc.* **1999**, *121*, 2643.

(38) Prince, R. B.; Brunsveld, L.; Meijer, E. W.; Moore, J. S. *Angew. Chem. Int. Ed.* **2000**, *39*, 228.

(39) Hou, J.-L.; Shao, X.-B.; Chen, G.-J.; Zhou, Y.-X.; Jiang, X.-K.; Li, Z.-T. *J. Am. Chem. Soc.* **2004**, *126*, 12386.

(40) Inouye, M.; Waki, M.; Abe, H. *J. Am. Chem. Soc.* **2004**, *126*, 2022.

(41) Abe, H.; Murayama, D.; Kayamori, F.; Inouye, M. *Macromolecules* **2008**, *41*, 6903.

(42) Abe, H.; Masuda, N.; Waki, M.; Inouye, M. *J. Am. Chem. Soc.* **2005**, *127*, 16189.

(43) Waki, M.; Abe, H.; Inouye, M. *Angew. Chem. Int. Ed.* **2007**, *46*, 3059

(44) Prince, R. B.; Barnes, S. A.; Moore, J. S. *J. Am. Chem. Soc.* **2000**, *122*, 2758.

(45) Tanatani, A.; Mio, M. J.; Moore, J. S. *J. Am. Chem. Soc.* **2001**, *123*, 1792.

(46) Tanatani, A.; Hughes, T. S.; Moore, J. S. *Angew. Chem. Int. Ed.* **2002**, *41*, 325.

(47) Stone, M. T.; Moore, J. S. *Org. Lett.* **2004**, *6*, 469.

(48) Goto, K.; Moore, J. S. *Org. Lett.* **2005**, *7*, 1683.

(49) Heemstra, J. M.; Moore, J. S. *J. Am. Chem. Soc.* **2004**, *126*, 1648.

(50) Smaldone, R. A.; Moore, J. S. *J. Am. Chem. Soc.* **2007**, *129*, 5444.

(51) Smaldone, R. A.; Moore, J. S. *Chem. Eur. J.* **2008**, *14*, 2650.

(52) Khan, A.; Hecht, S. *Chem. Eur. J.* **2006**, *12*, 4764.

(53) Sinkeldam, R. W.; Hoeben, F. J. M.; Pouderoijen, M. J.; De Cat, I.; Zhang, J.; Furukawa, S.; De Feyter, S.; Vekemans; Meijer, E. W. *J. Am. Chem. Soc.* **2006**, *128*, 16113.

(54) Garric, J.; Leger, J.-M.; Huc, I. *Angew. Chem. Int. Ed.* **2005**, *44*, 1954.

(55) Ferrand, Y.; Kendhale, A. M.; Kauffmann, B.; Grelard, A.; Marie, C.; Blot, V.; Pipelier, M.; Dubreuil, D.; Huc, I. *J. Am. Chem. Soc.* **2010**.

(56) Huisgen, R. *Angew. Chem. Int. Ed.* **1963**, *2*, 565.

(57) Bock, V. D.; Hiemstra, H.; van Maarseveen, J. H. *Eur. J. Org. Chem.* **2006**, 51.

(58) Hlasta, D. J.; Ackerman, J. H. *J. Org. Chem.* **1994**, *59*, 6184.

(59) Clarke, D.; Mares, R. W.; McNab, H. *J. Chem. Soc., Perkin Trans. 1* **1997**, 1799.

(60) Baskin, J. M.; Prescher, J. A.; Laughlin, S. T.; Agard, N. J.; Chang, P. V.; Miller, I. A.; Lo, A.; Codelli, J. A.; Bertozzi, C. R. *Proc. Natl. Acad. Sci.* **2007**, *104*, 16793.

(61) Baskin, J. M.; Bertozzi, C. R. *AldrichimicaACTA* **2010**, *43*, 15.

(62) Tornoe, C. W.; Christensen, C.; Meldal, M. *J. Org. Chem.* **2002**, *67*, 3057.

(63) Rostovtsev, V. V.; Green, L. G.; Fokin, V. V.; Sharpless, K. B. *Angew. Chem. Int. Ed.* **2002**, *41*, 2596.

(64) Kolb, H. C.; Finn, M. G.; Sharpless, K. B. *Angew. Chem. Int. Ed.* **2001**, *40*, 2004.

(65) Rodionov, V. O.; Presolski, S. I.; Dı´az, D. D. a.; Fokin, V. V.; Finn, M. G. *J. Am. Chem. Soc.* **2007**, *129*, 12705.

(66) Himo, F.; Lovell, T.; Hilgraf, R.; Rostovtsev, V. V.; Noodleman, L.; Sharpless, K. B.; Fokin, V. V. *J. Am. Chem. Soc.* **2005**, *127*, 210.

(67) Meldal, M.; Tornøe, C. W. *Chem. Rev.* **2008**, *108*, 2952.

(68) Rodionov, V. O.; Fokin, V. V.; Finn, M. G. *Angew. Chem., Int. Ed.* **2005**, *44*, 2210.

(69) Straub, B. F. *Chem. Commun.* **2007**, 3868.

(70) Meldal, M. *Macromol. Rapid Commun.* **2008**, *29*, 1016.

(71) Nolte, C.; Mayer, P.; Straub, B. F. *Angew. Chem. Int. Ed.* **2007**, *46*, 2101.

(72) Scriven, E. F. V.; Turnbull, K. *Chem. Rev.* **1988**, *88*, 297.

(73) Bräse, S.; Gil, C.; Knepper, K.; Zimmermann, V. *Angew. Chem. Int. Ed.* **2005**, *44*, 5188.

(74) Saxon, E.; Bertozzi, C. R. *Science* **2000**, *287*, 2007.

(75) Kiick, K. L.; Saxon, E.; Tirrell, D. A.; Bertozzi, C. R. *Proc. Natl. Acad. Sci.* **2002**, *99*, 19.

(76) Moses, J. E.; Moorhouse, A. D. *Chem. Soc. Rev.* **2007**, *36*, 1249.

(77) Droumaguet, B. L.; Velonia, K. *Macromol. Rapid Commun.* **2008**, *29*, 1073.

(78) van Dijk, M.; Rijkers, D. T. S.; Liskamp, R. M. J.; van Nostrum, C. F.; Hennink, W. E. *Bioconjugate Chem.* **2009**, *20*, 2001.

(79) Amblard, F.; Cho, J. H.; Schinazi, R. F. *Chem. Rev.* **2009**, *109* 4207.

(80) Lundberg, P.; Hawker, C. J.; Hult, A.; Malkoch, M. *Macromol. Rapid Commun.* **2008**, *29*, 998.

(81) Iha, R. K.; Wooley, K. L.; Nystrom, A. M.; Burke, D. J.; Kade, M. J.; Hawker, C. J. *Chem. Rev.* **2009**, *109*, 5620.

(82) Sumerlin, B. S.; Vogt, A. P. *Macromolecules* **2009**, *43*, 1.

(83) Binder, W. H.; Sachsenhofer, R. *Macromol. Rapid Commun.* **2007**, *28*, 15.

(84) Binder, W. H.; Sachsenhofer, R. *Macromol. Rapid Commun.* **2008**, *29*, 952.

(85) Johnson, J. A.; Finn, M. G.; Koberstein, J. T.; Turro, N. J. *Macromol. Rapid Commun.* **2008**, *29*, 1052.

(86) Flory, P. J. *Principles Of Polymer Chemistry*; Cornell University Press: Ithaca, 1953.

(87) Odian, G. *Principles Of Polymerization*; Fourth ed.; Wiley Interscience: New Jersey, 2004.

(88) Akeroyd, N.; Pfukwa, R.; Klumperman, B. *Macromolecules* **2009**, *42*, 3014.

(89) Lutz, J.-F. *Angew. Chem. Int. Ed.* **2007**, *46*, 1018.

(90) Baut, N. L.; Díaz, D. D.; Punna, S.; Finn, M. G.; Brown, H. R. *Polymer* **2007**, *48*, 239.

(91) Diaz, D. D.; Punna, S.; Holzer, P.; McPherson, A. K.; Sharpless, K. B.; Fokin, V. V.; Finn, M. G. *J. Polym. Sci., Part A: Polym. Chem.* **2004**, *42*, 4392.

(92) Zhu, Y.; Huang, Y.; Meng, W.-D.; Li, H.; Qing, F.-L. *Polymer* **2006**, *47*, 6272.

(93) Tsarevsky, N. V.; Sumerlin, B. S.; Matyjaszewski, K. *Macromolecules* **2005**, *38*, 3558.

(94) Golas, P. L.; Tsarevsky, N. V.; Sumerlin, B. S.; Matyjaszewski, K. *Macromolecules* **2006**, *39*, 6451.

(95) Udo, S.; Philip, C. Z.; Bernhard, R. *Macromol. Rapid Commun.*, *31*, 545.

(96) Ye, Y.-S.; Yen, Y.-C.; Cheng, C.-C.; Syu, Y.-J.; Huang, Y.-J.; Chang, F.-C. *Polymer* **2010**, *51*, 430.

(97) Binauld, S.; Damiron, D.; Hamaide, T.; Pascault, J.-P.; Fleurya, E.; Drockenmuller, E. *Chem. Commun.* **2008**, 4138.

(98) Karim, M. A.; Cho, Y.-R.; Park, J. S.; Kim, S. C.; Kim, H. J.; Lee, J. W.; Gal, Y.-S.; Jin, S.-H. *Chem. Commun.* **2008**, 1929.

(99) Karim, M. A.; Cho, Y.-R.; Park, J. S.; Ryu, T. I.; Lee, M. J.; Song, M.; Jin, S.-H.; Lee, J. W.; Gal, Y.-S. *Macromol. Chem. Phys.* **2008**, *209*, 1967.

(100) Angelo, N. G.; Arora, P. S. *J. Am. Chem. Soc.* **2005**, *127*, 17134.

(101) van Dijk, M.; Nollet, M. L.; Weijers, P.; Dechesne, A. C.; van Nostrum, C. F.; Hennink, W. E.; Rijkers, D. T. S.; Liskamp, R. M. J. *Biomacromolecules* **2008**, *9*, 2834.

(102) van Dijk, M.; Mustafa, K.; Dechesne, A. C.; van Nostrum, C. F.; Hennink, W. E.; Rijkers, D. T. S.; Liskamp, R. M. J. *Biomacromolecules* **2007**, *8*, 327.

(103) van Steenis, D. J. V. C.; David, O. R. P.; van Strijdonck, G. P. F.; van Maarseveen, J. H.; Reek, J. N. H. *Chem. Commun.* **2005**, 4333.

(104) Bakbak, S.; Leech, P. J.; Carson, B. E.; Saxena, S.; King, W. P.; Bunz, U. H. F. *Macromolecules* **2006**, *39*, 6793.

(105) Qin, A.; Lam, J. W. Y.; Tang, L.; Jim, C. K. W.; Zhao, H.; Sun, J.; Tang, B. Z. *Macromolecules* **2009**, *42*, 1421.

(106) Qin, A.; Tang, L.; Lam, J. W. Y.; Jim, C. K. W.; Yu, Y.; Zhao, H.; Sun, J.; Tang, B. Z. *Adv. Funct. Mater.* **2009**, *19*, 1891.

(107) Binauld, S.; Fleury, E.; Drockenmuller, E. *J. Polym. Sci., Part A: Polym. Chem.* **2010**, *48*, 2470.

(108) Duxbury, C. J.; Cummins, D.; Heise, A. *J. Polym. Sci., Part A: Polym. Chem.* **2009**, *47*, 3795.

(109) Besset, C. l.; Binauld, S.; Ibert, M.; Fuertes, P.; Pascault, J.-P.; Fleury, E.; Bernard, J.; Drockenmuller, E. *Macromolecules* **2009**, *43*, 17.

(110) Meudtner, R. M.; Hecht, S. *Macromol. Rapid Commun.* **2008**, *29*, 347.

(111) Meudtner, R. M.; Ostermeier, M.; Goddard, R.; Limberg, C.; Hecht, S. *Chem. Eur. J.* **2007**, *13*, 9834.

(112) Li, Y.; Huffman, J. C.; Flood, A. H. *Chem. Commun.* **2007**, 2692.

(113) Meudtner, R. M.; Hecht, S. *Angew. Chem. Int. Ed.* **2008**, *47*, 4926.

(114) Li, Y.; Flood, A. H. *J. Am. Chem. Soc.* **2008**, *130*, 12111.

(115) Li, Y.; Flood, A. H. *Angew. Chem. Int. Ed.* **2008**, *47*, 2649

(116) Kassimi, N. E.-B.; Doerksen, R. J.; Thakkar, A. J. *J. Phys. Chem.* **1995**, *99*, 12790.

(117) Juwarker, H.; Lenhardt, J. M.; Pham, D. M.; Craig, S. L. *Angew. Chem. Int. Ed.* **2008**, *47*, 3740.

(118) Juwarker, H.; Lenhardt, J. M.; Castillo, J. C.; Zhao, E.; Krishnamurthy, S.; Jamiolkowski, R. M.; Kim, K.-H.; Craig, S. L. *J. Org. Chem.* **2009**, *74*, 8924.

(119) Wang, Y.; Bie, F.; Jiang, H. *Org. Lett.* **2010**, *12*, 3630.

(120) Wang, Y.; Li, F.; Han, Y.; Wang, F.; Jiang, H. *Chem. Eur. J.* **2009**, *15*, 9424.

(121) Kobayashi, S.; Itomi, K.; Morino, K.; Iida, H.; Yashima, E. *Chem. Commun.* **2008**, 3019.

(122) Juwarker, H.; Suk, J.; Jeong, K. *Chem. Soc. Rev.* **2009**, *38*, 3316.

(123) Alper, J. *Science* **2002**, *295*, 2396.

(124) Cuccia, L. A.; Lehn, J.-M.; Homo, J.-C.; Schmutz, M. *Angew. Chem. Int. Ed.* **2000**, *39*, 233.

(125) Brunsveld, L.; Meijer, E. W.; Prince, R. B.; Moore, J. S. *J. Am. Chem. Soc.* **2001**, *123*, 7978.

(126) Delsuc, N.; Hutin, M.; Campbell, V. E.; Kauffmann, B.; Nitschke, J. R.; Huc, I. *Chem. Eur. J.* **2008**, *14*, 7140.

(127) Delsuc, N.; Massip, S.; Léger, J. M.; Kauffmann, B.; Huc, I. *J. Am. Chem. Soc.* **2011**, *133*, 3165.

(128) Berl, V.; Huc, I.; Khoury, R. G.; Krische, M. J.; Lehn, J.-M. *Nature* **2000**, *407*, 720.

(129) Berl, V.; Huc, I.; Khoury, R. G.; Lehn, J.-M. *Chem. Eur. J.* **2001**, *7*, 2810.

(130) Petitjean, A.; Cuccia, L. A.; Lehn, J.-M.; Nierengarten, H.; Schmutz, M. *Angew. Chem., Int. Ed.* **2002**, *41*, 1195.

(131) Petitjean, A.; Cuccia, L. A.; Schmutz, M.; Lehn, J.-M. *J. Org. Chem.* **2008**, *73*, 2481.

Chapter 3. *para*-Aryl triazole foldamer system

Introduction

An essential aspect of foldamer research is the need to identify and design new backbones with specific conformational preferences in solution. Foldamer systems based on *m*-linked aryl triazole have been reported (see Chapter 2). The crescent shape in a meta-linked system is coded for by the 1,3-nature of the substitution around the benzene ring and regiospecific 1,4-di-substitution pattern around the triazole moiety. The driving force for folding was provided by a preference for *anti-anti* conformation in 2,6-bis(1,2,3-triazol-4-yl)pyridines (BTPs),[1,2] and anion binding.[3,4] In amphiphilic systems (apolar aromatic backbone and polar oligo(ethylene glycol) side chains) the inherent solvophobicity abetted the folding process and helped to stabilize the folded conformation as well.[1,2] The subsequent helically folded conformation was also enthalpically stabilized by π-π interactions between stacked aromatic rings.[2] We envisaged that a helical conformation could be attained with a *p*-aryl triazole system. The key features to inducing a crescent shape into linear poly[*p*-bis(1,2,3-triazol-4yl)-aryl] rings include a strict adherence to 1,4-di-substitution about the triazole moiety and the adoption of an extended *cisoid* conformation.

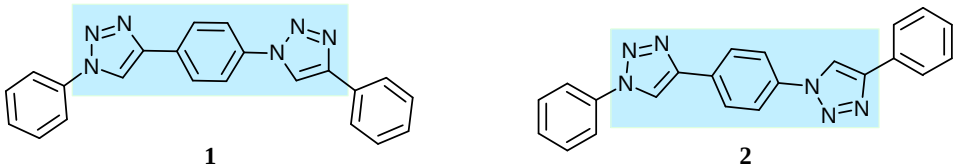

1 *cisoid* **2** *transoid*

Figure 3.1: Illustration of the *cisoid* and *transoid* conformations around p-aryl triazole linkages.

The *cisoid* conformation (highlighted on **1**, Figure 3.1) is crescent shaped and defines the helicity codon[5-7] for this helical system. Adoption of the *cisoid* conformation by the whole polytriazole should then enforce helical winding of the polymer.

A simple molecular modeling study was then performed to verify that the presence of the crescent shape, in a P(*p*-AT) with an extended *cisoid* conformation leads to helical folding in oligomers with a sufficiently large degree of polymerization. The modeling entailed a simple energy minimization of an all *cisoid* P(*p*-AT), with Spartan software (HF/3–21G* in vacuo). The model predicted a helical conformation, Figure 3.2, with 14 repeat units to complete a turn with a large internal diameter of approximately 30.6 Å, defined by the internal triazole hydrogens. In the helically folded conformation, each aryl ring stacks a triazole ring above and below it as clearly shown from the side view in Figure 3.2.

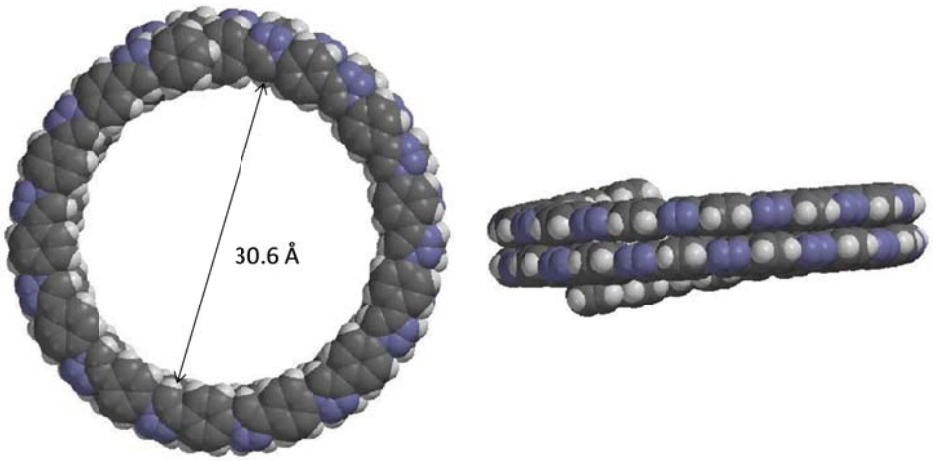

Figure 3.2: Top (left) and side (right) view of space filling molecular models of the putative helical conformation of the P(*p*-AT) with two complete turns. Side chains were omitted for clarity.

The helical pitch is approximately 3.8 Å. This is in good agreement with theoretical and experimental values for helical foldamers.[8,9] It also puts the turns of the helix to within the distance for making van der Waals contact.[8] Another interesting structural feature is the extensive inter–ring co–planarity shown explicitly in the side view of the helical foldamer. It is evident that the *para* di–substitution around the aryl rings and the 1,4–triazole di–substitution around the triazole ring reduces the torsion of the curve coding for a helix with a huge diameter. This inter–ring co–planarity should enable efficient π–π stacking interactions in the helical foldamer. The co–planarity in aryl–triazole–aryl linkages has also been utilized in the synthesis of planar triazolophanes.[10-12]

In the polymeric versions of **2** there is no inherent drive to force the P(*p*-AT) into an extended syn-syn conformation, *i.e*. fold into a helix. The unsubstituted polytriazole is also very insoluble.[13] To impart both solubility and a driving force for the helical folding, we turned to oligo(ethylene glycol) (oEG) side chains pioneered by Moore.[14,15] oEG chains are amphiphilic with good solubility in apolar solvents like $CHCl_3$, dioxane and polar solvents like DMF, acetonitrile and water. Therefore, attaching the oEG side chains to the aryl rings should introduce an amphiphilic character to the P(*p*-AT), since the aromatic backbone is inherently apolar. In good solvents, where the whole molecule is effectively solvated, a random coil is expected to prevail. However, in bad solvents, a solvophobically driven collapse into the putative helically folded conformation occurs.[16,17] It has been shown that the nature of the side chain linking group has a direct effect on the stability of the helically folded conformation. *m*PE foldamers with ester linked oEG side chains were more stable than phenyl and benzyl ether linked oEG side chains.[18] We took this cue and attached oEG side chains to the aryltriazole backbones via ester linkages. Monomers **3** and **4** were then synthesized for this study. An enantiomerically pure side chain was installed on monomer **4** in order to track the solvent dependent conformational transition by CD spectroscopy.[19] The chiral side chain biases the screw sense of the helices, hence the helices become diastereomers with different free energies. The methyl group is on the first carbon of the chiral side chain placing the stereochemical information in close proximity to the heteroaromatic backbone in the subsequent P(*p*-AT).

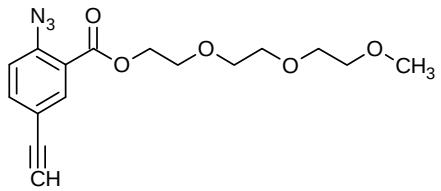

3

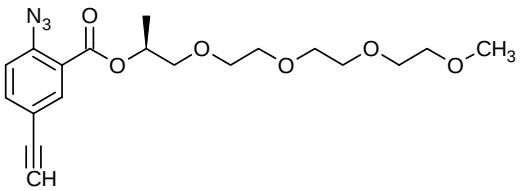

4

Figure 3.3: Monomers used for the formation of foldamers.

Synthesis and characterization of monomers

Achiral monomer synthesis

The synthesis of monomer **3** is shown in Scheme 3.1. First, 2-amino-5-iodobenzoic acid, **5**, was converted to the azido aryliodide **6**, via the diazonium salt. Then **6** was esterified with tetraethylene glycol mono methyl ether (TgOH) to give compound **7**.

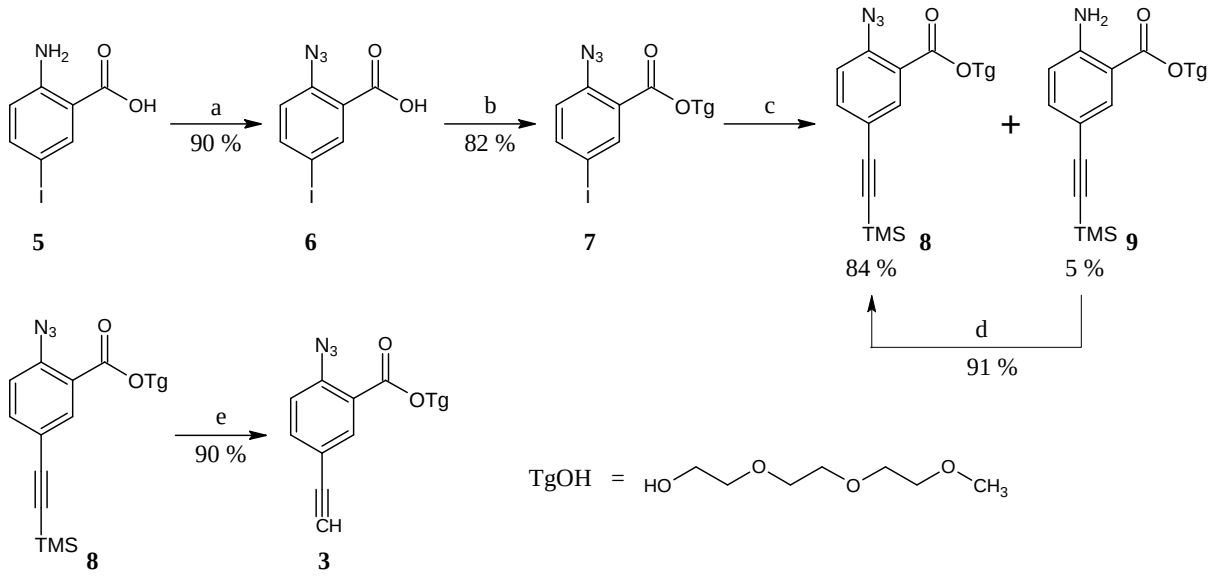

Scheme 3.1: Synthesis of achiral monomer; (a) HCl, $NaNO_2$, NaN_3, H_2O, 0 °C; (b) TgOH, DCC, DMAP, CH_2Cl_2, 0 °C to room temperature (r.t.); (c) Trimethylsilylacetylene (TMSA), $Pd(PPh_3)_4$, CuI, Triethyl amine (TEA), THF, r.t.; (d) *t*-$BuNO_2$, Trimethylsilyl azide (TMS-azide), THF, 0 °C to r.t.; (e) TBAF, THF, r.t.

A Sonogashira coupling[20] of compound **7** and TMS protected acetylene (TMSA) proceeded with complete conversion of the iodine moiety to the TMS protected alkyne to give **8**. Approximately ~ 5 % of the azide moiety, however, was reduced to amine functional compound **9**. This side reaction presumably is caused by a Staudinger reaction[21] between the azide moiety and triphenylphosphine from the palladium catalyst system. This type of side reaction also caused the loss of orthogonality in the Cu^I catalyzed step growth polymerization of azide-alkyne functional monomers using $Cu(PPh_3)_3Br$ as a catalyst.[22] Wang *et al*. recently reported a Sonogashira coupling of a meta-linked azido aryl iodide, with TMSA, with the same Pd catalyst and claimed a complete retention of azide functionality.[23] Nevertheless, the aryl amine, **9**, was

converted to the azide **8**, using *t*–$BuNO_2$ and TMS azide.[24] This brought the overall yield of the compound **8** close to ~ 90 %. Finally, monomer **3** was accessed by cleaving the TMS protection of **8** using TBAF, quantitatively, completing the synthesis.

Chiral monomer synthesis

The synthesis of the chiral side chain started with the protection of enantiopure methyl (*S*)–lactate (**10**) with 2,3-dihydro-2H-pyran (**11**) to give the protected ether **12** which was subsequently reduced, using $LiAlH_4$, to give **13** (Scheme 3.2). Compound **13** was then coupled with the tosylated triethylene glycol **15** to give compound **16**. Finally the tetrahydropyrane protection of compound **16** was removed, using pyridinium p-toluenesulfonate (PPTS) to yield the chiral oligo ethylene oxide **17**.

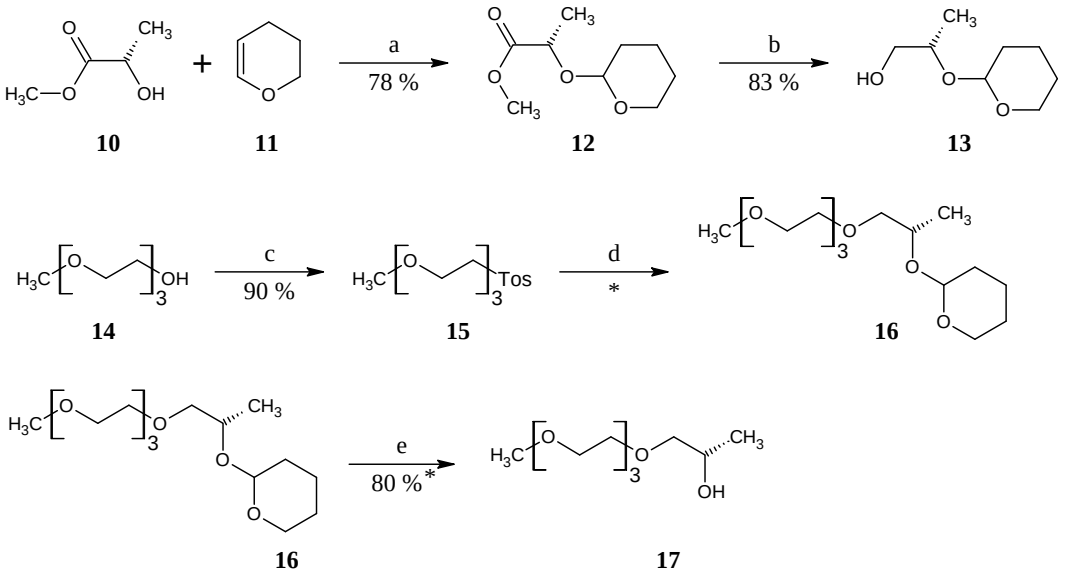

Scheme 3.2: Synthesis of chiral side chain; (a) HCl, neat, 0 °C to r.t.; (b) $LiAlH_4$, diethyl ether, 0 °C to r.t.; (c) NaOH, *p*-tosyl chloride, H_2O, THF, 0 °C to r.t.; (d) **13**, NaH, THF, reflux; (e) $TsOH.H_2O$, 0 °C to r.t.

The enantiomeric purity of the chiral alcohol was estimated by derivatisation of the chiral alcohol (**17**) with enantiomerically pure (*S*)-(+)-α-Methoxy-α-trifluoromethylphenylacetyl chloride (S-(+)-MTPA-Cl), Mosher's acyl chloride, **18** (Scheme 3.3). The subsequent Mosher ester (**20**/**21**) was then analyzed by ^{19}F NMR spectroscopy. Enantiomerically pure Mosher's reagent reacts with primary and secondary alcohols (and amines) forming diastereomeric esters

(and amides). The diastereomers can then be analyzed by either ^{1}H or ^{19}F NMR spectroscopy.[25,26] In the Newman projection, one of the groups attached to the chiral carbon is positioned close to the magnetically anisotropic phenyl ring, therefore this group resonates at higher field.[25] This enables the discrimination of the diastereomers and subsequently the determination of the absolute configuration of the secondary alcohol. There are no α hydrogen atoms to the carbonyl therefore there is no chance of racemization during this derivatisation. Also the presence of the CF_3 group enables the enantiomeric excess (*ee*) to be determined cleanly by ^{19}F NMR spectroscopic analysis.

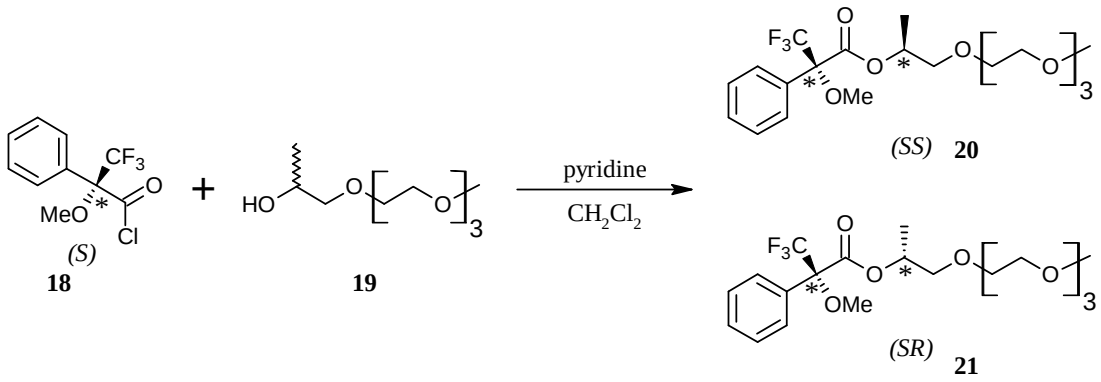

Scheme 3.3: Synthesis of Moscher Ester.

Figure 3.3 shows the ^{19}F NMR spectrum of the Mosher ester. This analysis followed the protocol reported by Hecht and coworkers who also prepared an identical chiral oligo(ethylene oxide) and deduced its *ee* to be 98 % percent, using Mosher ester analysis.[27] The chiral alcohol **17** was deduced, by ^{19}F NMR spectroscopy to have an *ee* of 97 %.

The synthesis of the chiral monomer began with the acylation of the azido aryl iodide **6** by refluxing compound **6** in thionyl chloride. The crude acyl halide, **22**, was first dried and then esterified with the chiral alcohol **17** in dry CH_2Cl_2, with DMAP catalysis to yield compound **23**. From here the synthesis followed the same protocol as in the synthesis of compound **3**.

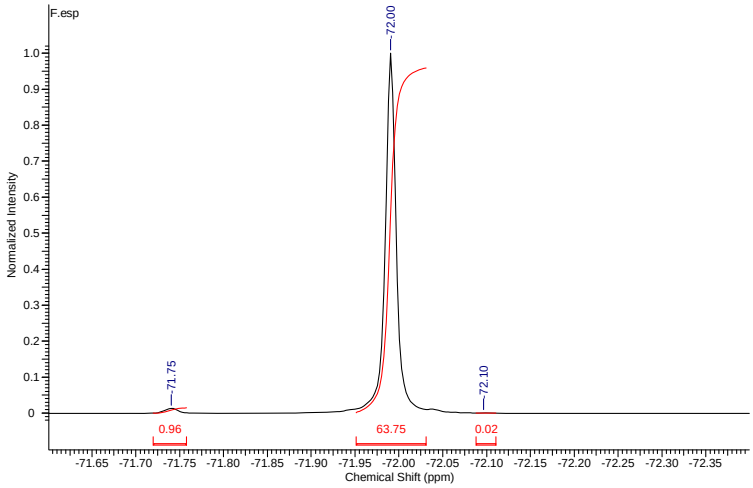

Figure 3.3: ^{19}F NMR spectrum of Mosher ester in $CDCl_3$ of 20 or 21.

In the conversion of **23** to **24**, about about ~ 6 % of the azide functionality was reduced to amine functionality, **25**. Compound **25**, however, was converted back to azido functionality bringing the overall yield of **24** to about 90 %. Finally the monomer **4** could be accessed by cleaving the TES protection on **24** with TBAF in complete conversion and the pure monomer was obtained after column chromatography.

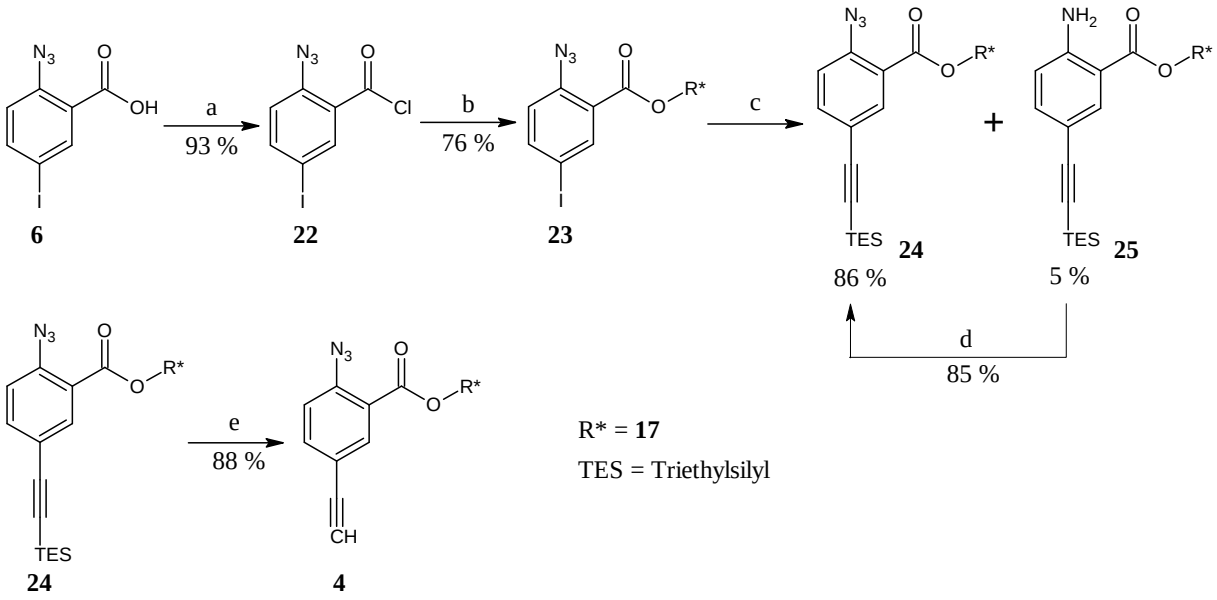

Scheme 3.4: Chiral monomer synthesis; (a) $SOCl_2$, reflux; (b) **17**, TEA, DMAP, CH_2Cl_2, 0 ^{o}C to (r.t.); (c) Triethylsilylacetylene, $Pd(PPh_3)_4$, CuI, TEA, THF, r.t.; (d) *t*-$BuNO_2$, TMS-azide, THF, 0 ^{o}C to r.t.; (e) TBAF, THF, r.t.

Polymer synthesis

CuAAC polymerization reactions proceed by a step growth mechanism. To reach high (useful) molecular weights via step growth polymerization strategies, a number of conditions should be met.[28] These include use of reactions which proceed with no side reactions, as they limit conversions, carrying out polymerizations at high concentrations (above 1 M) to minimize cyclization side reactions and to maximize reaction rates. Use of high temperatures, to increase reaction rate, and working under an inert atmosphere, to prevent oxidative degradation, also helps to increase conversions. Impure reagents drastically reduce polymer molecular weights in step growth systems and the use of high temperatures can present problems if the reactive functionalities are not thermally stable as this leads to loss of functionality. The CuAAC reaction offers a number of advantages, mainly a low tendency for side reactions, near quantitative conversions and it can be conducted efficiently at room temperatures.[29] The tendency to form cyclization side products is less with stiff aromatic monomers. The click monomers used here (**3** and **4**) are aromatic and stiff, reducing the possibility of cyclization side reactions. Click monomers **3** and **4** were subsequently polymerized via an AB CuAAC step growth polymerization, Scheme 3.5.

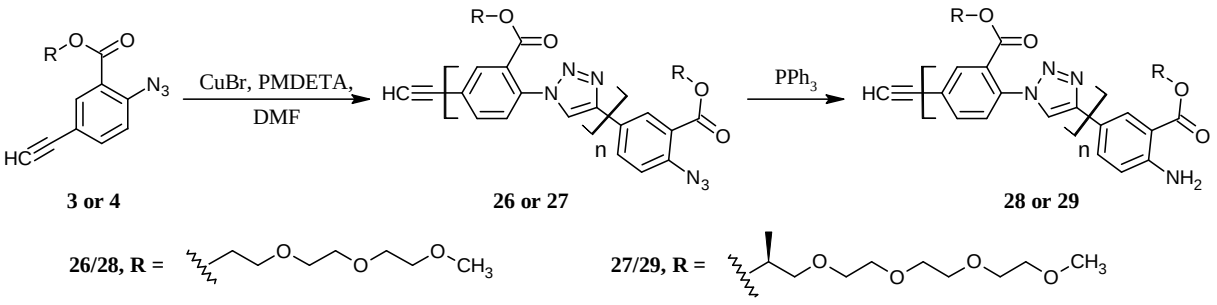

Scheme 3.5: Polymer synthesis.

Table 1: Reaction conditions for the polymerization of 3 and 4

Entry	Monomer	[a]Monomer / Cu^I / DMF	time	[b]M_n	[c]M_w	[d]$Đ$
1	3	0.5 g/5 mol %/1 mL	3 days	27 072	41 310	1.52
2	3	0.5 g/5 mol %/1 mL	3 days	23 273	41 561	1.79
3	3	0.5 g/5 mol %/0.5 mL	~ 30 mins	32 012	68 439	2.13
4	3	1 g/10 mol %/2 mL	~ 30 mins	32 273	41 561	1.79
5	4	0.5 g/5 mol %/0.5 mL	< 30 mins	42 581	67 858	1.59

- [a]Polymerizations were carried out 25 ^oC. Detailed conditions are given in the experimental section.
- [b]M_n and [c]M_w are the number average and weight average molecular weights determined by SEC in HFIP calibrated with low dispersity PMMA standards.
- [d]$Đ$ is the molar mass dispersity.[30]

CuBr was used as the Cu source and PMDETA as the ligand. Direct use of Cu^I salts precludes the need for reducing agents. It has been mentioned that this can proceed with formation of side products like diacetylenes, bistriazoles and 5-hydroxytriazoles. The formation of side products, however, is stopped by using one equivalent of a nitrogen base and excluding air.[31] The PMDETA ligand was used in a slight excess so as to fulfil the role of the nitrogen base. The reactions were also carried out under an inert atmosphere to prevent air oxidation of Cu^I.

The initial polymerization (entry 1) was carried out using optimized conditions reported for CuAAC AB step growth polymerization described by Hennink and Liskamp.[32] The protocol entailed dissolving 500 mg of monomer **3** into 1 mL of DMF and polymerizing with 5 mol % Cu^I to monomer. The reaction was stirred for 3 days after which the reaction mixture was very viscous. Cu ions were removed by several extraction steps using aqueous EDTA solution. The azide end-group was reduced to an amine end-group in order to prevent auto-polymerization during storage. The polymer was further purified by dialysis using dialysis tubing with molecular weight cut-off of 10 kDa. This also ensured that every P(*p*-AT) chain was above 10 kDa, and therefore long enough to fold into a minimum of two turns of the helix thereby maximizing enthalpic stabilization from π–π stacking interactions in the helical foldamer. A respectably high M_n of 27 kDa was obtained and the molar mass dispersity was also in the range typical for step growth polymerization systems, $Đ \approx 2$.[28] SEC analysis was carried out after an extensive

purification of the native polymer, which included a dialysis step that would have removed everything with a molecular weight below 10 kDa. The yield of the isolated polymer after purification was in excess of 80 % conversion of monomer. This implies that very little of the polymer was below 10 kDa. The resultant high molecular weight polymer obtained attested to the success of the CuAAC AB step growth polymerization technique. The result in entry 2 confirmed the reproducibility of the conditions therefore this protocol was considered optimum for making long P(*p*-AT)s.

An increase of the monomer concentration (entry 3) resulted in a dramatic acceleration of the reaction rate reflected in the reaction mixture, which became very viscous after just 20 minutes and was completely vitrified after about 30 minutes when no further stirring was possible. At this point, the reaction was considered complete and the polymer worked up. The isolated polymer had a higher molecular weight, M_n = 32 kDa. An increase of the catalyst loading to 10 mol %, entry 4, whilst keeping the same monomer concentrations as in entry 1, also resulted in the polymerization being essentially complete in under 30 minutes. Sumerlin *et al*. have also reported very high conversions in CuAAC step growth polymerizations in very short times, using CuBr/PMDETA as the catalyst system.[33]

The chiral monomer, **4**, was polymerized under the same conditions (entry 5) as those used in entry 3, and a higher molecular weight polymer was obtained than in entry 3. This was probably because the longer side chain of **4** resulted in the subsequent polymer staying in solution a little bit longer, allowing the functional groups to access each other and the chains to grow longer.

The high monomer concentrations used resulted in high molecular weight polymers. The apparent lack of bimodality in the SEC curves implies that cyclization side reactions were kept at a minimum, or were non-existent.

NMR spectroscopic analysis

Routine NMR spectroscopic analysis of the polymers was primarily carried out in DMSO-d_6, since it has been reported that ^{1}H NMR spectra of polytriazoles, in DMSO–d_6, are very well resolved.[34] Typical ^{1}H NMR spectra for the P(*p*-AT)s **28** and **29** are shown in Figure 3.4.

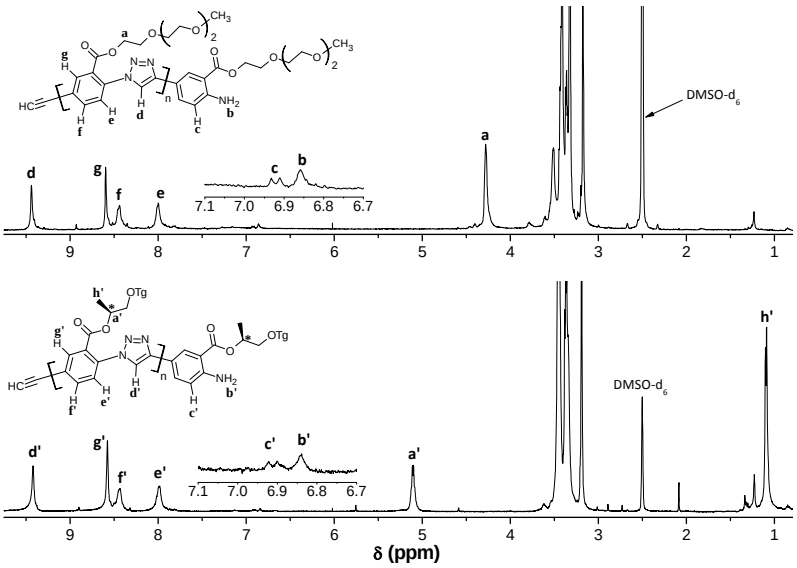

Figure 3.4: Typical ^{1}H NMR spectra in DMSO-d_6 of the P(*p*-AT)s 28 (top) and 29 (bottom).

The aromatic regions are identical as expected from the polymer structures. The triazole proton signal (d, d') appears at 9.45 ppm. It was assigned furthest downfield since it is the most de-shielded by the triazole ring. The signals e, e' and f, f' were assigned by comparing to monomer signals. The signal g, g' was assigned on the basis that it is *ortho* to an electronegative carbonyl functionality. The inserts show signals for the chain-end amine proton and the proton *ortho* to the amine functionality. These were assigned by comparing the signals of the amine functional side products **9** and **25** to those of the chain end.

Figure 3.5 shows a comparison of the ^{1}H NMR spectra of chiral P(*p*-AT)-**29** in DMSO-d_6, DMF-d_7 and in $CDCl_3$. The spectra in DMSO-d_6 and DMF-d_7 are almost identical, but the signals for the aromatic protons are shifted further downfield than in $CDCl_3$. The most significant downfield shifts are for the triazole and the chain-end amine protons, about 0.8 and 0.9 ppm respectively. This is caused by hydrogen bonding between the solvent and the respective protons. The aryl proton *meta* to the triazole ring also shifted downfield appreciably, indicating its hydrogen bonding ability. DMSO and DMF are good acceptors of localized positive charges such as hydrogen bonds.[4,35,36] This is reflected in the comparable downfield shifts of the triazole proton in DMSO-d_6 and DMF-d_7, Figure 3.5. The electropositive CH of the triazole, on the other hand, is a good hydrogen bond donor.[4,10]

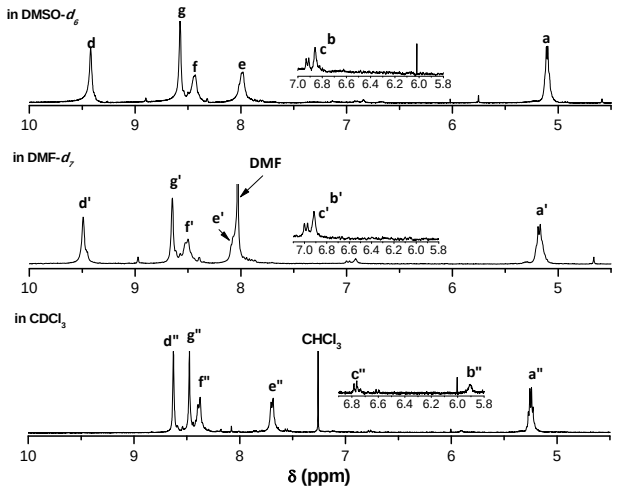

Figure 3.5: Comparisons of the ^{1}H NMR spectra of P(*p*-AT)-29 in DMSO-d_6, DMF-d_7 and in $CDCl_3$.

Variable temperature ^{1}H NMR spectroscopic analysis (VT ^{1}H NMR) of P(*p*-AT)-**29** in DMF-d_7, gave complimentary evidence to confirm the hydrogen bonding (Figure 3.6).

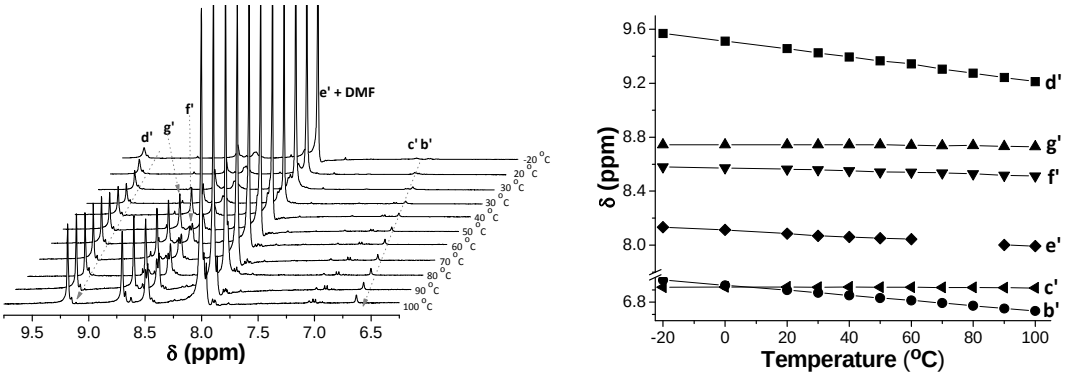

Figure 3.6: VT ^{1}H NMR of P(p-AT) in DMF-d_7. The gap between 70–80 °C for the aryl proton c' is because the signal could not be measured with certainty as it overlapped with that of the signal of the residual DMF solvent.

The chemical shifts of the triazole proton (d), the aryl proton *meta* to the triazole (e) and amine protons (b) shifted upfield most with increasing temperature, indicating a weakening of the hydrogen bond strength.

Helical folding of the P(*p*-AT)s

The folding behavior of the P(*p*-AT)s was investigated, in dilute solutions via UV-vis and CD spectroscopy. The expectation was that the amphiphilic nature of the polymers would result in

a helical folding of the polymers driven by solvophobic forces as the solvent is gradually reduced from a good solvent to a polar/bad solvent. In a good solvent, the whole molecule is equally solvated. In a bad solvent, a solvophobic environment is created around the hydrophobic heteroaromatic backbone, but selectively solvating the polar ethylene glycol side chains, forcing the P(*p*-AT) to fold into a helical conformation. The three nitrogens of the triazole moiety point out of the helix's cavity along with the polar side chains, whilst the less polar CH=C face is in the interior of the helix. The π–π stacking interactions in the helically folded conformation help to offset the considerable loss in entropy realized from undergoing the random coil to helix transition.[37] The face-centered nature of the π–π stacking also ensures a maximum reduction in the surface area of the hydrophobic aromatic surfaces exposed to the solvophobic environment.[38]

Considerations about the solvent

P(*p*-AT)s **28** and **29** dissolved completely in CH_2Cl_2, $CHCl_3$, CCl_4, HFIP, DMF, DMSO, partially dissolved in THF and acetonitrile (ACN) and sparingly dissolved in H_2O. It is likely, though, that the poor solubility in THF and ACN was due to the high M_n values of the polymers (> 25 kDa, Table 1). Small *meta*-linked oligo(aryl-triazoles) prepared by Hecht, with M_n values between 1.5 - 5 kDa were found to dissolve in ACN.[1]

In studies by Moore and co-workers on oligo *m*PE foldamers, with oEG side chains, a $CHCl_3$/ACN good solvent/bad solvent combination was used.[15] Meudtner *et al*. reported that *meta*-oligo aryl triazole foldamers, with oEG side chains displayed bisignate CD signals, in both CH_2Cl_2 and ACN, indicating that the foldamers adopted a helical backbone conformation in both apolar and polar solvents.[2] In a subsequent publication, however, it was mentioned that UV-vis spectra of the same foldamers in $CHCl_3$ and ACN did not differ substantially and significant amounts of water had to be added to induce the solvophobic folding process.[1] Another group also prepared foldamers with the same backbone appended with ionic side chains, which could be solvophobically driven into a helical conformation in aqueous solutions.[23] Increasing the strength of the solvophobic effect directly increases the stability of the helically folded conformation. In foldamers based on hydrophobic aryl backbones tethered with amphiphilic

oEG side chains, this entails increasing solvent polarity. Therefore, water will stabilize the helically folded conformation better than ACN. The solvent-dependent conformational transitions of P(*p*-AT)s **28** and **29** were therefore assessed in DMF/water as the respective good solvent/bad solvent combination. Although DMF is a polar solvent, its ability to interact, via hydrogen bonding (*vide supra*), with the apolar face of the P(*p*-AT) (Figure 3.7) makes it a good solvent capable of solvating the whole molecule equally. DMF mixes with water in all proportions therefore, the conformational transitions can be assessed as a function of solvent composition, without complications from solvent immiscibility.

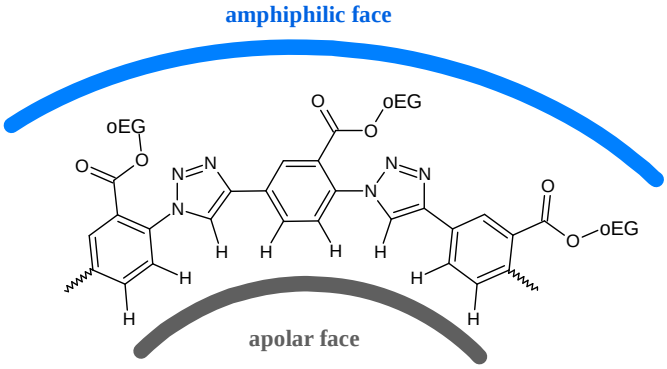

Figure 3.7: The two faces of the P(*p*-AT)s.

Conformational analysis of P(*p*-AT)-29

To establish conditions for helical folding, aqueous solutions of P(*p*-AT)-**29** were studied using UV-vis and CD spectroscopy as the primary analytical techniques. P(*p*-AT)-**29** was studied to observe solvent dependent conformational changes. Figure 3.8 depicts the UV-vis and CD spectra of P(*p*-AT)-**29** in $CHCl_3$, and in DMF. The spectra were identical with absorption maxima at 284 nm and a shoulder at ~ 310 nm. Also there was no CD activity in the UV-vis absorption region of the P(*p*-AT) backbone's π system. This is consistent with the fact that both $CHCl_3$ and DMF are good solvents which solvate the whole molecule equally and do not elicit helical ordering.

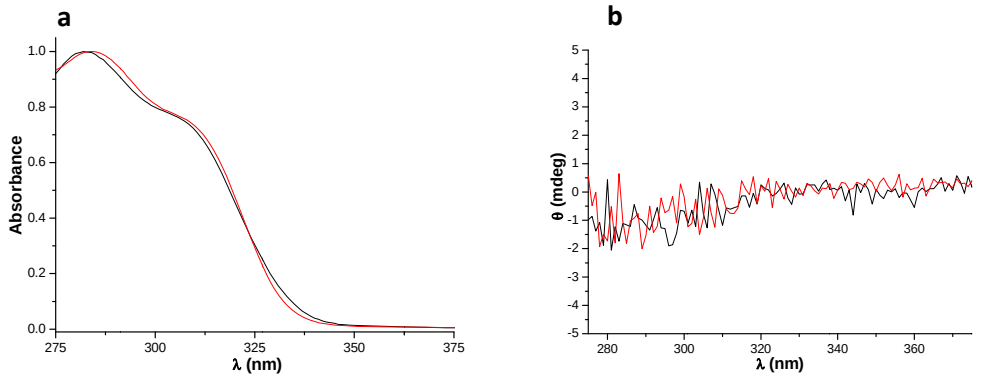

Figure 3.8: Normalized UV-vis and CD spectra of P(*p*-AT)-29 [0.9 µM] in $CHCl_3$ (black) and in DMF (red).

Next, the conformational preferences were studied in DMF/water solutions. Polymers were dissolved in DMF and the volume fraction of water was gradually increased, whilst keeping the concentration of the P(*p*-AT) and the total volume constant. The UV-vis absorption spectra were recorded (Figure 3.9a).

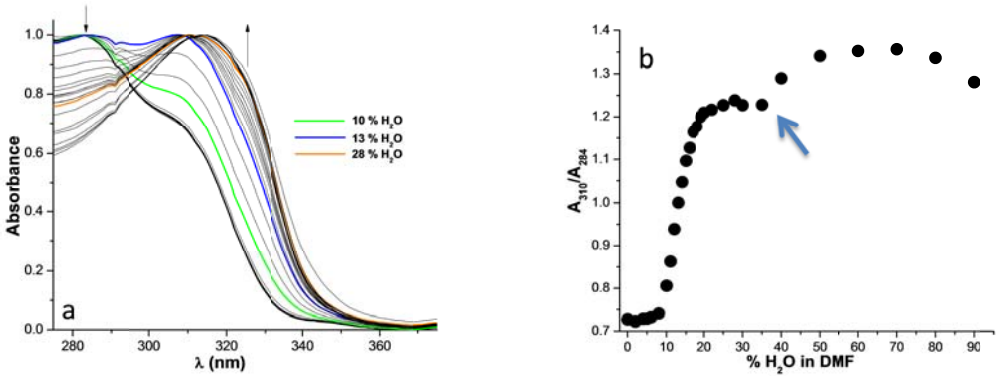

Figure 3.9: Normalized UV-vis spectra of P(*p*-AT)-29 [0.95 µM] in aqueous DMF solutions (a) and a plot of absorbance ratio (A_{310}/A_{284}) as a function of % H_2O in DMF/water. The colour coded spectra are visual guides.

Below 10% H_2O, the shape of the spectra barely changed. Upon increasing from 10 % H_2O, the shoulder peak at ~ 310 nm increased in intensity whilst the peak at 284 nm decreased. At 13 % H_2O, the peaks at 284 and 310 nm had equal intensities (blue spectrum, Figure 3.9a). With further increments in % H_2O the peak at 310 nm further amplified and became the main peak, and slightly red-shifted, whilst the peak at 284 nm attenuated. Figure 3.9b shows the plot of the absorbance ratio for the two peaks as a function of % H_2O in DMF. The absorbance ratio increased sharply after 10 % water and appeared to have levelled off after 20 % H_2O, but

increased again after 30 % H_2O (blue arrow, Figure 3.9b). This will be discussed later in this chapter.

The dramatic changes in the shape of the UV-vis spectra, with varying % H_2O were matched by the evolution of the CD spectra as a function of solvent composition (Figure 3.10). Foldamer solutions below 10 % H_2O were CD silent. A Cotton effect (CE) appeared at 10% water, in the UV-vis absorption region of the backbone's π system, growing in intensity with increasing % water, as well as evolving into a bisignate signal exhibiting negative exciton chirality. Maximum amplitude for the bisignate Cotton effect was realized at 28 % water with an intense negative couplet. This negative couplet suggested the formation of a helix with the M screw sense due to chirality transfer from the chiral side chain to the backbone.

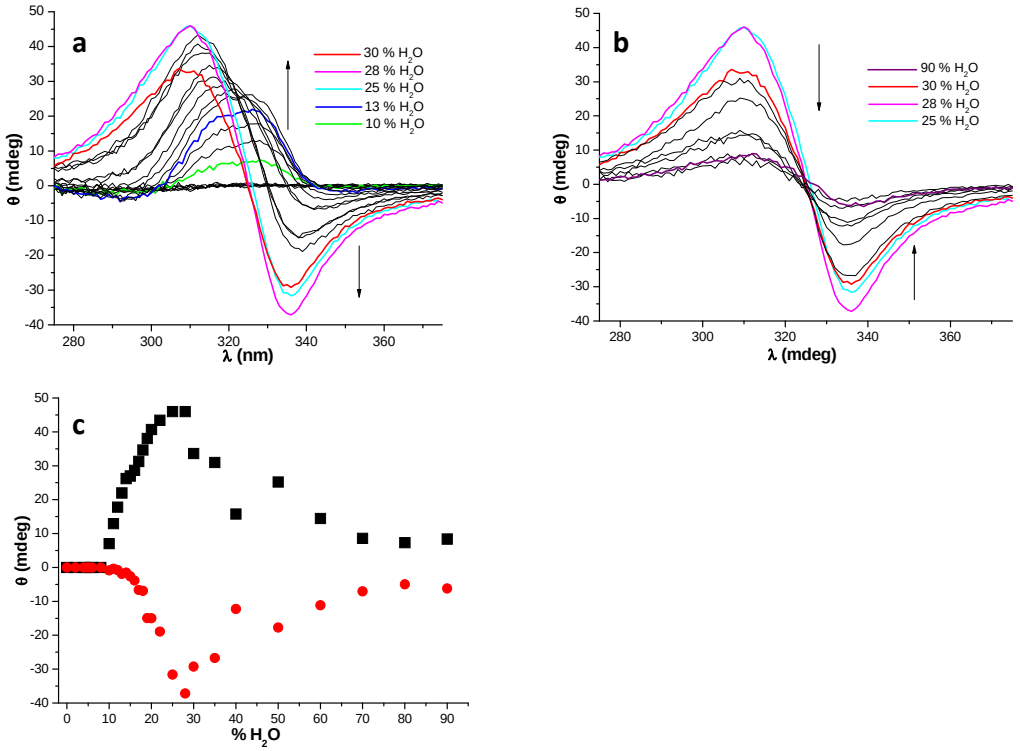

Figure 3.10: CD spectra of P(*p*-AT)-29 [0.95 µM] in aqueous DMF solutions for 0 – 30 % H_2O in DMF (a) 25 -90 % H_2O in DMF (b), the plots were split in order to improve clarity, and a plot of the positive (black) and negative (red) extrema (c). The colour-coded spectra are intended to be guides.

The intensely coupled CD had a negative extremum at 335 nm (Δε -37.3), a positive extremum at 310 nm (Δε 45.7) and a zero crossing at 324 nm. Further increasing the fraction of water

beyond 28 % resulted in a decrease in the amplitude of the Cotton Effect (Figure 3.10b). The decrease was drastic between 30 and 70 % H_2O and leveled off above 70 % water. It should be noted that above 25 % H_2O content, the overall shape of the CD spectra did not change, and neither did the position of the isodichroic point. UV-vis and CD spectroscopy report on two different structural elements, a stable helical conformation and a diastereomeric excess, respectively.[19] It is clear that the CD spectroscopic analysis faithfully reflects the solvent dependent spectral changes observed in the UV-vis spectroscopic analysis.

Analysis of the UV-vis and CD spectra reveals that below 10 % water, the shape of the UV-vis absorption spectra does not change, whilst the corresponding CD curves are silent, indicating that there is no helical ordering. The UV-vis band, at 310 nm, only starts to increase at around 10 % water and higher, matching the first appearance of CD activity. This is when the foldamer folds. The onset of a twist sense bias, monitored via the CD experiments, appears to match the coil to helix transition, monitored via the UV-vis experiments. This is contrary to the situation with *m*PE foldamers by Moore, in $CHCl_3$/ACN good/bad solvent system, where the twist sense bias as judged from CD lagged behind the coil to helix transition monitored by UV-vis.[19] The increase in the size of the CD signal from 10 % water matches with the changes in the absorption bands, *i.e*. the receding of the UV-vis absorption band at 284 nm and the increase in the band at 310 nm. The maximum amplitude of the bisignate CE is realized at 28 % water, in the region where the UV-vis absorbance ratio plot levels off (Figure 3.10b). It is apparent that the UV-vis spectrum with a maximum band at 284 nm represents the unfolded state. An increase in the volume fraction of water increases the hypochromicity of the absorption band at 284 nm, whilst the CD signal evolves into a fully bisignate signal, which is maximum at 28 % water, signifying the folded conformation. The UV-vis signature for a helically folded structure is when the absorption band at 310 nm is a maximum. The absorbance spectra at 13 % water, where the two absorption bands at 284 and 310 nm have equal intensities (Figure 3.10b) apparently reflects a solvent regime where the folded and unfolded conformations are in equilibrium. In the same way, the weak Cotton effects, *e.g*. the one for 13 % water, represent solutions in which the folded conformation is in equilibrium with the random coil. The reason

behind the deviating shape of the weak Cotton effects is not known and was not investigated further in this work.

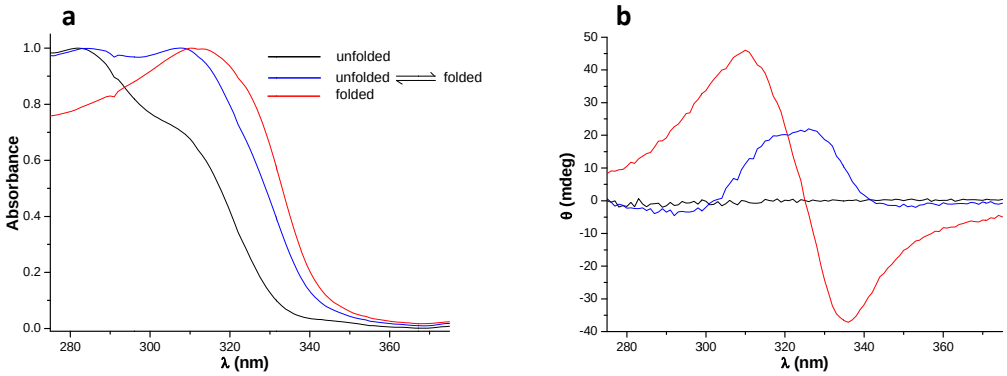

Figure 3.11: Comparison of UV-vis scpectra (a) and the complimentary CD spectra (b) with the spectroscopic signatures for the coil to helix transition.

The increase in the absorbance ratio from 30 % water in DMF is matched by the decrease in the amplitude of the CD signals (Figures 3.9b and 3.10c). The increase in the absorbance ratio is due to increased hypochromicity in the absorption band at 284 nm, implying a further stabilization of the helical conformation. Solvophobic driving forces instigate helical folding and the folded conformation is stabilized via π – π stacking interactions. The increased hypochromicity beyond 30 % water, however, means an increased stabilization of already folded P(p-AT)-**29**. The extra stabilization, therefore can be attributed to the stacking of the helices into columnar architectures.[39] Therefore, it appears that the coil to helix transition is complete at 28 % water, when the negative couplet has its maximum amplitude. The further increase in the absorbance ratio, from 30 % water, probably indicates the onset of the formation of higher order structures as illustrated in Scheme 3.6. The presumed formation of higher order structures in the solution state, as a function of solvent composition is investigated further in Chapter 4.

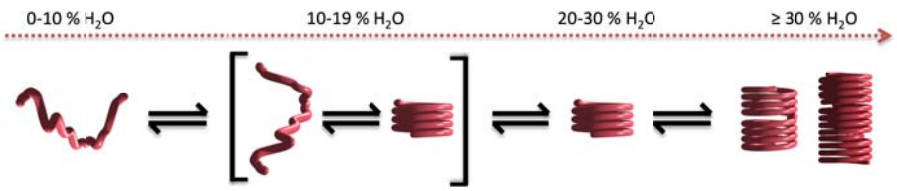

Scheme 3.6: Hypothesized folding and self-assembly of P(*p*-AT)-29 into columnar architectures.

As mentioned earlier, Figures 3.10b and c show that the amplitude of the negative couplet receded with increasing volume fraction of water beyond 30 %. The isodichroic point, however, was not lost and the overall shape of the couplet did not change. This is probably because the screw sense is maintained in the columnar architectures and the columns architectures are perhaps not interacting laterally. Hence, the stacked helices are essentially similar folded architectures to the stable single helices, albeit longer due to the stacking. The cause of decrease in the amplitude of the negative couplet, albeit without losing the isodichroic point was not investigated further in this work.

Conformational analysis of P(*p*-AT)-28

Similar solvent-dependent conformational transitions were detected in the solvent titration of P(*p*-AT)-**28** (Figure 3.12), albeit with some differences over the % H_2O at which the coil to helix transition took place. Figure 3.12b shows that helical folding began from just 2 % water.

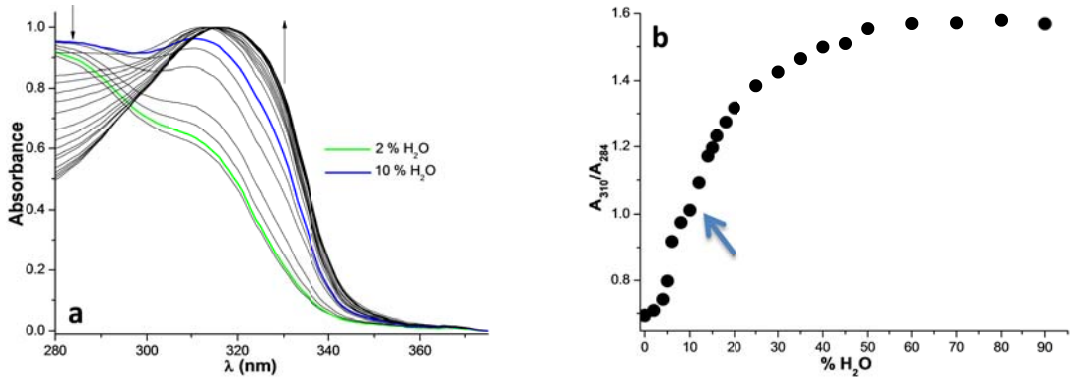

Figure 3.12: Normalized UV-vis spectra of P(p-AT)-28 [0.74 µM] in aqueous DMF solutions (a) and a plot of absorbance ratio (A_{310}/A_{284}) as a function of % H_2O in aqueous DMF. The colour coded spectra are visual guides.

The UV-vis absorption spectra in which the two bands at 284 and 310 nm had equal amplitudes was produced with 10 % water. This curve is the spectroscopic signature for the transition mid-point, *vide supra*. These results imply that P(*p*-AT)-**28** requires less water, *i.e*. less solvophobic driving force, than P(*p*-AT)-**29** to fold, since that latter foldamer required 13 % water in DMF to reach this point. This is probably an effect of the side chains, P(*p*-AT)-**29** has four ethylene glycol (EG) repeat units in its side chain compared to three in P(*p*-AT)-**28**. The two side chains do not

strictly represent a homologous series, since that of P(*p*-AT)-**29** also has an extra methyl group appended to it (Figure 3.3). It is apparent, however, that the extra EG repeat unit elicits the need for a stronger solvophobic force, *i.e.* higher % water in DMF, to induce helical folding.

More striking is the onset of the increase in the absorbance ratio for P(*p*-AT)-**28** (Figure 3.12b), which is proposed to signal the onset of the self-assembly of the helices. The absorbance ratio starts to increase after 10 % H_2O, which is the mid-point of the coil to helix transition. This increase is attributed to an increase in hypochromicity of the band at 284 nm implying a greater than expected stabilization of the folded state conformation, due to the formation of supramolecular stacks. These results suggest that with P(*p*-AT)-**28** stacking begins once helical structures are formed (Scheme 3.7) in contrast with P(p-AT)-**29** whereby stacking only begins after stable individual helices are formed.

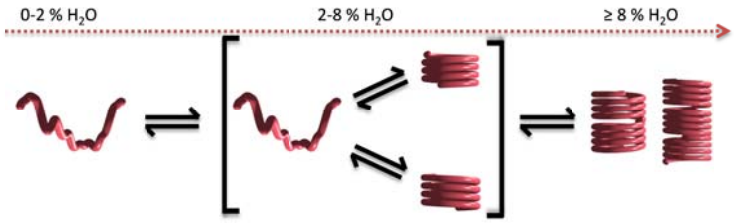

Scheme 3.7: Hypothesized folding and self-assembly of P(*p*-AT)-28 into columnar architectures.

TEM analysis

To obtain visual evidence of the formation of the higher order structures, conventional TEM analysis was carried out on P(*p*-AT)-**29,** on samples prepared from 28 %, 50 % and 80 % H_2O in DMF (Figure 3.13). For samples from 25 % H_2O, no discernible morphologies were seen. Samples prepared from 50 % H_2O revealed a threaded mesh architecture, however, no defined architectures were seen. With samples prepared from 80 % H_2O, fibers with lengths > 100 nm, could be clearly observed. The fibers are probably composed of columnar stacks of helical foldamers. The columns assemble to give bundles and in some parts wrap around each other (Figure 3.13f). CD analysis ruled out the possibility of lateral interaction amongst columns. The bundling up of the helical columns observed in Figure 3.13 is probably due to drying in effects during sample preparation.

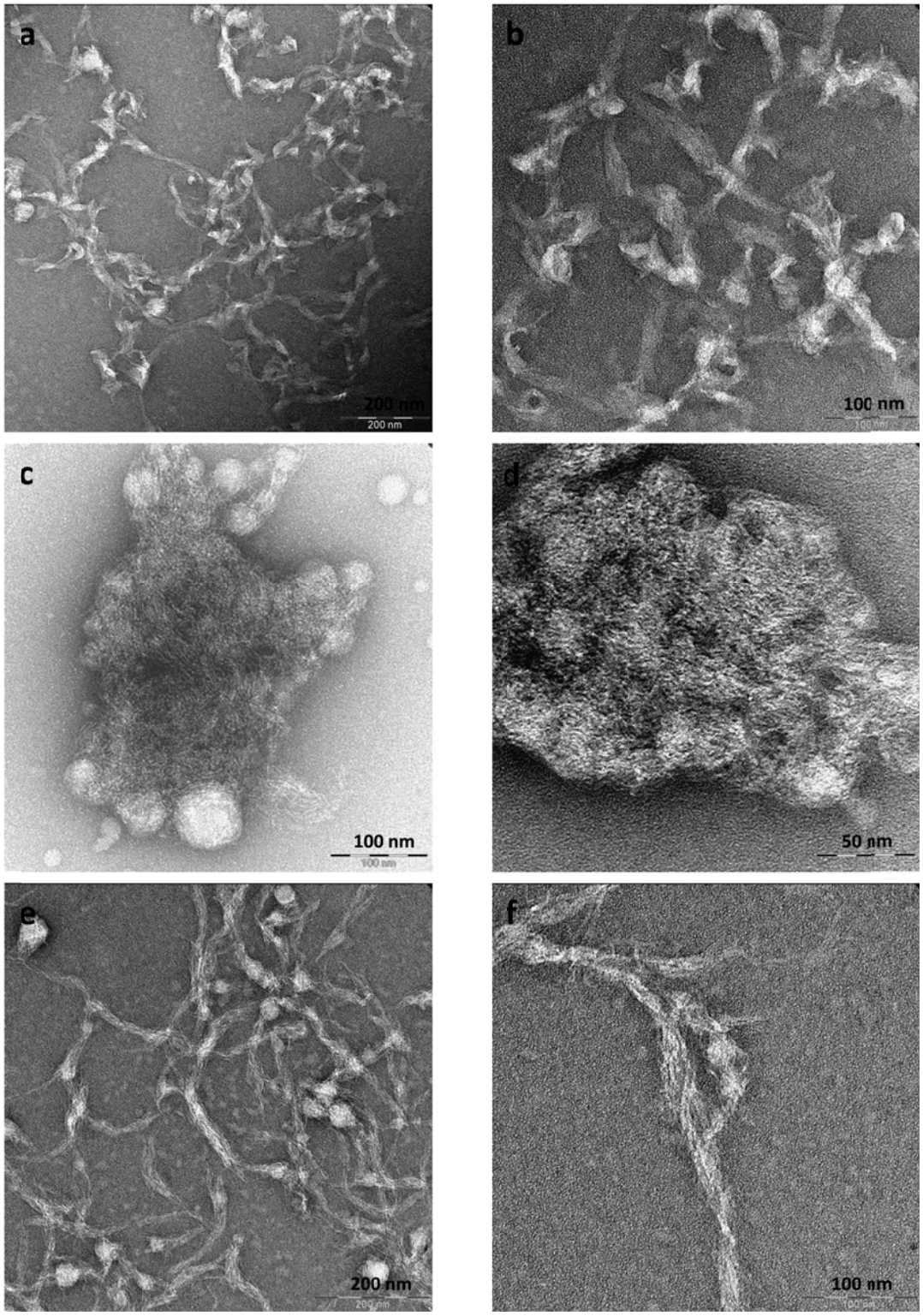

Figure 3.13: TEM images of P(*p*-AT)-29 prepared from 28 % H_2O (A, B), 50 % H_2O (C, D) and from 80 % H_2O in DMF (E, F).

Although the foldamer in 28 % water gave the highest amplitude for the bisignate Cotton effect, this solvent composition is not solvophobic enough to drive the formation of higher order structures. The images from samples prepared from 50 % H_2O were also inconclusive, the "string architectures" observed appear to indicate some form of higher order structure, but unlike the 80 % H_2O sample in which supramolecular stacks are seen, the solvophobic driving force is not strong enough to stabilise defined assemblies. The TEM samples were air dried before images were acquired. It is likely, therefore, that an uncertainty in the evaporation rates of the two solvents (DMF and water) during air drying, under an uncontrolled environment, could have resulted in water evaporating faster than DMF. This possibility would then result in the foldamer samples being exposed to an environment higher in DMF concentration, i.e. more denaturing environment. With increasing volume fraction of water in the samples, however, denaturing gets progressively less hence defined structures were observed in 80 % water.

Conclusion

A novel P(*p*-AT) foldamer system was developed. Facile synthetic protocols for the foldamer monomers were developed. A true polymer science approach to foldamer synthesis was used which enabled access to high molecular weight polytriazoles, via an AB-step growth polymerization strategy. The conformational preferences of the foldamers could be controlled by adjusting the volume fraction of water (a bad solvent) in DMF (a good solvent) and could be tracked by a combination of UV-vis and CD spectroscopy. CD spectroscopic analysis was possible by the addition of an enantiopure chiral side chain to the aryltriazole backbone, which biased the screw sense of the helix. Careful analysis of UV-vis and CD signals allowed a hierarchical self-assembly pathway to be proposed. A clear spectroscopic signature marking the onset of the self-assembly of the helices was observed and it should serve as a useful indicator for tracking the hierarchical information transfer process. The length of the side chain was shown to influence the sequence of the self-assembly protocols, polytriazole foldamers with triethylene glycol side chains began to assemble immediately after reaching equilibrium between the random coil and the helically folded conformations. The foldamers with a tetraethylene glycol side chains, however, first formed stable helices which further stacked with increasing solvophobic driving force. Finally, columns of helical stacks were visualized using TEM, upon driving the solvent system to 80 % water, giving visual evidence of the formation of higher order structures.

Experimental

General details

All chemicals and solvents used were purchased from commercial sources and used without further purification unless stated otherwise. All solvents were dried and distilled before use. Air and moisture sensitive reactions were carried out under either a nitrogen or an argon atmosphere, using standard Schlenk techniques. TLC plates (0.20 mm Silica gel 60, with fluorescent indicator UV254) and Silica gel 60 (0.063 - 0.2 mm/70 - 230 mesh) were purchased from Machery-Nagel. SnakeSkin® Pleated dialysis tubing, MW cutoff 10 000, was purchased from Thermoscientific. ^{1}H and ^{13}C NMR spectra were recorded on a Varian VXR 400 MHz instrument. NMR samples were prepared in deuterated solvents obtained from Cambridge Isotope labs. Proton and carbon chemical shifts are reported in parts per million (ppm) (δ) downfield from tetramethylsilane (TMS) using residual solvent protons as internal standards. Coupling constants (J) are reported in Hertz (Hz) and splitting patterns are designated as s (singlet), d (doublet), t (triplet), q (quartet), bs (broad singlet), m (multiplet). Mass spec was performed on a Waters GCT Premier or a Waters API Quattro Micro instrument. Size exclusion chromatography (SEC) was measured on a system equipped with a Waters 1515 Isocratic HPLC pump, a Waters 2414 refractive index detector (40 °C), a Waters 2707 autosampler, a PSS PFG guard column followed by 2 PFG-linear-XL (7 µm, 8*300 mm) columns in series at 40 °C. Hexafluoroisopropanol (HFIP, Biosolve) with potassium trifluoro acetate (3 g/L) was used as eluent at a flow rate of 0.8 mL min^{-1}. The molecular weights were calculated against poly(methyl methacrylate) standards (Polymer Laboratories, M_p = 580 Da up to M_p = $7.1*10^6$ Da). TEM samples [1.11 µM] (3 µL) samples were pipetted on to carbon coated 200 mesh copper grids and stained with 2 % aqueous uranyl acetate. The samples were air dried and then viewed using a LEO 912 Omega TEM (Zeiss, Oberkochen, Germany) at 120 kV. Images were collected using a Proscan CCD camera. UV-vis spectroscopy measurements were carried out on a Perkin Elmer Lambda 20 photodiode array spectrophotometer in 1 cm quartz cuvettes. Samples were in the µM concentration range. CD spectroscopy measurements were made on a Jasco J-815 instrument, in 1 cm quartz cuvettes. UV and CD spectroscopy titrations samples were prepared volumetrically, by mixing a fixed volume of P(*p*-AT), from the same stock solution, with the appropriate volume of water and/or DMF up to a constant total volume. UV-vis and CD spectroscopy experiments were carried out at 22 ^{o}C, unless stated otherwise.

Synthetic procedures

2-azido-5-iodobenzoic acid (6): This compound was prepared exactly as described in literature.[40] ^{1}H NMR (400 MHz, $CDCl_3$) δ: 8.40 (d, *J* = 2.2 Hz, 1H), 7.88 (dd, *J* = 8.5, 2.2 Hz, 1H), 7.02 (d, *J* = 8.5 Hz, 1H). 13C NMR (400MHz, $CDCl_3$) δ: 167.48, 143.12, 141.83, 140.40, 122.56, 121.61, 87.90. MS (ESI): *m/z* = 290.0 (calcd 289.94 for $[M + H]^+$), 307.0 (calculated: 306.97 for $[M + NH_4]^+$).

2-[2-(2-methoxyethoxy)ethoxy]ethyl 2-azido-5-iodobenzoate (7): To a 100 mL round bottom flask was added 2-azido-5-iodobenzoic acid (6,1.11 g, 3.83 mmol), dry distilled CH_2Cl_2 (50 mL), triethylethylene glycol mono methyl ether (0.69 g, 4.21 mmol) and DMAP (0.05 g, 0.42 mmol). The mixture was cooled to 0 ^{o}C in a sodium chloride/ice bath. DCC (0.87 g, 4.21 mmol) was then added in one portion and the reaction ran for an hour at 0 °C, before being allowed to run at room temperature for 16 h. Afterwards the reaction mixture was chilled, the white precipitate (dicyclohexylurea side product) filtered off and the product was then purified by column chromatography (pentane : EtOAC = 2:1, R.F. = 0.53) to yield **7** as a very viscous pale yellow liquid (1.38 g, 82.5 %). ^{1}H NMR (400 MHz, $CDCl_3$) δ: 8.14 (d, *J* = 2.1 Hz, 1H), 7.78 (dd, *J* = 8.5, 2.1 Hz, 1H), 6.97 (d, *J* = 8.5 Hz, 1H), 4.47 – 4.42 (m, 2H), 3.82 – 3.79 (m, 2H), 3.72 – 3.61 (m, 6H), 3.55 – 3.51 (m, 2H), 3.35 (s, 3H). ^{13}C NMR (400 MHz, $CDCl_3$) δ: 163.67, 141.87, 140.39, 140.07, 124.29, 121.76, 87.38, 71.96, 70.66, 70.62, 68.98, 64.67, 59.07. MS (ESI): *m/z* = 453.2 (calculated 453.06 for $[M + NH_4]^+$), 458.1 (calculated 458. 02 for $[M + Na]^+$), 474.2 (calculated: 473.99 for $[M + K]^+$).

2-[2-(2-methoxyethoxy)ethoxy]ethyl 2-azido-5-[(trimethylsilyl)ethynyl]benzoate (8): A typical procedure is described. A 50 mL Schlenk flask was charged with the aryl iodide (**7**) (1.2 g, 2.76 mmol), trimethylsilyl acetylene (0.30 g, 3.03 mmol), THF (5 mL) and TEA (5 mL) and the mixture was subjected to two freeze-pump-thaw cycles and backfilled with nitrogen each time. The mixture was then frozen again and the flask filled with nitrogen. The flask was opened and $Pd(PPh_3)_4$ (0.032 g, 0.027 mmol) and CuI (0.005 g, 0.027 mmol) were quickly added, the flask was immediately sealed and evacuated before being subjected to three freeze-pump-thaw cycles and backfilled with nitrogen. The flask was then immersed into an oil bath preheated to 30 °C to mark the start of the reaction. A clear yellow solution resulted and a white precipitate started forming after ~ 5 – 10 minutes. The color of the reaction abruptly changed from yellow to orange/brown after about 30 minutes. TLC analysis (pentane/ethyl acetate = 2:1) showed two news spots R.F. = ~0.5 and ~0.3. The reaction was stopped by opening to air and adding ethyl acetate. The crystalline white precipitate (triethylamine hydrobromide) was filtered off. The filtrate was mixed with aqueous sodium bicarbonate. The product was extracted into ethyl

acetate, the extracts combined, dried with Na_2SO_4 anhydrous and concentrated and purified by column chromatography (pentane/ethyl acetate = 2:1). The first fraction (R.F. = 0.5) (0.94 g, 84 %) was determined by NMR to be the requisite azide **8**: ^{1}H NMR (400 MHz, $CDCl_3$) δ: 7.96 (d, *J* = 2.0 Hz, 1H), 7.58 (dd, *J* = 8.4, 2.0 Hz, 1H), 7.16 (d, *J* = 8.4 Hz, 1H), 4.47 – 4.45 (m, 2H), 3.87 – 3.79 (m, 2H), 3.74 – 3.62 (m, 6H), 3.55 – 3.53 (m, 2H), 3.37 (s, 3H), 0.25 (s, 9H). ^{13}C NMR (400 MHz, $CDCl_3$) δ: 164.51, 140.16, 136.41, 135.58, 122.62, 119.95, 119.73, 103.23, 72.08, 70.79, 69.17, 64.62, 59.19, 0.01. MS (ESI): *m/z* = 423.3 (calcd 423.21 for $[M + NH_4]^+$]), 812.0 (calculated: 811.35 for $[2M + H]^+$).

The second fraction (R.F. = 0.3) (0.06 g) was determined by NMRspectroscopy to be an aromatic amine side product **9**, produced by reduction of the azide product, by PPh_3. ^{1}H NMR (400 MHz, $CDCl_3$) δ: 8.02 (d, *J* = 2.0 Hz, 1H), 7.33 (dd, *J* = 8.5, 2.0 Hz, 1H), 6.56 (d, *J* = 8.6 Hz, 1H), 5.91 (bs, 2H), 4.45 – 4.40 (m, 2H), 3.85 – 3.79 (m, 2H), 3.74 – 3.62 (m, 7H), 3.57 – 3.52 (m, 2H), 3.37 (s, 3H), 0.23 (s, 9H). ^{13}C NMR (400 MHz, $CDCl_3$) δ: 167.43, 150.51, 137.46, 135.80, 116.67, 110.62, 110.52, 105.30, 91.63, 72.10, 70.81, 70.79, 70.72, 69.26, 63.70, 59.14, 0.25. MS (ESI): *m/z* = 380.2 (calculated: 380.19 for $[M + H]^+$).

2-[2-(2-methoxyethoxy)ethoxy]ethyl 2-azido-5-[(trimethylsilyl)ethynyl]benzoate (8): A 50 mL round bottomed flask was charged with **9** (0.06 g, 0.16 mmol) and THF (2 mL). The mixture was cooled to 0 °C in a sodium chloride/ice bath and *t*-$BuNO_2$ (0.08 g, 0.79 mmol) was added dropwise and the mixture stirred for 5 minutes. TMS-N_3 (0.036 g, 0.32 mmol) was then added, dropwise, mixture stirred at 0 °C for 30 min and at room temperature for 2 h. Progress of reaction was followed by TLC (pentane/ethyl acetate = 2:1). Afterwards, the reaction mixture was concentrated and the product purified by column chromatography (pentane/ethyl acetate = 2:1) affording the azide **8** (0.058 g, 91 %) of **8** as a pale yellow viscous oil. ^{1}H NMR (400 MHz, $CDCl_3$) δ: 7.96 (d, *J* = 2.0 Hz, 1H), 7.58 (dd, *J* = 8.4, 2.0 Hz, 1H), 7.16 (d, *J* = 8.4 Hz, 1H), 4.47 – 4.45 (m, 2H), 3.86 – 3.79 (m, 2H), 3.75 – 3.61 (m, 6H), 3.55 – 3.53 (m, 2H), 3.37 (s, 3H), 0.25 (s, 9H). ^{13}C NMR (400 MHz, $CDCl_3$) δ: 164.51, 140.16, 136.41, 135.58, 122.62, 119.95, 119.73, 103.23, 95.93, 72.08, 70.80, 70.78, 70.76, 69.17, 64.62, 59.19, 0.01.

2-[2-(2-methoxyethoxy)ethoxy]ethyl 2-azido-5-ethynylbenzoate (3): TMS protected aryl alkyne **8** (0.45 g, 1.11 mmol) was dissolved in THF (20 mL), in a 50 mL round bottomed flask and TBAF.$3H_2O$ (0.64 g, 2.01 mmol) added. The reaction was ran for one minute and filtered through a short silica gel plug, concentrated and purified by column chromatography (pentane/ethyl acetate = 2:1, R.F. = 0.3) yielding **3** (0.33 g, 89%) as a pale yellow/colorless oil, which solidified in the freezer overnight and melted at room temperature. ^{1}H NMR (400 MHz, $CDCl_3$) δ: 7.98 (d, *J* = 2.0 Hz, 1H), 7.60 (dd, *J* = 8.4, 2.0 Hz, 1H), 7.17 (d, *J*

= 8.4 Hz, 1H), 4.49 – 4.41 (m, 2H), 3.85 – 3.77 (m, 2H), 3.74 – 3.60 (m, 6H), 3.56 – 3.49 (m, 2H), 3.35 (s, 3H), 3.11 (s, 1H). ^{13}C NMR (400 MHz, $CDCl_3$) δ: 164.35, 140.56, 136.54, 135.71, 122.70, 120.06, 118.60, 81.97, 78.57, 72.04, 70.77, 70.74, 70.71, 69.10, 64.65, 59.13. MS (ESI): *m/z* = 351.2 (calculated 351.2 for $[M + NH_4]^+$]), 667.6 (calculated: 666.2 for $[2M + H]^+$).

Methyl (2*S*)-2-(tetrahydro-2*H*-pyran-2-yloxy)propanoate (12): A solution of methyl (*S*)-lactate (**10**) (10 g, 96 mmol) and 3,4-dihydro-2*H*-pyran (**11**) (13.16 g, 156 mmol) was cooled to 0 °C and 3 drops of concentrated HCl added. The mixture was stirred for 10 h, reaching room temperature on its own accord. Na_2CO_3 (3 g) was added and the stirring was continued for a further 10 h. After that, the reaction mixture was filtered, concentrated and the product was purified by distillation (69 - 76 °C at 39 hPa) yielding the tetrahydropyranyl ether **12** (14.2 g, 78 %) as a colorless oil, as a mixture of diastereomers. ^{1}H NMR (400 MHz, $CDCl_3$) δ: δ 4.69–4.65 (m, 2H), 4.40 (q, *J* = 7.0 Hz, 1H), 4.19 (q, *J* = 6.8 Hz, 1H), 3.94 – 3.74 (m, 2H), 3.711 (s, 3H), 3.707 (s, 3H), 3.54 – 3.38 (m, 2H), 1.91 – 1.46 (m, 12H), 1.43 (d, *J* = 6.9 Hz, 3H), 1.37 (d, *J* = 6.9 Hz, 3H).). ^{13}C NMR (400MHz, $CDCl_3$) δ: 173.92, 173.81, 98.41, 97.73, 72.49, 70.07, 62.57, 62.55, 52.02, 52.00, 30.57, 30.48, 25.47, 25.36, 19.31, 19.27, 18.92, 18.12. MS (ESI): *m/z* = 189.2 (calculated 189.1 for $[M + H]^+$, 206.1 (calculated: 206.1 for $[M + NH_4]^+$).

(2*S*)-2-(tetrahydro-2*H*-pyran-2-yloxy)propan-1-ol (13): A solution of **12** (20 g, 106,2 mmol) in Et_2O (50 mL) was added to a suspension of $LiAlH_4$ (4.96 g, 131 mmol) in Et_2O (50 mL), at 0 °C, under a nitrogen atmosphere over 8 h. Afterwards, the reaction was ran for 12 h at room temperature and refluxed for 5 h. The reaction was quenched by adding, in succession, ethyl acetate (4 g), 10 % NaOH (aq) and water (40 mL). The white granular precipitate was filtered off and the filtrate concentrated. The crude product was purified by distillation (60 – 65 ^{o}C at 40 hPa) to obtain the pure alcohol (**13**) (14.2 g, 83.4%), as a mixture of diastereomers. ^{1}H NMR (400 MHz, $CDCl_3$) δ: 4.70 (dd, *J* = 5.1, 2.7 Hz, 1H), 4.52 (dd, *J* = 6.3, 2.6 Hz, 1H), 4.01 – 3.72 (m, 4H), 3.69 – 3.37 (m, 6H), 1.87 – 1.64 (m, 5H), 1.61 – 1.43 (m, 8H), 1.18 (d, *J* = 6.4 Hz, 3H), 1.10 (d, *J* = 6.5 Hz, 3H). ^{13}C NMR (400 MHz, $CDCl_3$) δ: δ 99.99, 99.14, 77.75, 74.96, 67.27, 66.25, 64.64, 63.24, 31.67, 31.17, 25.44, 25.18, 21.00, 20.14, 17.81, 17.29. MS (ESI): *m/z* = 161.1 (calculated 161.1 for $[M + H]^+$]), 183.1 (calculated: 183.1 for $[M + Na]^+$).

2-[2-(2-methoxy-ethoxy)-ethoxy]-ethyl p-tosylate (15): This compound was prepared exactly as reported in literature.[41] ^{1}H NMR (400 MHz, $CDCl_3$) δ: 7.78 (d, *J* = 8.3 Hz, 2H), 7.33 (d, *J* = 7.9 Hz, 2H), 4.16 – 4.13 (m, 2H), 3.69 – 3.66 (m, 2H), 3.61 – 3.56 (m, 6H), 3.53 – 3.50 (m, 2H), 3.35 (s, 3H) 2.43 (s, 3H). ^{13}C NMR (400 MHz, $CDCl_3$) δ: 144.89, 133.12, 129.91, 128.07, 72.00, 70.84, 70.66, 70.64, 69.34, 68.77,

59.13, 21.74. MS (ESI): *m/z* = 319.3 (calculated 319.1 for $[M + H]^+$]), 336.3 (calculated: 336.1 for $[M + NH_4]^+$).

(13*S*)-2,5,8,11-tetraoxatetradecan-13-ol (17): The procedure was adapted from literature.[42] NaH (60 %) (2.12 g, 52.9 mmol of NaH component) was added to a solution of compounds **13** (the THP protected) (3.0 g, 18.7 mmol) and **15** (the tosylated alcohol) (6.72 g, 21 mol) in THF (100 mL). The mixture was refluxed for 12 h. Afterwards the reaction was cooled and quenched by adding water. The THF was evaporated and the product was extracted into CH_2Cl_2 (3 x 50 mL). The organic layer was washed with brine, dried over Na_2SO_4 (anhydrous) and the product was concentrated. The solution of the crude product (**16**) in MeOH (50 mL) was cooled to 0 °C and $TsOH.H_20$ (0.6 g, 3.18 mmol) was added. The mixture was allowed to warm to room temperature and the reaction stirred for 4 h. The reaction was quenched by adding aqueous $NaHCO_3$ and brine (100 mL) successively. Then the product was extracted into CH_2Cl_2 (3 x 50 mL). The organic layer was dried over Na_2SO_4 (anhydrous) and concentrated. The product (**17**) was purified by column chromatography (pentane : EtOAc = 2:1 to 1:1; R.F. = 0.4 in pentane :E tOAc = 1:1) yielding 3.3 g (80 %) as a colorless oil. (Mosher ester: > 94 % *ee* ^{19}F NMR, Scheme 3.3 Figure 3.3) ^{1}H NMR (400 MHz, $CDCl_3$) δ: δ 3.99 – 3.90 (m, 1H), 3.69 – 3.61 (m, 10H), 3.55 – 3.51 (m, 2H), 3.47 (dd, *J* = 9.9, 3.0 Hz, 1H) 3.36 (s, 3H), 3.24 (dd, *J* = 9.9, 8.4 Hz, 1H), 2.90 (s, 1H), 1.10 (d, *J* = 6.4 Hz, 3H). ^{13}C NMR (400MHz, $CDCl_3$) δ: 77.18, 71.97, 70.61, 70.60, 70.52, 70.51, 66.30, 59.06, 18.55. MS (ESI): *m/z* = 223.2 (calculated 223.1 for $[M + H]^+$]), 245.2 (calculated: 245.1 for $[M + Na]^+$).

Synthesis of Mosher ester:[27] To a solution of the chiral alcohol (**19**) (30 mg, 0.135 mmol) in dry CH_2Cl_2 and dry pyridine (0.75 mL of each) was added (S-(+)-MTPA-Cl) and the reaction ran for 40 h. Afterwards, the mixture was diluted with CH_2Cl_2 (7 mL), washed with 2 N HCl (2 x ~ 1mL), saturated $NaHCO_3$ aq. (2 x 1 mL), water (2 x 1 mL) and dried over Na_2SO_4 anhydrous. The solvent was evaporated and the crude product further dried with a vacuum pump overnight.

(S)-1-{2-[2-(2-methoxyethoxy)ethoxy]ethoxy}propan-2-yl 2-azido-5-iodobenzoate (23): 2-azido-5-iodobenzoic acid (**6**) (1.5 g, 5.19 mmol) was dissolved in $SOCl_2$ (60 mL) and the mixture was refluxed for 3 h. Excess $SOCl_2$ was removed *in vacuo* and the product was further dried under vacuum overnight yielding crude 2-azido-5-iodobenzoyl chloride (**22**) (1.5, 93 %) as an orange-red solid, which was used without further purification. Crude **22** (1.4 g, 4.6 mmol) was added to a solution of **17** (chiral alcohol) (1.27 g, 5.7 mmol), TEA (0.63 g, 6.27 mmol), DMAP (7.7 mg, 0.063 mmol) in CH_2Cl_2 (20 mL) at 0 °C. The mixture was stirred for 18 h, warming to room temperature on its own accord. Afterwards the organic

layer was washed with brine (2 x 20 mL) and saturated NH_4Cl (aq.) solution (2 x 20 mL) successively and concentrated. The product was purified by column chromatography (Pentane : EtOAc = 1:1; R.F. = 0.4) yielding the product **23** (1.96 g, 76.3 %, based on compound **6**) as a pale yellow oil. ^{1}H NMR (400 MHz, $CDCl_3$) δ: 8.08 (d, *J* = 2.1 Hz, 1H), 7.76 (dd, *J* = 8.5, 2.1 Hz, 1H), 6.95 (d, *J* = 8.5 Hz, 1H), 5.32 – 5.23 (m, 1H), 3.73 – 3.57 (m, 12H), 3.55 – 3.51 (m, 2H) 3.35 (s, 3H), 1.33 (d, *J* = 6.5 Hz, 3H). ^{13}C NMR (400MHz, $CDCl_3$) δ: 163.33, 141.72, 140.25, 140.00, 124.93, 121.79, 87.44, 77.16, 73.58, 72.00, 70.98, 70.83, 70.72, 70.69, 70.58, 59.09, 16.73. MS (ESI): *m/z* = 511.2 (calculated 511.1 for $[M + NH_4]^+$]), 516.2 (calculated: 516.1 for $[M + Na]^+$).

(S)-1-{2-[2-(2-methoxyethoxy)ethoxy]ethoxy}propan-2-yl 2-azido-5-[2-(triethylsilyl)ethynyl]benzoate (24): The synthesis of **24** followed the same procedure as for compound **8**; using **23** (1.37 g; 2.78 mmol), triethylsilyl acetylene (0.48 g, 3.4 mmol), $Pd(PPh_3)_4$ (0.036 g, 0.031 mmol) and CuI (0.0059 g, 0.031 mmol). Similarly to the synthesis of **8**, the color of the reaction changed abruptly after about 30 min. TLC analysis (pentane : ethyl acetate = 2:1, R.F. = 0.43 for azido derivative and 0.24 for amine side product) showed complete consumption of starting azido aryl iodide (**23**). The reaction was worked up as described for **8** and purified by column chromatography (pentane : ethyl acetate = 2:1) affording 1.21 g (2.39 mmol, 86 %) of the requisite compound **24** and 0.07 g of the amine side product which was converted into the azide as described below. Spectral data for **24** (aryl azide): ^{1}H NMR (400 MHz, $CDCl_3$) δ: 7.89 (d, *J* = 2.0 Hz, 1H), 7.57 (dd, *J* = 8.4, 2.0 Hz, 1H), 7.14 (d, *J* = 8.4 Hz, 1H), 5.36 – 5.24 (m, 1H), 3.73 – 3.57 (m, 12H), 3.54 – 3.50 (m, 2H), 3.36 (s, 3H), 1.35 (d, *J* = 6.5 Hz, 3H), 1.03 (t, *J* = 7.9 Hz, 9H), 0.67 (q, *J* = 7.9 Hz, 6H). ^{13}C NMR (400MHz, $CDCl_3$) δ: 164.17, 139.88, 136.38, 135.29, 123.20, 119.87, 104.90, 104.50, 93.42, 73.68, 72.05, 70.89, 70.83, 70.77, 70.76, 70.74, 70.63, 59.13, 16.81, 7.60, 4.46. MS (ESI): *m/z* = 523.4 (calculated 523.3 for $[M + NH_4]^+$]), 524.4 (calculated: 524.3 for $[M + H_3O]^+$).

Spectral data for **25** (aryl amine side product): ^{1}H NMR (400 MHz, $CDCl_3$) δ: 7.97 (d, *J* = 2.0 Hz, 1H), 7.33 (dd, *J* = 8.5, 2.0 Hz, 1H), 6.56 (d, *J* = 8.5 Hz, 1H), 5.92 (bs, 2H), 5.35 – 5.22 (m, 1H), 3.72 – 3.57 (m, 12H), 3.55 – 3.50 (m, 2H), 3.36 (s, 3H), 1.34 (d, *J* = 6.4 Hz, 3H), 1.03 (t, *J* = 7.9 Hz, 9H), 0.66 (q, *J* = 7.9 Hz, 6H). MS (ESI): *m/z* = 480.4 (calculated 480.3 for $[M + H]^+$]), 481.3 (calculated: 481.3 for $[M + 2H]^+$).

Conversion of aryl amine side product 25 into aryl azide 24: The synthesis followed the same procedure as that laid down for the conversion of **9** to **8**. The crude product was purified by column chromatography (pentane : ethyl acetate = 2:1) affording **25** (0.063 g, 0.69 mmol, 85 %) as a pale yellow viscous oil. This brought the overall yield of the aryl azide to 1.27 g (2.51 mmol, 90 %).^{1}H NMR (400 MHz,

$CDCl_3$) δ: 7.89 (d, *J* = 2.0 Hz, 1H), 7.57 (dd, *J* = 8.4, 2.0 Hz, 1H), 7.14 (d, *J* = 8.4 Hz, 1H), 5.36 – 5.24 (m, 1H), 3.73 – 3.57 (m, 12H), 3.54 – 3.50 (m, 2H), 3.36 (s, 3H), 1.35 (d, *J* = 6.5 Hz, 3H), 1.03 (t, *J* = 7.9 Hz, 9H), 0.67 (q, *J* = 7.9 Hz, 6H).

(S)-2,5,8,11-tetraoxatetradecan-13-yl 2-azido-5-ethynylbenzoate (4): The synthesis of **4** followed the same procedure as for compound **3**; using **25** (0.6 g, 1.19 mmol) and TBAF (1 M THF solution, 3.57 mL). The reaction was worked up as described for **3** and the crude product was purified by column chromatography (pentane : ethyl acetate = 2:1, R.F. = 0.21) affording **4** (0.41 g, 1.05 mmol, 88 %) as a pale yellow oil. ^{1}H NMR (400 MHz, $CDCl_3$) δ: 7.95 (d, *J* = 2.0 Hz, 1H), 7.60 (dd, *J* = 8.4, 2.0 Hz, 1H), 7.18 (d, *J* = 8.4 Hz, 1H), 5.37 – 5.24 (m, 1H), 3.74 – 3.57 (m, 12H), 3.55 – 3.51 (m, 2H), 3.36 (s, 3H), 3.12 (s, 1H), 1.35 (d, *J* = 6.5 Hz, 3H). ^{13}C NMR (400MHz, $CDCl_3$) δ: 163.94, 140.48, 136.37, 135.53, 123.26, 120.05, 118.57, 104.90, 82.06, 78.54, 73.66, 72.04, 70.90, 70.85, 70.77, 70.73, 70.62, 59.13, 16.78. MS (ESI): *m/z* = 409.3 (calculated 409.2 for $[M + NH_4]^+$]), 410.2 (calculated: 410.2 for $[M + H_3O]^+$).

General polymerization procedure: To a 25 mL Schlenk flask was added monomer **3** (0.43 g, 1.29 mmol), PMDETA (0.022 g, 0.13 mmol), ascorbic acid (0.0011 g, 0.064 mmol) and triethylamine (0.013 g, 0.13 mmol). The mixture was dissolved in DMF (0.8 mL). The reaction flask was freeze-pump-thawed and backfilled with nitrogen twice, frozen again, filled with argon, opened and CuBr (0.0185 g, 0.13 mmol) quickly added and the flask sealed. The mixture was freeze-pump-thawed and backfilled with nitrogen thrice and the reactions were allowed to proceed at 30 °C. When the polymerization was considered finished, extra DMF was added, to dilute the mixture. The polymer was precipitated from an aqueous EDTA solution and the mixture vigorously stirred for an hour and centrifuged. The pellet was re-dissolved in DMF, precipitated from aq. EDTA, stirred and centrifuged again. This process was carried out three times. The polymer was dissolved in $CHCl_3$ and lyophilized for 24h, in dialysis tubing with a cut-off of 10 kDa, and obtained in ~ 90 % yield. To prevent any further polymerization during storage, the azide chain-ends were reduced to amine chain-ends by a Staudinger reduction as follows. The isolated polymer was dissolved in a mixture of $CHCl_3$/THF/water 9/0.5/0.5 mL followed by addition of an excess of PPh_3 (with respect to moles of azide chain end). The reaction was allowed to run for 20 h @ 50 °C. Afterwards the solvent was removed under reduced pressure, the polymer stirred in toluene, to remove any residual PPh_3 oxide and isolated by filtration. Finally the polymer was dried under reduced pressure overnight.

References

(1) Meudtner, R. M.; Hecht, S. *Macromol. Rapid Commun.* **2008**, *29*, 347.

(2) Meudtner, R. M.; Hecht, S. *Angew. Chem. Int. Ed.* **2008**, *47*, 4926.

(3) Juwarker, H.; Lenhardt, J. M.; Pham, D. M.; Craig, S. L. *Angew. Chem. Int. Ed.* **2008**, *47*, 3740.

(4) Juwarker, H.; Lenhardt, J. M.; Castillo, J. C.; Zhao, E.; Krishnamurthy, S.; Jamiolkowski, R. M.; Kim, K.-H.; Craig, S. L. *J. Org. Chem.* **2009**, *74*, 8924.

(5) Hanan, G. S.; Lehn, J.-M.; Kyritsakas, N.; Fischer, J. *J. Chem. Soc., Chem. Commun.* **1995**, 765.

(6) Cuccia, L. A.; Lehn, J.-M.; Homo, J.-C.; Schmutz, M. *Angew. Chem. Int. Ed.* **2000**, *39*, 233.

(7) Gardinier, K. M.; Khoury, R. G.; Lehn, J.-M. *Chem. Eur. J.* **2000**, *6*, 4124.

(8) Lee, O.-S.; Saven, J. G. *J. Phys. Chem. B* **2004**, *108*, 11988.

(9) Kelley, R. F.; Rybtchinski, B.; Stone, M. T.; Moore, J. S.; Wasielewski, M. R. *J. Am. Chem. Soc.* **2007**, *129*, 4114.

(10) Li, Y.; Flood, A. H. *Angew. Chem. Int. Ed.* **2008**, *47*, 2649

(11) Li, Y.; Flood, A. H. *J. Am. Chem. Soc.* **2008**, *130*, 12111.

(12) Zahran, E. M.; Hua, Y.; Li, Y.; Flood, A. H.; Bachas, L. G. *Anal. Chem.* **2009**, *82*, 368.

(13) Baldwin, M. G.; Johnson, K. E.; Lovinger, J. A.; Parker, C. O. *Polymer Letters* **1967**, *5*, 803.

(14) Nelson, J. C.; Saven, J. G.; Moore, J. S.; Wolynes, P. G. *Science* **1997**, *277*, 1793.

(15) Ray, C. R.; Moore, J. S. *Adv. Polym. Sci.* **2005**, *177*, 91.

(16) Hill, D. J.; Moore, J. S. *Proc. Natl. Acad. Sci. U. S. A.* **2002**, *99*, 5053.

(17) Prince, R. B.; Saven, J. G.; Wolynes, P. G.; Moore, J. S. *J. Am. Chem. Soc.* **1999**, *121*, 3114.

(18) Lahiri, S.; Thompson, J. L.; Moore, J. S. *J. Am. Chem. Soc.* **2000**, *122*, 11315.

(19) Prince, R. B.; Brunsveld, L.; Meijer, E. W.; Moore, J. S. *Angew. Chem. Int. Ed.* **2000**, *39*, 228.

(20) Chinchilla, R.; Nájera, C. *Chem. Rev.* **2007**, *107*, 874.

(21) Bräse, S.; Gil, C.; Knepper, K.; Zimmermann, V. *Angew. Chem. Int. Ed.* **2005**, *44*, 5188.

(22) Binauld, S.; Fleury, E.; Drockenmuller, E. *J. Polym. Sci., Part A: Polym. Chem.* **2010**, *48*, 2470.

(23) Wang, Y.; Li, F.; Han, Y.; Wang, F.; Jiang, H. *Chem. Eur. J.* **2009**, *15*, 9424.

(24) Barral, K.; Moorhouse, A. D.; Moses, J. E. *Org. Lett.* **2007**, *9*, 1809.

(25) Parker, D. *Chem. Rev.* **1991**, *91*, 1441.

(26) Hoye, T. R.; Jeffrey, C. S.; Shao, F. *Nat. Protocols* **2007**, *2*, 2451.

(27) Khan, A.; Kaiser, C.; Hecht, S. *Angew. Chem. Int. Ed.* **2006**, *45*, 1878

(28) Odian, G. *Principles Of Polymerization*; Fourth ed.; Wiley Interscience: New Jersey, 2004.

(29) Kolb, H. C.; Finn, M. G.; Sharpless, K. B. *Angew. Chem. Int. Ed.* **2001**, *40*, 2004.

(30) Stepto, R. F. T. *Pure Appl. Chem.* **2009**, *81*, 351.

(31) Rostovtsev, V. V.; Green, L. G.; Fokin, V. V.; Sharpless, K. B. *Angew. Chem. Int. Ed.* **2002**, *41*, 2596.

(32) van Dijk, M.; Mustafa, K.; Dechesne, A. C.; van Nostrum, C. F.; Hennink, W. E.; Rijkers, D. T. S.; Liskamp, R. M. J. *Biomacromolecules* **2007**, *8*, 327.

(33) Golas, P. L.; Tsarevsky, N. V.; Sumerlin, B. S.; Matyjaszewski, K. *Macromolecules* **2006**, *39*, 6451.

(34) Qin, A.; Lam, J. W. Y.; Tang, L.; Jim, C. K. W.; Zhao, H.; Sun, J.; Tang, B. Z. *Macromolecules* **2009**, *42*, 1421.

(35) Gutmann, V. *Coord. Chem. Rev.* **1975**, *15*, 207.

(36) Gutmann, V. *Coord. Chem. Rev.* **1967**, *2*, 239.

(37) Hill, D. J.; Mio, M. J.; Prince, R. B.; Hughes, T. S.; Moore, J. S. *Chem. Rev.* **2001**, *101*, 3893.

(38) Cubberley, M. S.; Iverson, B. L. *J. Am. Chem. Soc.* **2001**, *123*, 7560.

(39) Brunsveld, L.; Meijer, E. W.; Prince, R. B.; Moore, J. S. *J. Am. Chem. Soc.* **2001**, *123*, 7978.

(40) Latli, B.; Tomizawa, M.; Casida, J. E. *Bioconjugate Chem.* **1997**, *8*, 7.

(41) Stone, M. T.; Moore, J. S. *Org. Lett.* **2004**, *6*, 469.

(42) Hirose, T.; Matsuda, K.; Irie, M. *J. Org. Chem.* **2006**, *71*, 7499.

Chapter 4. TMV like complex by hierarchical information transfer

Introduction

Self-assembly is central to all life forms. Living cells are filled with functional self-assembled domains working to sustain life. Understanding how nature assembles her machinery will shed light on life processes. An equally important spinoff will be in the field of materials science, were the need to design and create functional materials for nanotechnology is ever apparent.[1] Rapid advances in nanotechnology demand precise control and understanding of shape, size and structure of the assembled domains. Viruses are the foremost examples of precise self-assembly from the bottom up *i.e.* hierarchical self-assembly to precise nano architectures. They have regular shapes, monodisperse structures and an incredible range of functional groups (in the form of amino acid residues), precisely placed on virus surfaces, which can be manipulated for the benefits of materials science. Viruses are now frequently used as templates for making nano materials.[2-5]

Tobacco mosaic virus (TMV) is one of the best understood hierarchical self-assembled biological systems and is a popular model for study.[6,7] Native TMV comprises 2130 identical protein subunits arranged around a RNA helix (6400 bases), in a helical fashion. The overall structure is a rigid asymmetric complex 300 nm long, 18 nm wide and an internal cavity 4 nm wide (Figure 4.1a).[7,8] This picture is elegant and simple, however, the mechanism of assembly is extremely complex. Under physiological conditions, the individual protein molecules can assemble into a two layer disk structure, each a ring comprising 17 protein molecules. A hairpin loop, of the RNA's initiation region, inserts into the central hole of the protein disk, in a gap between the two layers, dislocating the disk into a helical structure. Two turns of the final helix (16.33 subunits per turn) trap the RNA initiating helical growth. The helix then grows by addition of further disks (Figure 4.1b). The length of the full assembly is precisely controlled by the RNA template, whilst the capsid determines the shape.

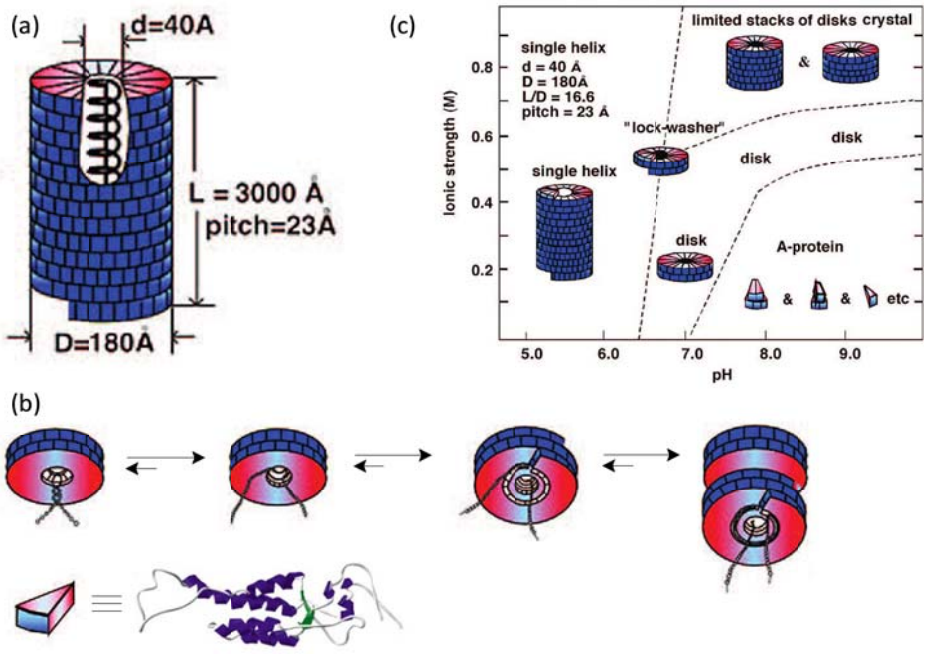

Figure 4.1: Cartoon of TMV (a), schematic illustration TMV assembly (b) and phase diagram showing the effect of pH and ionic strength on TMV protein aggregates in the absence of RNA (c). Images adapted from reference 13.

A complete and fully infective TMV can be reconstituted from the isolated RNA and capsid proteins, which means that the information required for its assembly and structure are in its subunits.[6] At low pH, the discs assemble on their own, without RNA, into helices with varying lengths (Figure 4.1c).

A number of very important lessons have been drawn from TMV's assembly, for the benefit of supramolecular chemistry:[1,9,10]

- Stable subunits are first constructed and then assembled into larger structures.
- Assembling subunits is much easier and more efficient than direct construction.
- Using multiple weak non-covalent interactions, in assembling subunits, enables better control over the assembly and disassembly processes since the process is dynamic.
- Directions for the assembly process are built into the subunits, equipping the system with a built in error-checking system.

- The use of subunits with complimentary shapes maximizes the formation of weak non-covalent interactions used in the assembly process.
- The use of templates, in self-assembly, enables structural control, *e.g.* control of length, and it also helps to reduce errors.

Several others have used the TMV model as an inspiration for supramolecular self-assembly. The most prominent examples being the low molecular weight dendronized polymers, prepared by Percec and coworkers, which have tapered shapes, and self-organize into disk-like supramolecules, and subsequently into helical cylindrical superstructures and then hexagonal columnar phases.[11-13] This system resembles TMV in that self-assembled helical cylindrical objects are formed.[11] In other work, Stupp and coworkers demonstrated length control by assembling peptide amphiphiles around the hydrophobic core of a dumbbell shaped oligo(*p*-phenylene ethynylene) template in aqueous solutions.[14] Without the template, the amphiphiles self-assemble into high aspect ratio fibers. When presented with the template, small monodisperse nanostructures were observed via AFM and TEM, implying templating. The authors, however, did not give spectroscopic evidence of interaction between the template and the amphiphiles.[14] They also pointed out that the amphiphiles assembled in the same fashion with or without the template.

Our approach

We envisaged that embedding a poly(γ-benzyl-L-glutamate) (PBLG) (template) inside the cavity of P(*p*-AT) helical foldamers, would result in a self-assembled complex in which the length and chirality of the system could be regulated by the polymer template. PBLG is a hydrophobic synthetic polypeptide, which adopts a rigid α-helix conformation, both in solution and solid state, stabilized by intramolecular hydrogen bonds. P(*p*-AT) foldamers exist in a random coil conformation in a good solvent *e.g.* DMF and fold into a helical conformation in DMF/water. The helical conformation has an apolar interior and an amphiphilic exterior. The P(*p*-AT)'s conformational preferences can be controlled by subtly adjusting the DMF/water ratios. At low volume fractions of water a random coil prevails, on slightly increasing the water content there

exists an equilibrium between the folded and unfolded conformations. A further increase in water content beyond this point makes the system solvophobic enough to stabilize the helically folded conformation and ultimately results in stacking of the helices and subsequent formation of long bundles with high aspect ratios. These conformational transitions can be tracked by UV-vis and CD titrations as a function of solvent quality (Chapter 3). PBLG is soluble in DMF, without losing its α-helical conformation,[15] but crucially it is insoluble in water and also in DMF/water mixtures.[16] Therefore, presenting the P(*p*-AT) foldamer with a PBLG will result in templated self-assembly of the foldamer by the PBLG, driven by solvophobic forces.

Hierarchical self-assembly without a template

In order to fully assess the hierarchical self-assembly of the P(*p*-AT)s, with and without a template, it was paramount to determine the full extent of the P(*p*-AT)s' solubility and self-assembly in water. The triethylene glycol and tetraethylene glycol side chains used in chapter 3 resulted in P(*p*-AT)s (**28** and **29**) that were sparingly soluble in water. It has been shown that hexa-ethylene glycol (h-EG) side chains appended to *m*PE foldamers conferred extra water solubility to the foldamers.[17,18] For this reason a h-EG side chain was synthesized anticipating that the longer side chains would confer water solubility to the subsequent P(*p*-AT).

Monomer and polymer synthesis

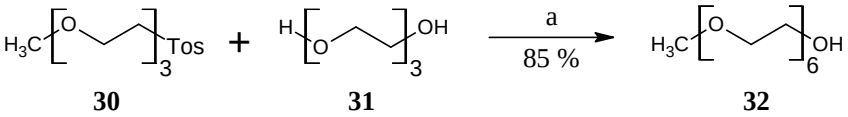

30 **31** **32**

Scheme 4.1: Synthesis of h-EG side chain. (a) NaOH, neat, Δ.

The synthesis of the h-EG proceeded by the coupling of a tosylated triethylene glycol monomethyl ether (**30**) with neat triethylene glycol (**31**), under basic conditions.[18] Subsequently, the compound **32** was coupled to 2-azido-5-iodobenzoic acid (**6**) giving compound **33**. Ethynylation of **33**, by a Sonogashira coupling, with TMS-protected alkyne

followed by the removal of the TMS protecting group, using TBAF, yielded the requisite monomer **36**. The structure of **36** was confirmed by ^{1}H and ^{13}C NMR and by mass spectroscopy.

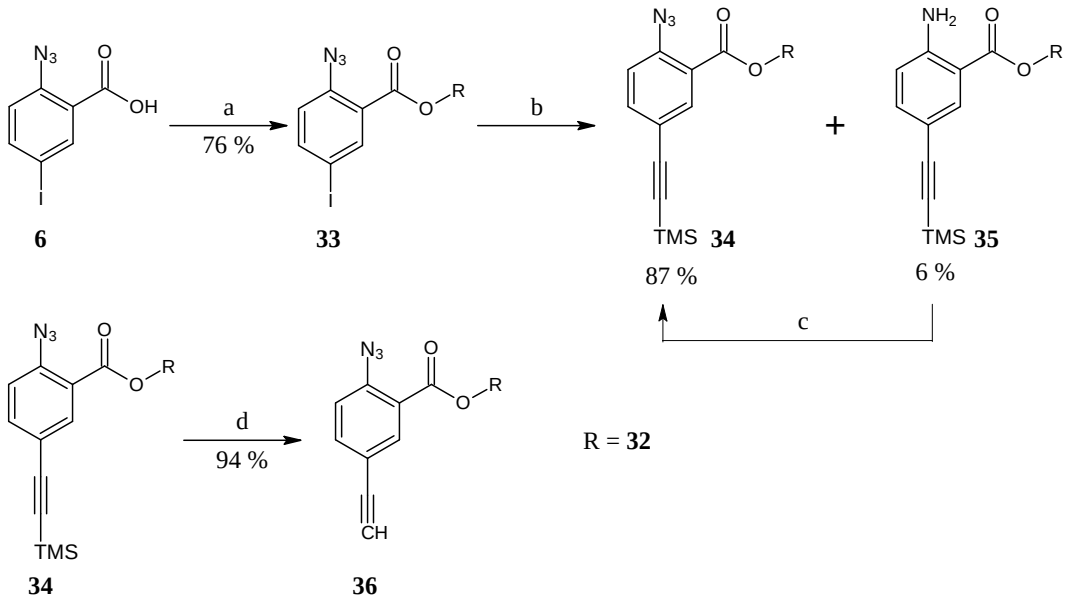

Scheme 4.2: Monomer synthesis. (a) **32**, DCC, DMAP, THF, 0 °C to r.t.; (b) TMSA, $Pd(PPh_3)_4$; CuI, TEA, THF, 30 °C; *t*-$BuNO_2$, TMS-azide, THF, 0 °C to r.t.; (e) TBAF, THF, r.t.

The CuAAC AB step growth polymerization of **36**, using optimized conditions from Chapter 3, yielded a high molecular weight P(p-AT)-**38** (Table 4.1). The protocol entails carrying out the polymerization with a very concentrated monomer solution, 500 mg in 1 ml of solvent, using a Cu^{I} catalyst. Direct use of a Cu^{I} source has been shown to be better than using a Cu^{II} salt and then reducing it *in-situ* to the active Cu^{I} catalyst.[19]

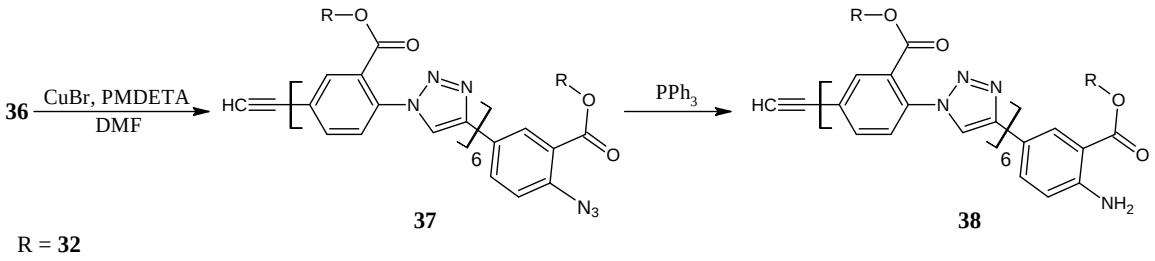

Scheme 4.3: CuAAC AB step growth polymerization of 36.

The polymer was isolated by precipitation into an aqueous EDTA solution. The process was repeated three times, so as to remove Cu ions. The azide-end group was then reduced to a amine functionality in order to prevent auto-polymerization during storage and finally the polymer was dialyzed against DMF, overnight and dried.

Table 4.1: Reaction conditions for the polymerization.

Entry	Monomer	Monomer / Cu^{I} / DMF	time	M_n	M_w	*Đ*
1	**36**	0.5 g/5 mol %/1 ml	3 days	33 538	45 148	1.35
2	**4**	0.5 g/5 mol %/1 ml	3 days	31 348	49 750	1.59

The M_n^{SEC} of 33.5 kDa Da (entry 1) confirmed the success of the polymerization protocol in realizing respectably high molecular weight polymers by the CuAAC step growth polymerization techniques. The *Đ* value of 1.35 is much lower than the values typical of step growth systems, *Đ* ≈ 2.[20] The SEC analysis was done after extensive purification of the polymer during which lower molecular weight oligomers were removed. Monomer **4** was also successfully polymerized (entry 2), yielding a high molecular weight polymer.

P(*p*-AT)-**38** completely dissolved in $CHCl_3$, CH_2Cl_2, HFIP, DMSO, NMP and DMF, giving bright yellow solutions. It was also soluble in water at concentrations of 2 mg/ml, yielding a viscous pale yellow solution.

Conformational analysis and self-assembly

The primary analytical technique used, to assess the solvent dependent conformation transitions, for P(*p*-AT)-**38**, is UV-vis spectroscopy. Previously (Chapter 3) it was shown that the aryl triazole polymers have two characteristic absorption maxima around 284 nm and 310 nm. A conformational change from a random coil to a helical folded conformation was characterized by hypochromism in the band at 284 nm whilst the band at 310 nm amplified. The “good solvent/bad solvent” combination used was DMF/water. A good solvent completely solvates the whole polymer, whilst a bad solvent selectively solvates parts of it.[21] In the “foldamer

chemistry" sense, switching from a good to a bad solvent induces a conformational transition from a random coil to a helically folded conformation due to solvophobicity.[22]

Figure 4.2a shows the UV-vis spectra recorded as a function of volume percent of water in DMF. The solvent quality was gradually changed from 100% DMF to 100% H_2O in small increments.

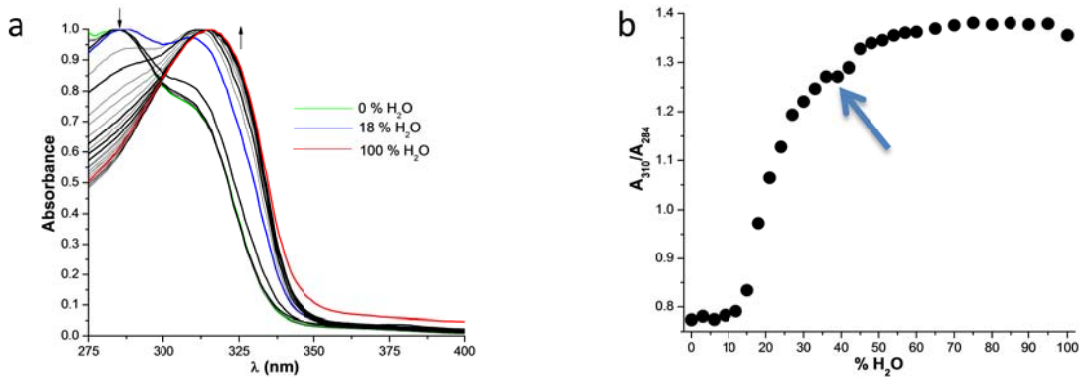

Figure 4.2: Normalized UV-vis spectra of P(*p*-AT)-38 [0.95 µM] as a function of volume % H_2O in DMF (a) and the absorbance ratio A_{310}/A_{284} as a function of volume % H_2O in DMF.

Increasing the volume fraction of H_2O resulted in the hypochromicity of the absorption band at 284 nm whilst the band at 310 nm amplified. This evolution in the UV-vis spectra, with varying solvent composition, is consistent with the findings in Chapter 3. At 18 % H_2O the characteristic bands had (almost) equal amplitudes (Figure 4.2a), implying the presence of an (almost) equal population of foldamers in the random coil conformation and in the helically folded state. Since P(*p*-AT)-**38** has no configurationally chiral elements in its structure, a dynamic equilibrium should exist between the M and P helices, via the random coil, at 18 % H_2O. Further increments in % H_2O, beyond 18 %, resulted in an increased hypochromic effect for the band at 284 nm.

Figure 4.2b shows a plot of the absorbance ratio as a function of volume % H_2O. The absorbance ratio increased sharply after 12 % H_2O and appeared to be leveling off at 35 % H_2O, before an apparent further increase from 40 % H_2O. It is apparent that at 35 % H_2O, when the curve appears to flatten, a stable helical conformation is prevailing. The "kick" from 40 % H_2O reflects an increased hypochromicity in the absorption band at 284 nm, implying an increased stability of the helically folded conformation. In Chapter 3 we tentatively attributed the

increased stability of the helical foldamers to the formation of tertiary structures, i.e. helical stacks, due to stronger solvophobic driving forces caused by increasing the volume % of H_2O.[23]

The plot in Figure 4.2b can be split into two parts representing firstly the formation of a stable helical conformation from the random coil (Figure 4.3a) and the subsequent formation of a higher order structures (Figure 4.3b).

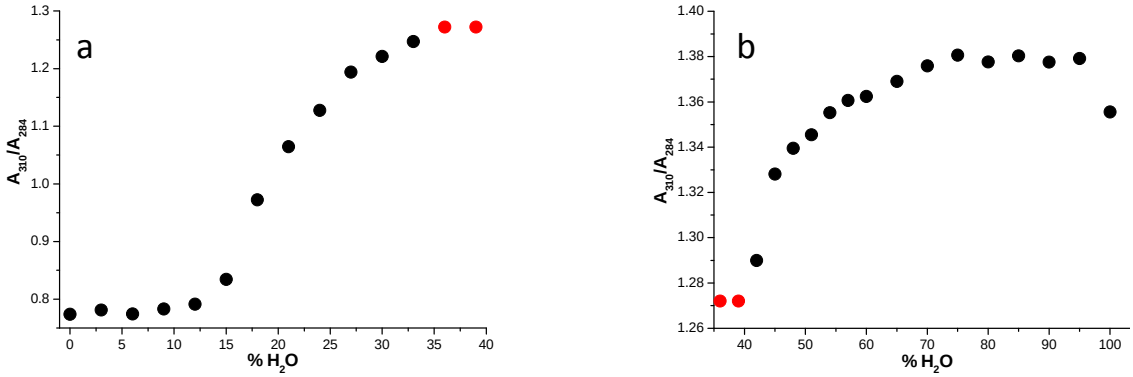

Figure 4.3: (a) Absorbance ratio A_{310}/A_{284} as a function of volume % H_2O in DMF up to 40% water. (b) The absorbance ratio beyond 40% water.

The plot for the coil to helix transition (Figure 4.3a) is sigmoidal, a typical feature of cooperative conformational transitions.[24] It could also be argued that this conformational transition is a two-state cooperative conformational transition. In a two-state cooperative transition, only the folded and the unfolded conformations are present in appreciable amounts.[24] The prime characteristic of a two-state system is the observation of two distinct populations near the transition mid-point.[24] Two distinct populations are indeed identifiable at 18 % H_2O which are assignable to the folded and unfolded conformations (Figure 4.2a). Two-state behavior in aryl based helical foldamers has been demonstrated for *m*PE foldamers.[22] Although, with *m*PE foldamers, two distinct populations were not identified, the validity of a two-state assumption was demonstrated by the linear dependency between the stability of the helically folded state and chain length of the foldamer.[22]

The data in Figure 4.3a was further analyzed with the assumption that the system obeys a two-state mechanism, using protocols that are applied to protein denaturation studies.[25] Since only

the folded and unfolded conformations are assumed to be present in appreciable amounts, equation *i* can be assumed to hold at all times:

$$F_u + F_f = 1 \qquad i$$

F_u and F_f stand for the fractions unfolded and folded of the P(*p*-AT)s respectively. The absorbance ratio data, in Figure 4.3a, can then be normalized, using equation *ii*, enabling the analysis to be done in terms of fraction unfolded as a function of solvent quality.

$$F_u = (A_f - A_r)/(A_f - A_u) \qquad ii$$

A_r is the absorbance ratio, A_u and A_f are absorbance ratios of the fully unfolded and the fully folded confomers respectively. The equilibrium constant and the free energy of the folding reaction are then accessible via equations *iii* and *iv* below:

$$K = F_u/F_f = F_u/(1 - F_u) \qquad iii$$

$$\Delta G = -RT\ln K = -RT\ln[F_u/(1 - F_u)] \qquad iv$$

R is the molar gas constant and *T* is the absolute temperature, (295.15 K, for this experiment). A_u and A_f were determined by extrapolation from the pre and post transition baselines respectively. Finally, the data in Figure 4.3a could be re-plotted as shown in Figure 4.4a.

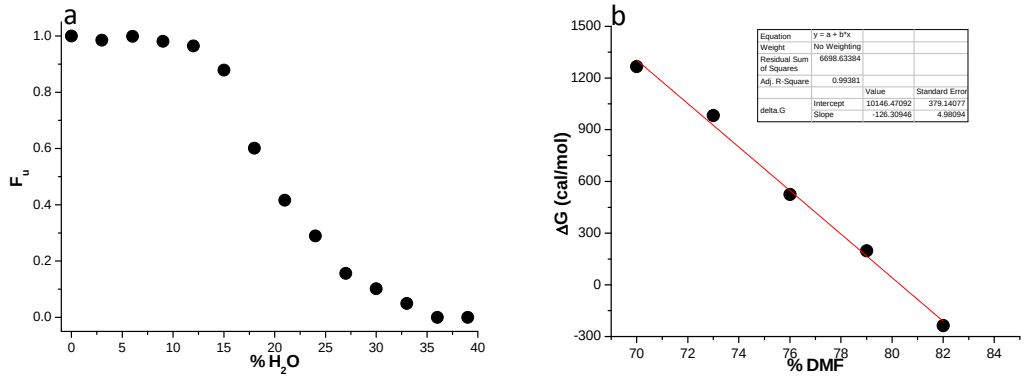

Figure 4.4: (a) Fraction unfolded as a function of volume fraction of water in DMF derived using equation *ii* and (b) the variation of ΔG as a function of denaturant, *i.e.* volume fraction of DMF, calculated using equation *iv*.

Figure 4.4b shows the variation of free energy with solvent composition in the transition region. The free energy varied linearly with volume fraction of denaturant, DMF, in the transition region, a typical feature of two-state systems. This linear relationship between denaturant and the free energy is expressed in equation *v*:

$$\Delta G = \Delta G(H_2O) - m[\%\ DMF] \qquad v$$

were *m* measures the dependency of the ΔG on volume fraction. The intercept of the plot, in Figure 4.4b, gives $\Delta G(H_2O)$ and the solvent composition required to reach the transition midpoint, *i.e.* when ΔG = 0, or $[\%\ DMF]_{1/2}$, is then given by $\Delta G(H_2O)/m$. The $[\%\ DMF]_{1/2}$ was 80.33 % DMF, conversely 19.67 % H_2O in DMF. This value was in good agreement with the experimentally observed mid-point where the two absorption bands had *almost* equal intensities.

The plot for the formation of higher order structures, as a function of solvent composition, (Figure 4.3b) is not sigmoidal. Similar shaped curves have been observed in the hierachichal self-assembly of oligo(*p*-phenylenevinylene) (OPV) derivatives, which form hydrogen bonded dimers, that further stack and grow into long helical fibers.[26,27] It was observed that the formation of the hydrogen bonded dimers was crucial for overcoming the energy barrier to the formation of helical fibers. Judged exclusively by the shape of the curve, (Figure 4.3b), it appears that the hypothesized tertiary structure formation occurs by a solvent dependent cooperative self-assembly mechanism.[26,27] In this case, the critical nucleus required for self-assembly to commence is the formation of the helical conformation of a finite length. More work will be required to fit the data to either cooperative self-assembly models or to isodesmic self-assembly models.[27] Figure 4.3b shows that stable helical columns are obtained above 70 % water. The UV-vis spectra of the sample in 100 % water showed less hypochromicity than spectra for samples from 70 – 95 % water. This was perhaps due to the complete absence of DMF which could alter the conformation of the self-assembled structure in order to minimize contact with water.[18]

cryo-TEM analysis

To get a clearer picture on the self-assembled structure of the helical foldamers in the solution state, the sample in 100 % water was imaged by cryo-TEM since this technique reveals the solution state structure.

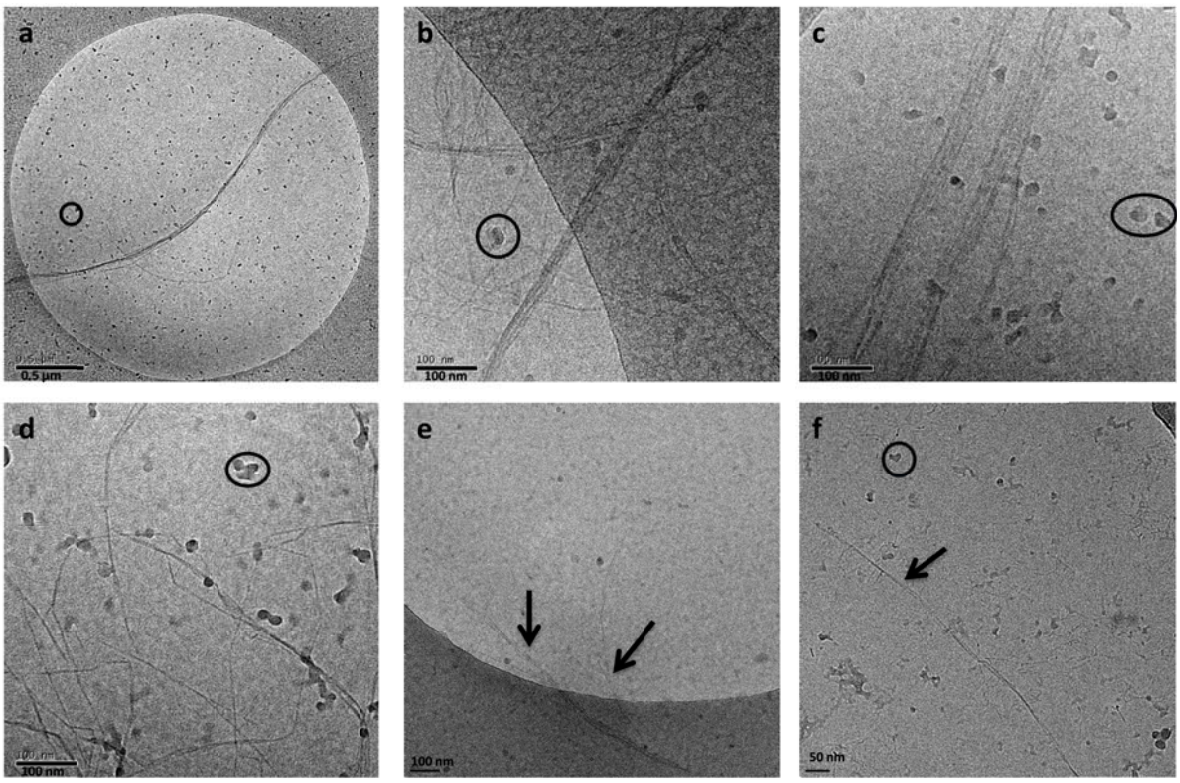

Figure 4.5: cryoTEM images of the self-assembled helical P(*p*-AT)-38 foldamer in water. P(*p*-AT)-38 concentrations were 29.8 µM, for images A – D, and 1.2 µM for images E – F. The irregular shaped dark blots, examples indicated by the black circles, are ice crystals contaminating the sample.

The cryo-TEM images in Figure 4.5, provided definite evidence of the formation of long extensive fibers up to several microns long (e.g. Figure 4.5a). The fibers are composed of helices that stack together into the long extensive structures. It is also apparent that in the solution state, the fibers do not coil around each other, but simply bundle parallel to each other. In Chapter 3, aqueous DMF solutions of P(*p*-AT)-**28**, with stacked helices, still had the same isodichroic point as the solution with "monomeric" helices, implying that the supramolecular

stacks were not interacting laterally. This assertion is confirmed explicitly in Figure 4.5b and c which shows several stacks running parallel to each other. The supramolecular stacks were of mixed lengths.

A clear picture of the hierarchical self-assembly can now be drawn, and is illustrated schematically in Figure 4.6.

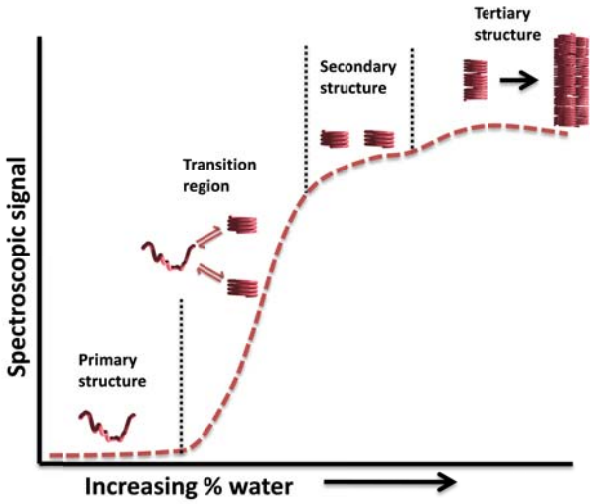

Figure 4.6: Hierarchical self-assembly.

First the *primary structure* (the random coil polymer) is synthesized with information for folding in the form of specific linkages and an amphiphilic character. The solvent dependent structural evolution then passes through a *transition phase* whereby the folded conformation is in equilibrium with the unfolded. Then the *secondary structure*, in the form of the stable helical conformation is formed. On further increasing solvent polarity, the stable helices stack and form long fibers, *i.e.* the *tertiary structure*.

This picture, however, is not complete. A clearer mechanistic picture must still be sought, so as to fully understand the role of the solvent composition (polarity) in abetting or frustrating the growth of the fibers. Also critical is the need to have a deeper understanding of the thermodynamic and kinetic parameters. Figure 4.3b shows clearly that solvent composition has a dramatic role in influencing the growth and stability of the fibers. At the highest accessible

solvent polarity, in pure water, it is clear that the fibers are of very long varying lengths and assemble. This is at the most extreme solvophobic environment. It will be of interest to study the assembly length of the fibers in water/DMF mixtures between 60 and 90 % water and to see how they grow. A mechanistic investigation into the self-assembly process will be carried out in the future.

Templated self-assembly

The challenge to ensure that molecular components assemble into nano-objects with pre-determined sizes and shapes, without falling into a kinetic trap, is the overall goal of this thesis. The self-assembly of TMV operates in a dynamic equilibrium, enabling the systems to error check, ensuring high reliability in the assembly process. Stable sub-assemblies are made first and the use of a template helps to reduce errors, regulate length and introduce asymmetry. In the preceding section it was shown that helical P(*p*-AT)-**38** foldamers can assemble into high aspect ratio fibers, however with indeterminate lengths. The self-assembly is induced by solvophobic forces.

We postulated that the hydrophobic PBLG α-helix could template the self-assembly of helical foldamers into long stacks, with control over length and chirality. The α-helix is a tight wound coil conformation with 3.6 repeat units per turn, a residue translation of 0.15 nm, along the helical axis and the helical pitch is 0.54 nm.[28] Hydrogen bonds, formed between the N-H group and the amide carbonyl four repeat units before, hold the structure stable.

PBLG was chosen as the guest template for several reasons. It dissolves in DMF, and does not associate in that solvent.[15] It is, however, insoluble in water and sparingly soluble in water/DMF mixtures. This solubility allows the use of solvophobic forces to drive it into the apolar cavity of the P(*p*-AT) foldamers thereby controlling the assembly process. The diameter of PBLG is approximately 1.6 nm,[29] whilst the cavity of the putative P(*p*-AT) helix is ~ 3 nm, bringing the PBLG to ~ 53 % of the volume of the host cavity. This resonates with the findings by Rebek who showed that, in host guest systems, “a favorable recognition event” occurred when the guest occupied approximately 55 % of the volume of the host cavity.[30]

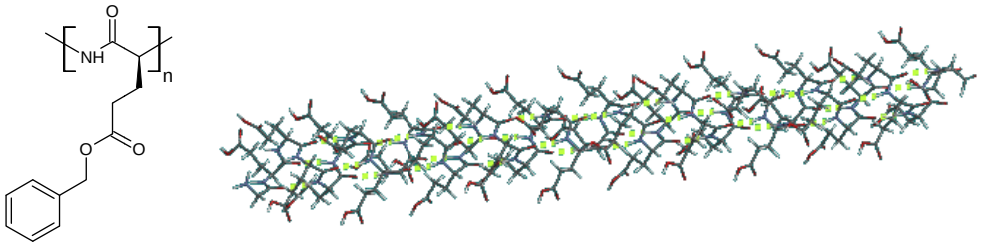

11 12

Figure 4.7 Poly(γ-benzyl-L-glutamate) repeat unit and the tube model of the α-helical poly(L-glutamatic acid) with a D.P. of 30. The bright green streaks represent hydrogen bonds, formed between the the *i*-th and the residue in the *i*-4 position. Structure was drawn using the peptide template in Spartan.

To ensure a dynamic self-assembly process, the templating was implemented in the transition region of P(*p*-AT)-**38**, using the 18 % H_2O in DMF solution. P(*p*-AT)-**38** has no chiral bias. In the transition region it equilibrates between the M and P helical conformations, via the random coil and is hence CD inactive. It was anticipated that the enantiopure chiral PBLG template would selectively self-assemble with the enantiomer of the helical foldamer with a matching screw sense. The self-assembled structure is stabilized by van de Waals interactions between stacked helices. It occupies a thermodynamic minimum, which makes it much more stable than the assembly subunits, creating a sink in the direction of the diastereomeric complex (Scheme 4.4). This strategy introduces asymmetry and the control over length of the self-assembled object, which is regulated by the template. The formation of the diastereomeric complex can be tracked by CD spectroscopy, monitoring the appearance of a Cotton effect in the wavelength region of the foldamer, where the guest is not CD active.

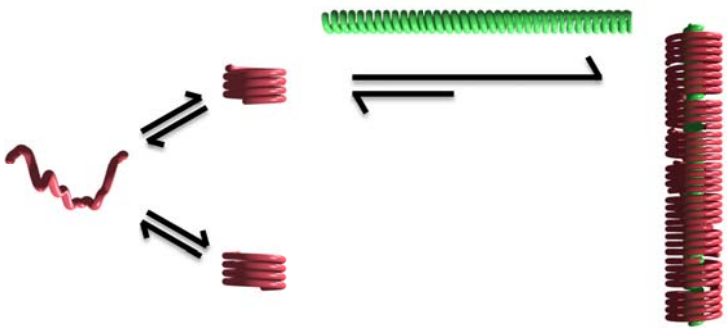

Scheme 4.4: Schematic depiction of the dynamic self-assembly method introduced in this work.

Probing the templated self-assembly

CD spectroscopy was used to probe interaction between the P(*p*-AT)-**38** and the PBLG template. Important is that absorptions of the PBLG and the P(*p*-AT)-**38** helical foldamer are well separated in the UV-vis region, therefore apparent CD activity in the region of the P(*p*-AT) foldamer can be used as evidence of complex formation.

A prediction for the stoichiometry of the initial experiment to prove interaction was carried out using structural information of the helical foldamer and the α-helical PBLG template. First the thickness of the helical foldamer "disk" (*h*) was determined. The helical pitch (*p*), of P(*p*-AT)-**38**, was estimated to be 3.8 Å (Chapter 3) with 14 repeat units to complete a turn. Dividing the D.P. of P(*p*-AT)-**38** by 14 gives the number of turns of the helix. The product of the number of turns and the helical pitch then gives the value of *h*:

h = (D.P.)/(14)*p = (33 538/465.5)/(14) * 3.8 = 19.56 Å.

The residue translation in the polypeptide PBLG is 1.5 Å. Therefore the length of the α-helix rod is the product of the D.P. and the residue translation, *i.e.* D.P. * 1.5 Å. Finally, the theoretical number of P(*p*-AT) "disks" [$N^{P(p\text{-AT})}$] required to fully template the PBLG α-helix is the ratio of the α-helix rod length to the stack length of the P(*p*-AT).

Table 4.2. Characterization of PBLG α-helix used.

[a] M_n (kDa)	[b] D.P.	[c]Rod length (nm)	[d]Generic name	[e]$N^{[P(p\text{-AT})]}$
41	187	28.0	Template A	14
92.6	422	63.3	Template B	32
162.9	743	111.4	Template C	57

- [a]M_n^{PBLG}, details provided by supplier, Sigma Aldrich.
- [b]D.P.^{PBLG} = $M_n^{(polymer)}/M_n^{(repeat\ unit)}$ (M_n repeat unit = 219.24 g/mol).
- [c]Residue translation is 0.15 nm,[31] therefore rod length = D.P.*0.15 nm.
- [d]Generic names for templates used in this work.
- [e]$N^{[P(p\text{-AT})]}$ is the calculated number of helical foldamer disks required to fully cover the PBLG template.

Three different sizes of commercial PBLG α-helix were assayed. The molecular weight details and physical characteristics are given in Table 4.2. It can be seen that for a short polymer template (template A) the number of helical foldamers required to cover it is 14, whilst for the long polymer (template C) it is 57.

To provide evidence for the complexation, between PBLG (template B) and P(*p*-AT)-**38**, mixtures of P(*p*-AT)-**38** with (and without) template B were analyzed by CD spectroscopy, in 100 % DMF and in 18 % H_2O in DMF. The mixture of P(*p*-AT)-**38** and template B, in 100 % DMF, was CD silent in the region of the spectrum where P(*p*-AT)-**38** is active (Figure 4.8, black line). This is because in DMF, P(*p*-AT)-**38** exists in a random coil. The host subassembly is not constituted, therefore self-assembly cannot take place.

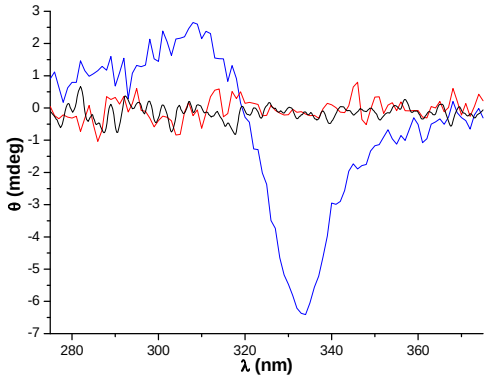

Figure 4.8: CD spectra of a mixture of P(*p*-AT)-38 (0.74 µM) and PBLG template B (0.025 µM) in DMF (black line), P(*p*-AT)-38 (0.74 µM) 18 % H_2O in DMF (red line) and a mixture of P(*p*-AT)-38 (0.74 µM) and PBLG template B (0.025 µM) (blue line).

P(*p*-AT)-**38** in 18 % water, *sans* the template, was also CD silent (Figure 4.8, red line). UV-vis analysis indicated the presence of a helical conformation, in equilibrium with the random coil, in this solvent composition, *vide supra*. P(*p*-AT)-**38** has no configurationally chiral components and in the helically folded state it exists as a racemic mixture of the M and P helices and hence is CD inactive. The mixture of P(*p*-AT)-**38** and template B (30:1 equivalents respectively) displayed CD activity in the region of the spectrum where only P(*p*-AT)-**38** absorbs (Figure 4.8, blue line). The negative bisignate Cotton Effect had a negative maximum at ~ 333 nm, a zero

crossing around 320 nm and a positive maximum around 307 nm. Clearly the chirality of the template was expressed in the self-assembled construct.

The stoichiometry between P(p-AT)-**38** and all the templates was studied using CD spectroscopy as the primary analytical technique. Titrations were run at 293.15 K in 18 % water in DMF solution. The P(p-AT) helical foldamer was treated as the host and its concentration was kept constant, whilst the concentration of the guest PBLG templates was gradually raised in small increments (Figure 4.9).

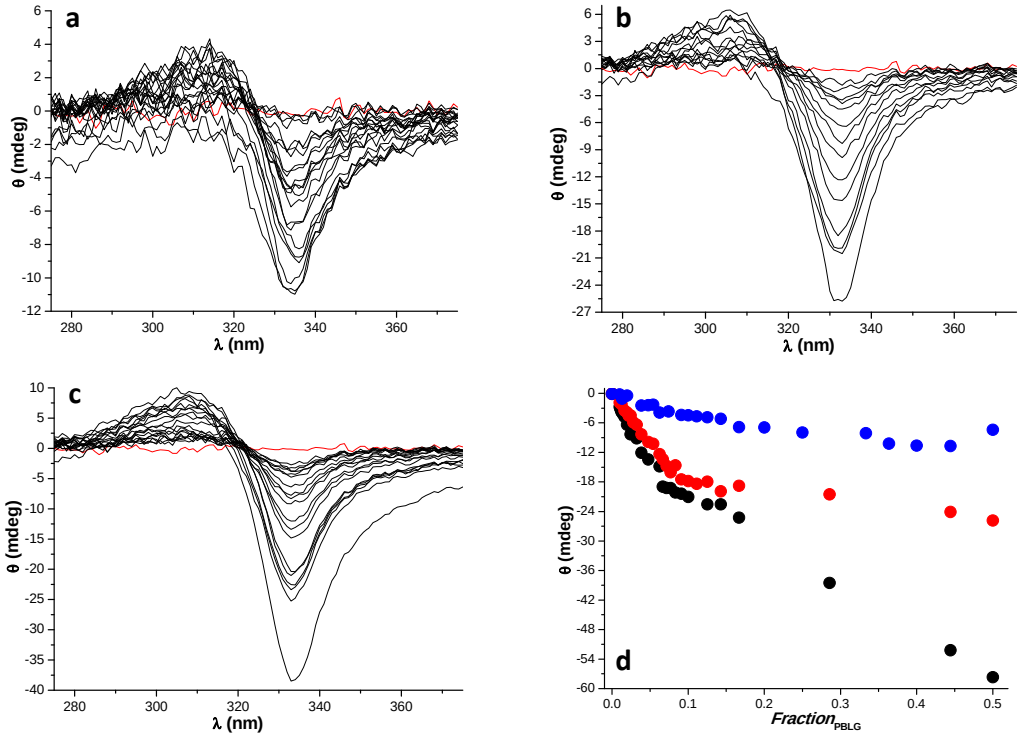

Figure 4.9: CD spectra of P(*p*-AT)-38 as a function of the guest template concentration, 0 – 0.248 µM for template A (a) and 0 – 0.149 µM for templates B and C, (b and c respectively) and a plot of the CD signal at 333 nm as a function of the mole fraction of template (d), the blue, red and black curves represent templates A, B and C respectively. P(*p*-AT) was held constant at 0.74 µM.

In all the CD spectra, the CD signal intensity increased with increasing amount of template before eventually saturating. Also, and more significantly, the strength of the CD signal increased with the size of the template demonstrating a remarkable template-length

dependent self-assembly. The CD signals displayed an isodichroic point around 320 nm, which was lost beyond saturation. The presence of an isodichroic point, at ~ 320 nm, before saturation, also implied that the self-assembly process was giving the same type of structures, regardless of length of the template. At molar ratios of PBLG:P(*p*-AT) of ~ 3:1, solutions with template C appeared cloudy white due to the excess amounts of PBLG template more than the foldamer host could entrap and keep solubilized in the aqueous DMF solutions.

To determine the stoichiometry and verify the length dependent templating effect (LDTE), the data in Figure 4.9d was converted into Job's plots. Carrying out a typical continuous variation (Job's method) experiment[32,33] for this system is not viable because the PBLG guest template precipitates from aqueous DMF solutions. In the typical continuous variation experiment, the mole fraction of the guest is varied whilst the total concentration, of the host and guest, is kept constant. The signal response is then plotted (as the dependent variable) against the mole fraction of the guest and the curve maxima gives the stoichiometry of the host to guest. The technique of increasing the guest concentration, whilst that of the host is kept constant is called the mole ratio method. Typically, in this method, when the signal response is plotted vs. the mole ratio, the curve displays a sharp "break point" at the point that matches the stoichiometry of the complex under study.[34] The mole ratio plot in Figure 4.9d does not show a sharp break point. Nevertheless a Job's plot was fashioned from the data in Figure 4.9d by normalizing the CD signal of each sample against the total concentration of monomers in that solution.

To equate the analysis, to one carried out at a constant total concentration, first the used concentrations were recalculated to reflect the total concentration of "monomers" in each solution. The concentration of monomers from the PBLG template is the product of the moles of PBLG used and the D.P. of the respective polymer, whilst each P(*p*-AT) foldamer helix was considered as a single monomer. Then the sum of the two monomer concentrations values is the total concentration of monomer in solution. Then each total monomer concentration was normalized against the total concentration of monomers in the solution of the first addition point to give a "normalization factor". This last step effectively, equates the analysis to one

carried out at a constant total concentration of host and guest. Finally, each CD reading was then also normalized against its corresponding "normalization factor". The normalized CD values were then plotted against the mole fraction of PBLG in solution (Figure 4.10a).

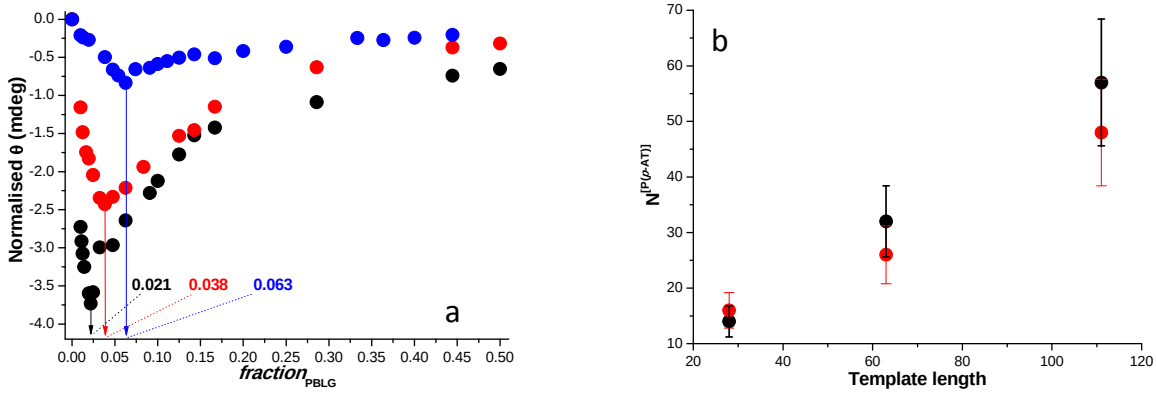

Figure 4.10: Job's plot of normalized CD signal intensity, at 333 nm as a function of mole fraction of PBLG (a) and a plot of the theoretical (black dots) and experimental (red dots) $N^{[P(p\text{-AT})]}$ (vide supra) required to completely entrap the respective templates (b). Error bars are based on the *Đ* of PBLG.

Table 4.3: Characterization of the self-assembled P(*p*-AT)-38/PBLG complexes

Template	Rod length (nm)	[a]$N^{[P(p\text{-AT})]}$	Mole fraction$_{PBLG}$	[b]$N^{[P(p\text{-AT})]}$
A	28.0	14	0.063	16
B	63.3	32	0.038	26
C	111.4	57	0.021	48

- [a]Theoretical value
- [b]Experimental value

As shown in Figure 4.10a after this manipulation, a clear break point could be observed, enabling the experimental $N^{[P(p\text{-AT})]}$ to be calculated. Figure 4.10b shows the close correlation between the theoretical and experimental $N^{[P(p\text{-AT})]}$ values, which have been depicted numerically in Table 4.3. These results show clearly that a LDTE was achieved. Templates A, B and C required 16, 26 and 48 helical foldamers to cover them, respectively, with a very good agreement between the theoretical and the experimental $N^{[P(p\text{-AT})]}$ values. This is without precedent in the self-assembly of dynamic helical foldamer systems.

The template mediates the self-assembly

The templated self-assembly was further assessed as a function of solvent composition. Earlier it was shown that, in the absence of a template, P(*p*-AT) foldamers self-assemble into helical stacks, driven by solvophobic forces. The onset of the self-assembly was signaled by an abrupt increase in the UV-vis absorbance ratio, as a function of solvent composition (Figures 3.9b and 4.2b). This was attributed to an increased stability of the helical conformation, due to the formation of stacks, which was reflected by an increased hypochromicity of UV-vis absorption band at 284 nm. It was rationalized that in the presence of a template the hierarchical self-assembly protocols presented in Figure 4.6 would be modified. UV-vis spectra of the optimum stoichiometry self-assembled complexes of P(*p*-AT)-**38** and P(*p*-AT)-**29**, with template B, were recorded as a function of increasing water content and the absorbance ratio values determined.

Comparisons of the UV-vis absorbance ratios for the templated hierarchical self-assembly complex above and the non-templated hierarchical self-assembly are shown in Figures 4.11a (ii) and b(ii) for P(*p*-AT)-**38** and P(*p*-AT)-**29** respectively. In the absence of a template, a stable helical conformation is formed first. Subsequently with increasing strength of the solvophobic driving force, these helices stack. The onset of the tertiary structure is marked by the “kick” in the absorbance ratio from 35 % water. As shown in Figure 4.11a (ii), in the presence of a template, this kick is not observed. This is because, in the presence of a template, the self-assembly already begins as soon as a helical conformation is present. This observation was reproduced when the same experiment was carried out with the chiral P(*p*-AT)-**29**, Figure 4.11b (ii). This showed that the template modifies the hierarchical self-assembly protocols presented in Figure 4.6 from the transition stage of secondary structure formation, to a quaternary structure as illustrated schematically in Figure 4.12.

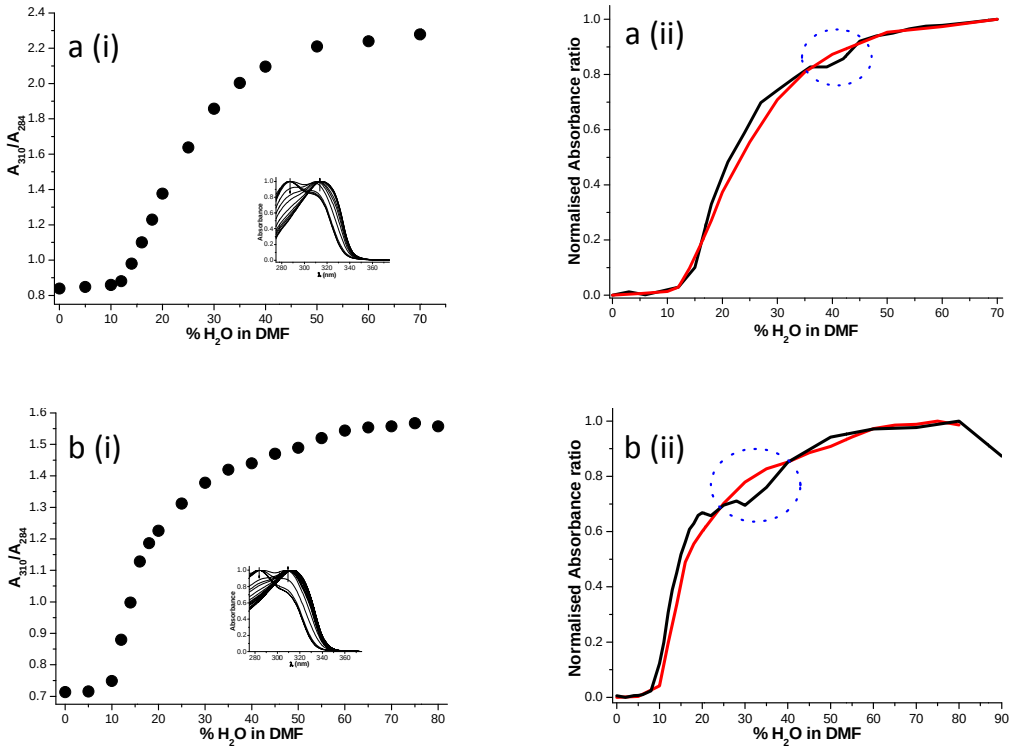

Figure 4.11: UV-vis absorbance ratios, as a function of solvent composition, of the template B complexes with P(*p*-AT)-38 (0.74 µM) and P(*p*-AT)-29 (0.91 µM), [a (i) and b (i), respectively] with respective template B concentrations of 0.028 µM and 0.035 µM, and comparisons of the absorbance ratios in the absence (black) and in the presence (red) of a template B [a (ii) and b (ii)]. Data for black curves in a (ii) and b (ii) was taken from earlier experiments, see Figure 4.2b and Figure 3.9 respectively.

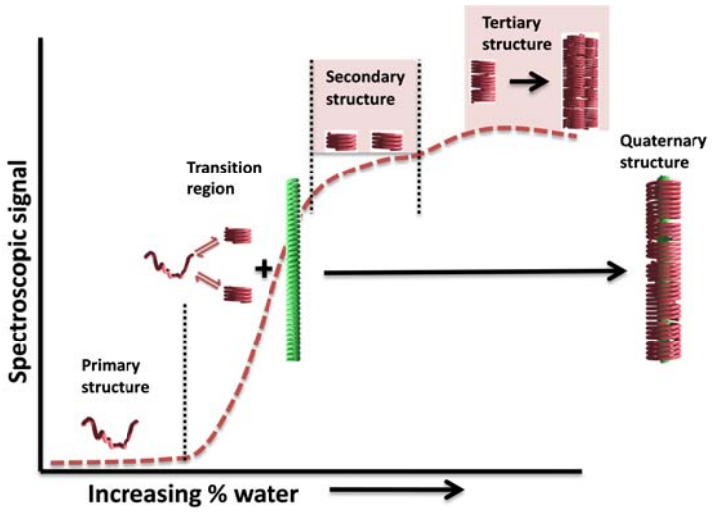

Figure 4.12: Schematic illustration of the template modified hierarchical self-assembly protocols.

The template stabilizes the helical conformation

To get a clearer picture of the stabilization, of the helically folded state, which the templated self-assembly induces, the assembly was studied with the chiral P(*p*-AT)-**29**. The solvent dependent conformational transitions of P(*p*-AT)-**29** are similar to those of P(*p*-AT)-**38**. However, the coil to helix transition mid-point of P(*p*-AT)-**29** occurs at 13 % water in DMF compared to 18 % H_2O in DMF for P(*p*-AT)-**38**. This is attributed to differences in the length of the oEG side chains. P(*p*-AT)-**38** has a hexa-oEG side chain, compared to the tetra-oEG side chain of P(*p*-AT)-**29**. Therefore the former is solubilized better in aqueous DMF solutions and hence requires a greater solvophobic driving force (*i.e.* higher volume fraction H_2O) to induce folding.

The CD spectrum of (P(*p*-AT)-**29** at 13 % H_2O features a weak Cotton effect. Templated self-assembly was expected to result in the stabilization of the helically folded conformer resulting in the evolution of the CD spectrum from a weak Cotton effect to a fully bisignate negative Cotton effect, typical of the stable helical conformation, see Chapter 3. The self-assembly was carried out as before, the concentration of the host foldamer and the solvent composition were kept constant whilst the concentration of the guest PBLG template was gradually increased and monitored by CD spectroscopy, Figure 4.13.

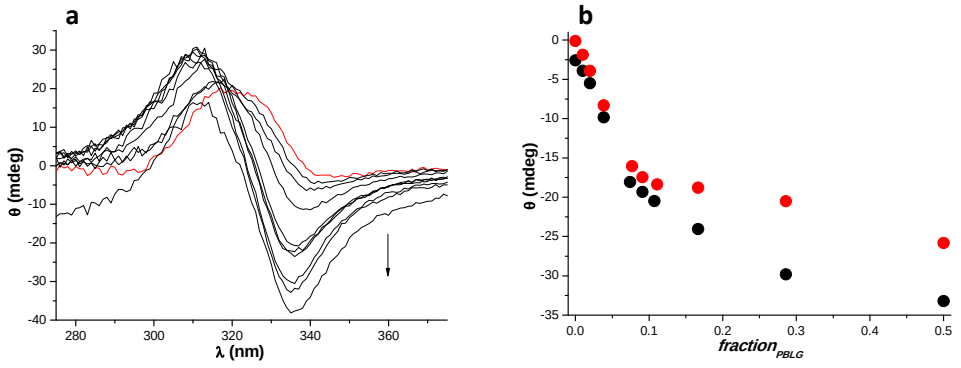

Figure 4.13: Illustration of the stabilizing effect of the template on the helical conformation using chiral P(*p*-AT)-29 (0.86 µM), and template B (0.033 µM) at 13 % H_2O in DMF and a comparison of CD signal intensities from the self-assembly experiments of P(*p*-AT)-29 (black) and P(*p*-AT)-38 (red, in 18 % H_2O in DMF, from Figure 4.9d).

With incremental addition of template, the weak Cotton effect (in red, Figure 4.13a) evolved into a bisignate negative Cotton Effect typical of the stable helices. This affirmed that the templated self-assembly strengthened the helical conformation. A comparison of the CD signal intensities from the complexes formed with the chiral and achiral foldamers showed that the signal intensities from the chiral foldamer system were marginally higher. The deviation between the two systems increased beyond 10 % mole fraction of PBLG. It is tempting to speculate that the physical significance is that it is easier to template with a foldamer that has a chiral bias matching that of the template. It is assumed that the guest PBLG template's screw sense matches that of the chiral P(*p*-AT)-**29** helical foldamer because both the PBLG α-helix and the helically folded P(*p*-AT)-**29** have a negative first Cotton Effect.[35,36] In such a case the self-assembly system has fewer errors to correct from screw sense mismatch.

To complement these findings, TEM analysis was carried out on non-templated P(*p*-AT)-**38** and on the templated self-assembled complexes of P(*p*-AT)-**38**, and templates A and B. In Chapter 3 it was shown that in order to visualize supramolecular stacks of the foldamer helices, by TEM, the samples must be prepared from solutions with a high volume fraction of water so as to stabilize defined assemblies during the TEM sample preparation. It was proposed that the template could stabilize defined supramolecular assemblies of the helical foldamers such that defined morphologies could be visualized from samples prepared from solutions with low volume fractions of water, like 50 % H_2O in DMF (Figure 4.14).

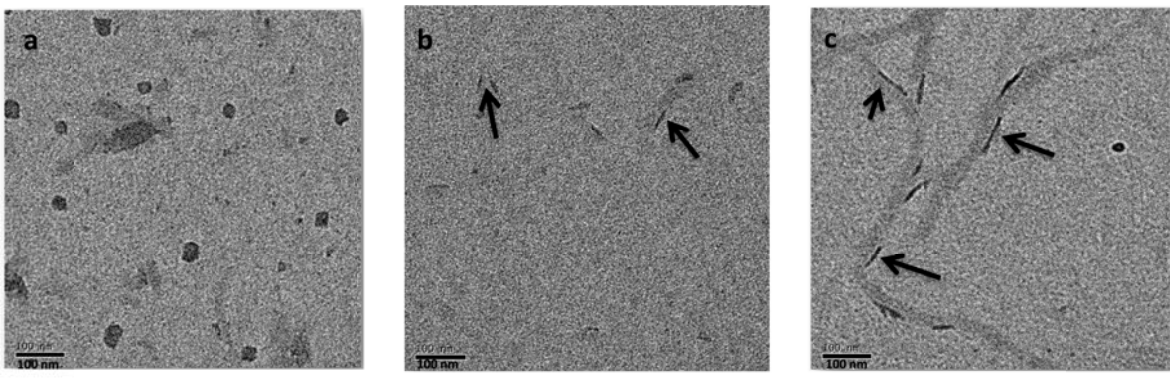

Figure 4.14: TEM images of P(*p*-AT)-38 (1.5 µM) without template (a), and the self-assembled complexes of P(*p*-AT)-38 with template A (b) and template B (c). Samples were prepared in DMF/Water = 1:1.

Without a template, in 50 % H_2O in DMF, no discernible morphologies were observable, except for ill-defined “smudges” (Figure 4.14a). This result was consistent with findings in Chapter 3, 50 % H_2O was not enough to stabilize supramolecular structures during the TEM sample preparation. In the presence of a template, small rod-like morphologies could be observed; with longer rods being observed when template B was used compared to the shorter template A. The presence of a template clearly served to stabilize the defined supramolecular morphologies as evidence by the appearance of rods when the template was present.

Conclusions

A water soluble P(*p*-AT) foldamer was developed. This enabled a full assessment of the hierarchical self-assembly of the P(*p*-AT) helical foldamers without template. Definite evidence for the formation of stable supramolecular stacks of helices, in the solution state, was provided by cryoTEM analysis. The helical foldamers stack into long fibers, which do not intertwine, but instead run parallel to each other. A facile yet elegant templated self-assembly process was developed. It is based on templating of a hydrophobic PBLG into the cavity of the helical foldamer. The subsequent diastereomeric complex was monitored with CD spectroscopy. This strategy was shown to introduce asymmetry as well as to control the lengths of the assembly, for the first time, closely matching the properties of TMV. The template mimicked the role of the RNA in TMV, driving the equilibrium to stable helical stacks of defined lengths.

Experimental

General details

General aspects concerning the synthesis and characterization of the monomer and the polymer, and the analysis of the solvent dependent conformational transition of P(*p*-AT) are the same as described in chapter 3. PBLG polymers were purchased from Sigma Aldrich and used as is. Cryo-TEM was carried out on a FEI Tecnai 20, type Sphera TEM instrument equipped with a LaB_6 filament operating at 200 KV. Sample vitrification was carried out using an automated vitrification robot (FEI Vitrobot™ Mark III). Images were recorded with a bottom mounted Gatan CCD camera. TEM analysis was carried out on the same instrument. A 3 µL sample [1.5 µM] was pipetted on to carbon coated 200 mesh copper grids and stained with 2% aqueous uranyl acetate and air dried. For the complexometric CD titration measurements, two stock solutions of the P(*p*-AT) foldamer host and the PBLG guest were prepared in spectrophotometric grade DMF. Solutions of varying guest concentrations, with constant host concentration, were then prepared and topped up with the appropriate volume of water. The total volume of all the samples was kept constant Samples were vigorously shaken to ensure thorough mixing and allowed to sit for 2 h before recording spectra. For the solvent dependent UV-vis titrations, (depicted in Figure 4.10) host guest concentrations were kept constant and whilst the volume fraction of water was gradually increased. The total volume of all the samples was kept constant. Then samples were shaken vigorously and allowed to sit for 2 h and finally the spectra were recorded. Sample concentrations used are given in the main text.

Synthetic procedures

2-[2-(2-methoxy-ethoxy)-ethoxy]-ethyl p-tosylate (30): was prepared as described in chapter 3, see compound **15**.

2-[2-(2-{2-[2-(2-Methoxy-ethoxy)-ethoxy]-ethoxy}-ethoxy)-ethoxy]-ethanol (32): was prepared as described in literature.[18] ^{1}H NMR (400 MHz, $CDCl_3$) δ: 3.73 – 3.68 (m, 2H), 3.67 – 3.61 (m, 18H), 3.60 – 3.56 (m, 2H), 3.54 – 3.50 (m, 2H), 3.37 (s, 3H). MS (ESI): *m/z* = 297.19 (calculated 297.19 for $[M + H]^+$]), 314.22 (calculated: 314.22 for $[M + NH_4]^+$) and 319.17 (calculated: 319.17 for $[M + Na]^+$).

2-azido-5-iodobenzoic acid (6): was prepared as in chapter 3.

2-[2-(2-{2-[2-(2-Methoxy-ethoxy)-ethoxy]-ethoxy}-ethoxy)-ethoxy]-ethyl 2-azido-5-iodobenzoate (33): To a 100 mL round bottom flask was added **6** (1.10 g, 3.83 mmol), freshly dry distilled THF (50 mL), **32** (1.354 g, 4.57 mmol) and DMAP (0.056 g, 0.46 mmol). The mixture was cooled to 0 ^{o}C in a sodium chloride/ice bath. DCC (0.94 g, 4.60 mmol) was then added in one portion and the reaction ran for an hour at 0 ^{o}C, before being allowed to run at room temperature overnight. Afterwards the reaction mixture was chilled, the white precipitate (dicyclohexylurea side product) filtered off and the crude product was purified by column chromatography (EtOAc = 100 %; R.F. = 0.3) affording **33** (1.63 g, 75.5 %, based on compound **6**) as a pale yellow oil.^{1}H NMR (400 MHz, $CDCl_3$) δ: 8.15 (d, *J* = 2.0 Hz, 1H), 7.78 (dd, *J* = 8.4, 2.0 Hz, 1H), 6.98 (d, *J* = 8.4 Hz, 1H), 4.47 – 4.41 (m, 2H), 3.84 – 3.77 (m, 2H), 3.72 – 3.58 (m, 18H); 3.56 – 3.50 (m, 2H), 3.36 (s, 3H). 13C NMR (400MHz, $CDCl_3$) δ: 163.61, 141.77, 140.30, 139.98, 124.21, 121.64, 87.26, 71.86, 70.53, 70.45, 68.88, 64.57, 58.97. MS (ESI): *m/z* = 585.14 (calculated: 585.14 for $[M + NH_4]^+$), 590.098 (calculated: 590.097 for $[M + Na]^+$).

2-[2-(2-{2-[2-(2-Methoxy-ethoxy)-ethoxy]-ethoxy}-ethoxy)-ethoxy]-ethyl 2-azido-5-[(trimethylsilyl)ethynyl] benzoate (34):

A 50 mL Schlenk flask was charged with the aryl iodide (**33**) (0.75 g, 1.3 mmol), trimethylsilyl acetylene (0.20 g, 2.0 mmol), THF (5 mL) and TEA (5 mL) and the mixture was subjected to two freeze-pump-thaw cycles and backfilled with nitrogen each time. The mixture was then frozen again and the flask filled with nitrogen. The flask was opened and $Pd(PPh_3)_4$ (0.015 g, 0.013 mmol) and CuI (0.0025 g, 0.013 mmol) were quickly added, the flask was immediately sealed and evacuated before being subjected to three freeze-pump-thaw cycles and backfilled with nitrogen. The reaction was worked up as described for **8**

(chapter 3) and purified by column chromatography (ethyl acetate = 100 %) affording 0.61 g (1.1 mmol mmol, 87 %) of the requisite compound **34** and 0.053 g of the amine side product **35** which was converted into the azide **34** as described in chapter 3 in 90 % yield. Spectral data for **34** (aryl azide): ^{1}H NMR (400 MHz, $CDCl_3$) δ: 7.95 (d, *J* = 2.0 Hz, 1H), 7.57 (dd, *J* = 8.4, 2.0 Hz, 1H), 7.15 (d, *J* = 8.4 Hz, 1H), 4.46 – 4.41 (m, 2H), 3.84 – 3.77 (m, 2H), 3.72 – 3.59 (m, 18H); 3.56 – 3.50 (m, 2H), 3.36 (s, 3H), 0.24 (s, 9H). 13C NMR (400MHz, $CDCl_3$) δ: 164.32, 139.95, 136.22, 135.38, 122.42, 119.77, 119.53, 103.04, 95.73, 71.88, 70.60, 70.51, 70.46, 68.96, 64.42, 58.97, -0.19. MS (ESI): *m/z* = 555.29 (calculated 555.28 for $[M + NH_4]^+$), 560.24 (calculated: 560.24 for $[M + Na]^+$). Spectral data for amine side product **35**, ^{1}H NMR (400 MHz, $CDCl_3$) δ: 7.95 (d, *J* = 2.0 Hz, 1H), 7.31 (dd, *J* = 8.4, 2.0 Hz, 1H), 6.56 (d, *J* = 8.4 Hz, 1H), 5.92 (bs, 2H), 4.46 – 4.40 (m, 2H), 3.84 – 3.78 (m, 2H), 3.72 – 3.58 (m, 18H); 3.56 – 3.50 (m, 2H), 3.36 (s, 3H), 0.22. MS (ESI): *m/z* = 512.27 (calculated 512.27 for $[M + H]^+$), 534.25 (calculated: 534.25 for $[M + Na]^+$).

2-[2-(2-{2-[2-(2-Methoxy-ethoxy)-ethoxy]-ethoxy}-ethoxy)-ethoxy]ethyl 2-azido-5-ethynylbenzoate (36): The synthesis of **36** followed the same procedure as for compound **3**, (see chapter 3); using **35** (0.68 g, 1.20 mmol) and TBAF (1 M THF solution, 3.57 mL). The crude product was purified by column chromatography (ethyl acetate = 100 %, R.F. = 0.20) affording **4** (0.52 g, 1.12 mmol, 93 %) as a pale yellow oil. ^{1}H NMR (400 MHz, $CDCl_3$) δ: 7.97 (d, *J* = 2.0 Hz, 1H), 7.59 (dd, *J* = 8.4, 2.0 Hz, 1H), 7.17 (d, *J* = 8.4 Hz, 1H), 4.47 – 4.41 (m, 2H), 3.84 – 3.77 (m, 2H), 3.71 – 3.56 (m, 18H); 3.56 – 3.49 (m, 2H), 3.35 (s, 3H), 3.13 (s, 1H). 13C NMR (400MHz, $CDCl_3$) δ: 164.15, 140.37, 136.35, 135.53, 122.52, 119.89, 118.44, 81.78, 78.48, 71.85, 70.58, 70.50, 70.43, 68.91, 64.47, 58.94. MS (ESI): *m/z* = 483.24 (calculated 483.24 for $[M + NH_4]^+$), 488.189 (calculated: 488.20 for $[M + Na]^+$).

The polymerization and the post polymerization modification followed exactly the same protocol as in Chapter 3.

References

(1) Whitesides, G. M.; Grzybowski, B. *Science* **2002**, *295*, 2418.

(2) Young, M.; Willits, D.; Uchida, M.; Douglas, T. *Annu. Rev. Phytopathol.* **2008**, *46*, 361.

(3) Knez, M.; Bittner, A. M.; Boes, F.; Wege, C.; Jeske, H.; Maiβ, E.; Kern, K. *Nano Letters* **2003**, *3*, 1079.

(4) Douglas, T.; Young, M. *Science* **2006**, *312*, 873.

(5) Xu, Y.; Ye, J.; Liu, H.; Cheng, E.; Yang, Y.; Wang, W.; Zhao, M.; Zhou, D.; Liu, D.; Fang, R. *Chem. Commun.* **2008**, 49.

(6) Creager, A. N. H.; Scholthof, K.-B. G.; Citovsky, V.; Scholthof, H. B. *The Plant Cell Online* **1999**, *11*, 301.

(7) Klug, A. *Phil. Trans. R. Soc. Lond. B* **1999**, *354*, 531.

(8) Klug, A. *Angew. Chem. Int. Ed.* **1983**, *22*, 565.

(9) Lindsey, J. S. *New. J. Chem.* **1991**, *15*, 153.

(10) Whitesides, G. M.; Mathias, J. P.; Seto, C. T. *Science* **1991**, *254*, 1312.

(11) Percec, V.; Heck, J.; Lee, M.; Ungar, G.; Alvarez-Castillo, A. *J. Mater. Chem.* **1992**, *2*, 1033.

(12) Percec, V.; Heck, J.; Tomazos, D.; Falkenberg, F.; Blackwell, H.; Ungar, G. *J. Chem. Soc. Perkin Trans. 1* **1993**, 2799.

(13) Rudick, J. G.; Percec, V. *Acc. Chem. Res.* **2008**, *41*, 1641.

(14) Bull, S. R.; Palmer, L. C.; Fry, N. J.; Greenfield, M. A.; Messmore, B. W.; Meade, T. J.; Stupp, S. I. *J. Am. Chem. Soc.* **2008**, *130*, 2742.

(15) Doty, P.; Bradbury, J. H.; Holtzer, A. M. *J. Am. Chem. Soc.* **1956**, *78*, 947.

(16) Russo, P. S.; Miller, W. G. *Macromolecules* **1984**, *17*, 1324.

(17) Stone, M. T.; Fox, J. M.; Moore, J. S. *Org. Lett.* **2004**, *6*, 3317.

(18) Stone, M. T.; Moore, J. S. *Org. Lett.* **2004**, *6*, 469.

(19) van Dijk, M.; Mustafa, K.; Dechesne, A. C.; van Nostrum, C. F.; Hennink, W. E.; Rijkers, D. T. S.; Liskamp, R. M. J. *Biomacromolecules* **2007**, *8*, 327.

(20) Odian, G. *Principles Of Polymerization*; Fourth ed.; Wiley Interscience: New Jersey, 2004.

(21) Flory, P. J. *Principles Of Polymer Chemistry*; Cornell University Press: Ithaca, 1953.

(22) Prince, R. B.; Saven, J. G.; Wolynes, P. G.; Moore, J. S. *J. Am. Chem. Soc.* **1999**, *121*, 3114.

(23) Brunsveld, L.; Meijer, E. W.; Prince, R. B.; Moore, J. S. *J. Am. Chem. Soc.* **2001**, *123*, 7978.

(24) Chan, H. S.; Bromberg, S.; Dill, K. A. *Phil. Trans. R. Soc. Lond. B* **1995**, *348*, 61.

(25) Pace, C. N.; Scholtz, J. M. In *Protein Structure: A Practical Approach*; Second ed.; Creighton, T. E., Ed.; IRL Press: Oxford, 1997, p 299.

(26) Jonkheijm, P.; van der Schoot, P.; Schenning, A. P. H. J.; Meijer, E. W. *Science* **2006**, *313*, 80.

(27) Smulders, M. M. J.; Nieuwenhuizen, M. M. L.; de Greef, T. F. A.; van der Schoot, P.; Schenning, A. P. H. J.; Meijer, E. W. *Chem. Eur. J.* **2010**, *16*, 362.

(28) Pauling, L.; Corey, R. B. *Proc. Natl. Acad. Sci.* **1951**, *37*, 235.

(29) Lecommandoux, S.; Achard, M.-F.; Langenwalter, J. F.; Klok, H.-A. *Macromolecules* **2001**, *34*, 9100.

(30) Mecozzi, S.; Rebek, J. *Chem. Eur. J.* **1998**, *4*, 1016.

(31) Parry, D. A. D.; Elliot, A. *Nat. Protocols* **1965**, *206*, 616.

(32) MacCarthy, P. *Anal. Chem.* **1978**, *50*, 2165.

(33) Hill, Z. D.; MacCarthy, P. *J. Chem. Educ.* **1986**, *63*, 162.

(34) Connors, K. A. *Binding Constants: The Measurement of Molecular Complex Stability*; John Wiley New york, 1987.

(35) Simmons, N. S.; Cohen, C.; Szent-Gyorgyi, A. G.; Wetlaufer, D. B.; Blout, E. R. *J. Am. Chem. Soc.* **1961**, *83*, 4766.

(36) “Chapter 3, this work..”

Chapter 5. Mechanistic insights into the templated self-assembly system

Introduction

In the preceding chapters a detailed description of the hierarchical information transfer in the solvent dependent self-assembly of helical P(*p*-AT) foldamers was described. A picture of the structural subunits involved in the non-templated self-assembly system is now clear, however, the mechanistic picture of the templated self-assembly process remains unclear. Intuitively, two routes can be imagined:

I. A guest template directly threads itself into the cavity of the helically folded P(*p*-AT) or

II. A transiently unfolded P(*p*-AT) wraps itself helically around the guest template.

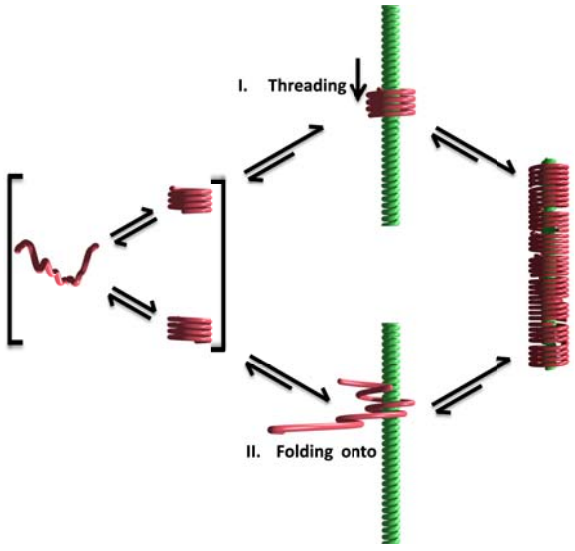

Scheme 5.1: The two possible routes for the templated self-assembly.

A similar question has been posed before by Moore and coworkers in their work on the molecular association between *m*PE foldamers and rod-like small guest molecules.[1] In their studies, they proposed a dynamic pathway in which both mechanisms were possible. To validate approach II, the authors used a dumbbell shaped template, with end-groups bigger

than the diameter of the cylindrical cavity of the host helical foldamer. This architectural blocking prevented the guest rod from directly threading itself onto the template as with route I. Despite this physical obstruction, assembly occurred, as confirmed by CD spectroscopy studies. This assembly could only have occurred via route II.

Stoddart and coworkers showed that single walled carbon nanotubes could be solubilized in aqueous solutions by wrapping starch around them.[2] The relevance of their work to this discussion is in the fact that the complexation only occurred when the starch had been preorganized into a helical conformation. The nanotube then directly threaded itself into the cavity of the helix, forcing out small solvent molecules inside.[2] This is in-line with route I.

Kinetic assessment of the self-assembly

The dynamics of the complexation between the P(*p*-AT)-**38**, and the PBLG template B were examined in order to better understand the assembly mechanism. In the experiment, water was added to a DMF solution of P(*p*-AT)-**38** and the PBLG template to give an 18 % H_2O in DMF solution, and then the time dependent CD and UV-vis spectra were recorded 60 seconds after mixing. The molar ratios, of P(p-AT)-**38** to PBLG, used were calculated give the $N^{P(p\text{-AT})}$ required to fully entrap the PBLG template B.

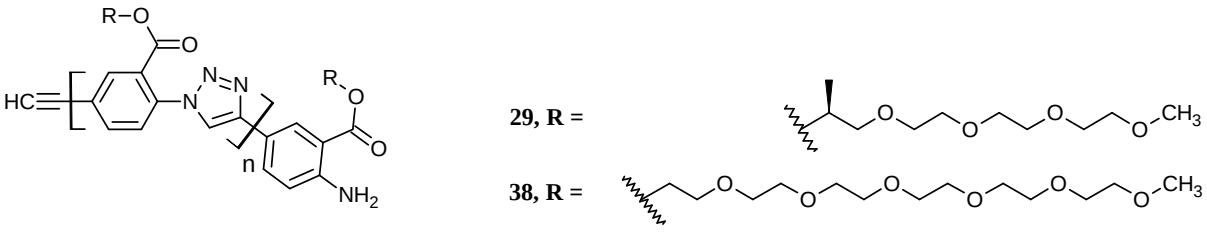

Figure 5.1: Structures of the P(*p*-AT)s used for the mechanistic studies.

Figure 5.2a (black curve) highlights that a diastereomeric bias, implying complexation between P(*p*-AT)-**38** and PBLG, was observed for the first measurement, which was acquired after 60 seconds. The recorded ellipticity, at 333 nm, only increased by ~15 %, in the first ~ 1 000 s and did not change appreciably afterwards.

The change in the concomitant UV-vis spectra from the experiment described above was also analyzed. In Chapter 3 it was demonstrated that the absorption bands at 310 nm and

284 nm are sensitive to backbone conformation. Hypochromicity of the latter band can be related to polymer backbone folding into a helical conformation. An increase in the absorbance ratio A_{310}/A_{284}, as a function of % H_2O in DMF, can be correlated to this conformational transition and in turn to the stability of the helically folded conformation. Figure 5.2b shows that higher absorbance ratios were realized for the templated self-assembled systems than for the non-templated system (black curve vs. the blue curve). This increased absorbance ratio implies an increase in the hypochromicty of the absorbance band at 284 nm, which indicates an increased stability of the helically folded conformation.

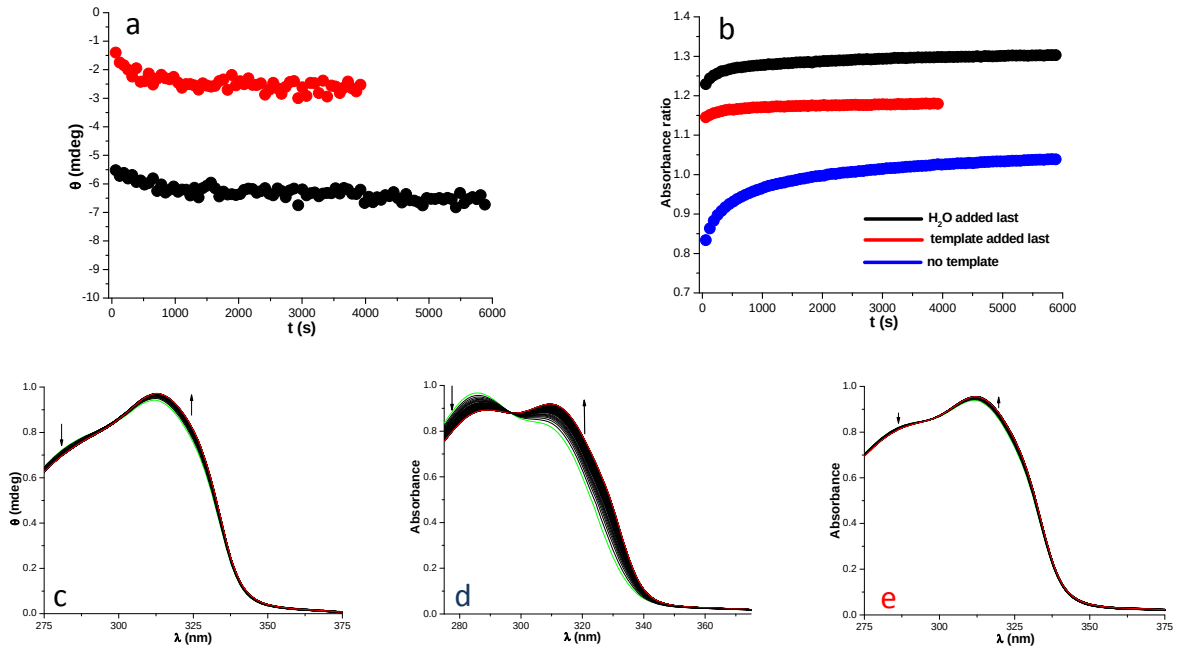

Figure 5.2: Kinetics of the complexation between P(*p*-AT)-38 [0.75 µM] and PBLG template [0.026 µM] in 18 % H_2O in DMF, monitored by (a) CD spectroscopy tracking the negative extremum, of the CD couplet, at 333 nm (black symbols: water added last, red symbols: template added last*) and (b) UV-vis spectroscopy tracking the absorbance ratios (A_{310}/A_{284}) determined from the concomitant UV-vis spectra (blue symbols: template free P(*p*-AT)-38 [0.75 µM] system) . Figures c (water added last), d (no template) and e (template added last), show the actual absorption curves from which the absorbance ratios were determined.

*In this variant of the kinetic experiments, the template was added last to an aqueous DMF solution of P(*p*-AT)-**38** and the subsequent CD and UV-vis spectra recorded as a function of time. This was done so as to underscore a practical consideration in the sample preparation for this self-assembly system. The recorded ellipticity at 333 nm and the UV-vis absorption ratios were lower than when water was added last to a DMF solution of the template and P(*p*-AT)-**38** (red curves, Figure 5.2) because the hydrophobic character of the PBLG template limited its availability for self-assembly since it precipitates when added to aqueous DMF solutions.

The discussion above qualitatively relates the kinetic data of the absorbance ratios to an ensuing, increasing stability of the helical conformation, due to templated self-assembly. It is also apparent, however, that helical stability rapidly increased, within the first 1 000 s, consistent with time-dependent CD spectroscopy experiments. This indicates that the self-assembly between the helical P(*p*-AT) foldamers and PBLG is a rapid process, consistent with a direct threading through process.[1] A direct threading process requires the helical folded conformation, threading onto the template, consistent with approach I (Scheme 5.1). This is akin to the self-assembly of pseudo-rotaxanes.[3]

Assessment of dynamic character of the templated self-assembly system

In Chapter 4 it was proposed that the highest diastereomeric bias, implying the most efficient complex formation, is obtained when the templated self-assembly system operates in a dynamic equilibrium. This entails using a solvent system in which the P(*p*-AT) rapidly interconverts between the helically folded and the unfolded conformations. The template-mediated self-assembly was therefore assessed as a function of solvent composition. It was expected that maximum CD signal intensity would be obtained at the solvent composition at which a dynamic equilibrium between the random coil and the helical conformation exist. Maximum CD signal amplitude would imply optimum self-assembly conditions.

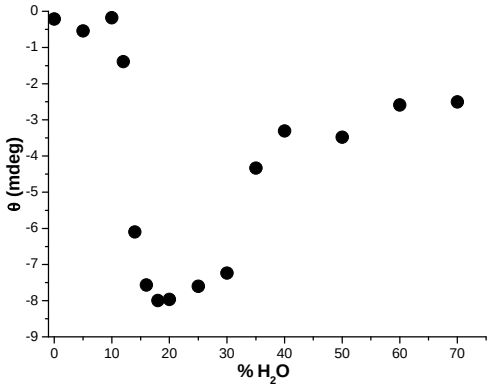

Figure 5.3: Solvent titrations of the optimum stoichiometry P(*p*-AT)-38 [0.75 µM] - PBLG template B [0.026 µM] complex showing plot of CD signal at 333 nm.

Figure 5.3 shows the plot of the negative extremum of the CD couplet as a function of % H_2O in DMF for P(*p*-AT)-**38** in the presence of the template. Solutions below 10 % H_2O in DMF were CD silent since in this solvent regime, P(*p*-AT)-**38** exists as a random coil and the

requisite helical subassembly is not yet constituted. Upon slightly increasing the solvent composition beyond 10 % H_2O, the CD signal intensity increased sharply and leveled off at 18 % H_2O, then sharply decreased between 30 and 35 % H_2O and appeared to level off again above 35 % H_2O. The coil to helix transition mid-point for P(*p*-AT)-**38** occurs at 18 % H_2O in DMF and a maximum negative extremum was observed also in this solvent composition for the self-assembled complex. The above observation confirmed that this was the ideal solvent system for the templated self-assembly for the achiral P(*p*-AT)-**38.**

P(*p*-AT)-**38** has no chiral bias. Therefore it folds into an equal population of both left and right-handed helices. The dynamic equilibrium between the two helical screw senses, in 18 % H_2O, ensures a continuous presence of helical conformers with a matching screw sense into which the template can thread. The template then interacts more favorably with the helical P(*p*-AT)-**38** with a matching screw sense, driving the overall equilibrium towards a chiral self-assembled complex (green arrow route, Scheme 5.2), with a diastereomeric excess. The highest CD activity was therefore observed in this solvent system.

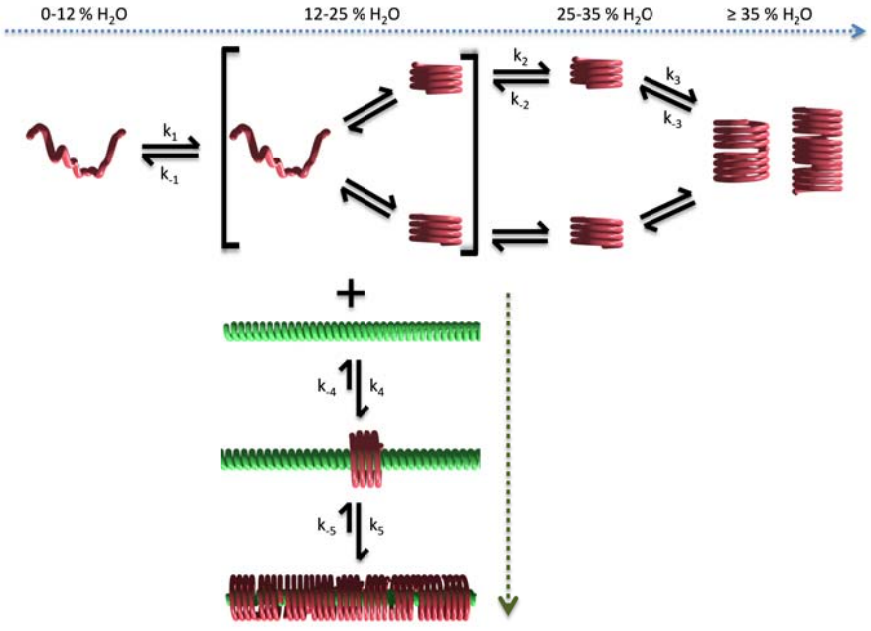

Scheme 5.2: The hierarchical self-assembly protocols of P(*p*-AT)-38, solvent mediated (blue arrow route) and template mediated (green arrow route).

In solutions with higher water volume fractions, above 18 % H_2O, the desire of the template to thread is greater, due to a stronger solvophobic driving force. The dynamic character,

however, is lower, *i.e.* $k_2 > k_{-2}$ goes to $k_2 >> k_{-2}$ (blue arrow route, Scheme 5.2). This is because the helical conformation is better stabilized, by solvophobic forces and subsequently by self-assembly of the helices (blue arrow route, Scheme 5.2). The helices are essentially trapped and cannot readily unwind back to an unfolded polymer, and the balance imparted by a dynamic character is lost to the self-assembly system. Upon threading onto the template, the concentration of the matching chiral foldamer is depleted, but cannot be replenished since the more strongly solvophobic environment prevents unfolding. The templated self-assembly system therefore falls into a kinetic trap, with a reduction of the dynamic equilibrium character and hence the CD signal intensity levels above 18 % H_2O.

The drastic decrease in CD signal intensity observed from 35 % H_2O in DMF is perhaps attributable to two causes. First the kinetic traps, induced by the more strongly solvophobic environment mentioned above. The second cause is a more practical issue. It is possible that some of the hydrophobic template can precipitate out of solution before it can thread, reducing its effective concentration. During the sample preparation, particularly of solutions with volume fractions of water greater than 30 %, great care was taken to add the water to the DMF solutions as slowly as possible to minimize the presumed precipitation of the template.

To verify the conclusions above, the solvent dependency of the CD signal intensity, in the templated self-assembly system, was also measured using the chiral P(*p*-AT)-**29** helical foldamer (Figure 5.4a).

Solutions below 10 % H_2O were CD silent as expected (Figure 5.4a), since the helical conformer was not yet constituted. A rapid increase in CD activity was observed between 10 and 25 % H_2O, the maximum negative extremum being realized between 25 – 30 % H_2O, before leveling and slowly decreasing in magnitude with further increments in volume fraction of water.

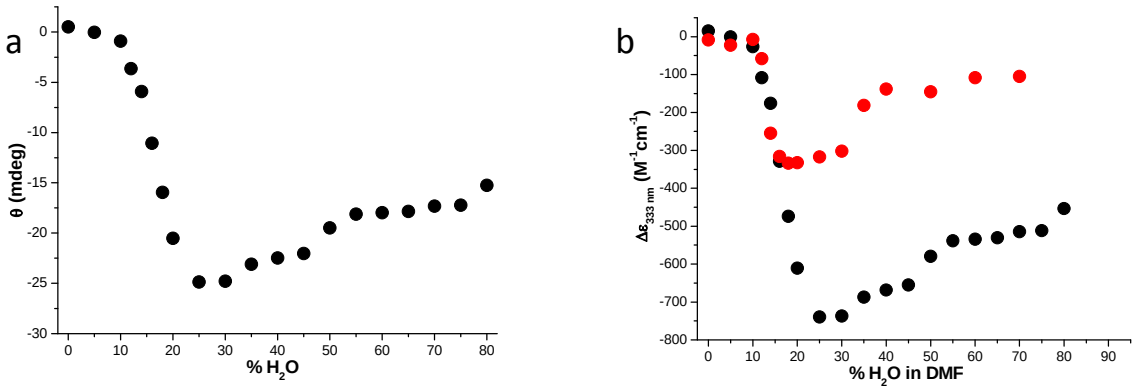

Figure 5.4: Solvent titrations of the optimum stoichiometry P(*p*-AT)-29 [0.98 µM] - PBLG template B [0.035 µM] complex* showing CD signal of the negative extremum, at 333 nm, as a function of water content (a) and an overlay of the plots from Figure 5.3 and 5.4a in the form differential molar ellipticity (Δε)♦,4 at 333 nm of the template B complexes of the chiral P(*p*-AT)-29 (black) and the achiral P(*p*-AT)-38 (red) (b).

The coil to helix transition mid-point of P(*p*-AT)-**29** falls at 13 % H_2O in DMF, individual helices are stable between 25 – 30 % H_2O and self-assembly/stacking of the helices begins from ≥ 30 % H_2O in DMF (blue arrow route, Scheme 5.3). In Figure 5.4a the maximum negative extremum, however, was realized at 25 – 30 % H_2O. This suggested that, with helical P(*p*-AT)-**29**, threading/self-assembly was optimum when carried in a solvent regime with stable individual helices. This is contrary to the system with the achiral P(*p*-AT)-**38**, whereby the maximum CD activity was observed in the solvent regime at the transition mid-point for P(*p*-AT)-**38**'s coil to helix transition. As remarked in Chapter 4, the screw senses of the guest PBLG template and the chiral host P(*p*-AT)-**29** helical foldamer are assumed to be the same because both the helices have a negative first Cotton Effect.[5,6] These results indicated that optimum self-assembly is realized with (firstly) a stable host helical foldamer conformation with (secondly) a matching screw sense as the guest template. The former requirement lends credence to the earlier assertion that the guest template threads into the hollow of the host helices. Under dynamic equilibrium conditions for P(*p*-AT)-**29**, in 13 % H_2O in DMF, the effective concentration of the helical foldamers is lower; therefore, the

* The M_n of P(*p*-AT)-**29** used for the experiment in Figure 5.4 was 31 348 g/mol (see Table 1, entry 2 Chapter 4). The thickness of its helical foldamer disk (*h*) is 2.17 nm. The rod length of the PBLG template B is 63.3 nm, therefore the theoretical $N^{P(p\text{-AT})}$ is 29.2. The experimental $N^{P(p\text{-AT})}$, according to the molar ratios, given in Figure 5.4, is 28.

♦ The CD spectra, recorded as ellipticity (θ) in millidegrees, was converted to Δε using the equation Δε = θ/32980*c*l, where c is the concentration in mol/l and l is the path length (= 1 cm). Δε has units of $M^{-1}cm^{-1}$.

recorded CD activity is lower. With stable individual helices, however, of a matching screw sense, as with P(*p*-AT)-**29** in 25 – 30 % H_2O in DMF, the effective concentration of helical foldamers is higher hence threading/self-assembly is optimum (green arrow route, Scheme 5.3).

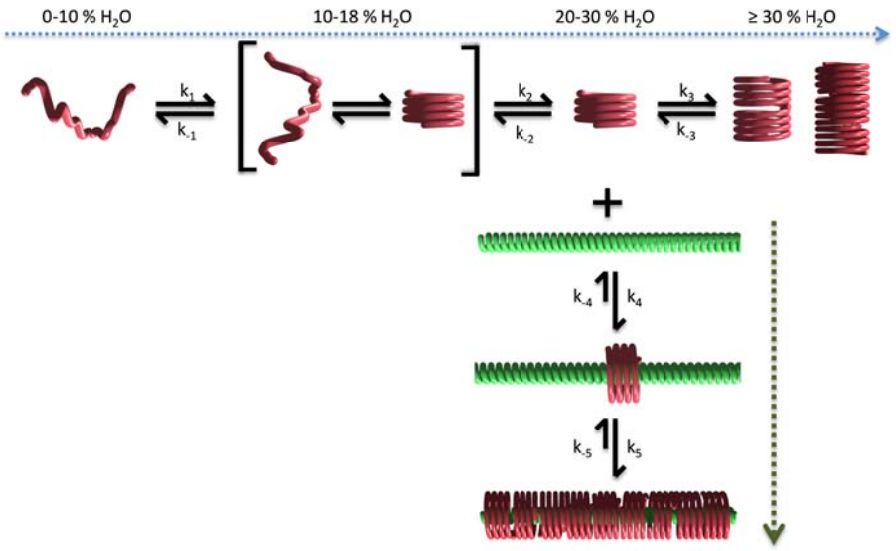

Scheme 5.3: The hierarchical self-assembly protocols of P(*p*-AT)-29, solvent mediated (blue arrow route) and template mediated (green arrow route).

This system can therefore be considered to be similar to pseudo-rotaxanes in which the helically folded disk is the rotor and the PBLG template is the axle.[3] With the assumption of a threading through, pseudo-rotaxane like, self-assembly mechanism, the resultant supramolecular structure is akin to main chain polyrotaxanes formed between cyclodextrins and linear polymers, pioneered by Harada. In this instance the helically folded conformer is the "rotor" whilst the polypeptide template is the axle.[7-10]

CD activity (Figure 5.4a) gradually decreased beyond 30 % H_2O in DMF. It is likely that this was a practical issue, *i.e.* that some of the hydrophobic template perhaps precipitated out of solution, because of the more strongly solvophobic environment, before it could thread, reducing its effective concentration. As remarked before, during the sample preparation, particularly of solutions with volume fractions of water greater than 30 %, great care was taken to add the water to the DMF solutions as slowly as possible to minimize the presumed precipitation of the template.

Figure 5.4b shows an overlay of the plots from Figures 5.3 and 5.4a, plotted as differential molar ellipticity (ΔƐ) so as to overcome the dependency of the magnitude of the CD signal on the sizes and the concentration of the two different host polymers, P(*p*-AT)s **29** and **38**. P(*p*-AT)s **29** and **38** have different side chains, which do not exactly represent a perfect homologous series. The aryltriazole backbones, however, are the same and they undergo similar solvent dependent coil to helix transitions, with similar UV-vis spectroscopic signatures, therefore the comparisons are reasonable. Figure 5.4b (red) shows that when a foldamer without a chiral bias was used (*i.e.* P(*p*-AT)-**38**), the intensity of the Cotton Effect was approximately 50 % of the Cotton Effect obtained when the foldamer had a matching screw sense (*i.e.* with P(*p*-AT)-**29**) with the guest template.

The achiral P(*p*-AT)-**38** helix folds into an equal population of M and P helices, whilst the chiral P(*p*-AT)-**29** helix folds into M helices (see Chapter 3). In the P(*p*-AT)-**38** system, it is likely that the desire of the hydrophobic PBLG template to avoid the unfavorable solvent conditions results in it threading into the host helices faster than it can discriminate against the helical foldamer screw sense. It is suggested that this imbalance in the self-assembly system can be corrected by increasing the amount of template. This is because in the continuous variation plots in Figure 4.12, Chapter 4, comparable ellipticity values, as a function of template concentration, are obtained for the templated self-assembled complexes of P(*p*-AT)-**38** and P(*p*-AT)s-**29**. Since P(*p*-AT)-**29** and PBLG are assumed to have the same screw sense, the $\Delta\varepsilon_{333\ nm}$ value of the P(*p*-AT)-**29** system in 25 % H_2O can be assumed to represent a templated self-assembled construct with a 100 % screw sense match. In 25 % water both P(*p*-AT)-**29** and P(*p*-AT)-**38** are proposed to exist as stable helices, based on the solvent dependent UV-vis absorbance ratio profiles (see Chapters 3 and 4 respectively). Then, when the $\Delta\varepsilon_{333\ nm}$ values of the constructs for both P(*p*-AT) **29** and P(*p*-AT)-**38** foldamers in 25 % H_2O, in Figure 5.4, are compared (737 $M^{-1}cm^{-1}$ and 318 $M^{-1}cm^{-1}$ respectively) the ability of the template to discriminate against a mismatching foldamer screw sense mismatch is approximately 70 %.

Temperature dependent unfolding and refolding

To obtain a deeper view on the mechanism of the templated self-assembly system, between helical P(*p*-AT) foldamers and PBLG, variable temperature (VT) CD and UV-vis spectroscopy studies were carried out, using the P(*p*-AT)-**38**/PBLG-template B complex, Figure 5.5.

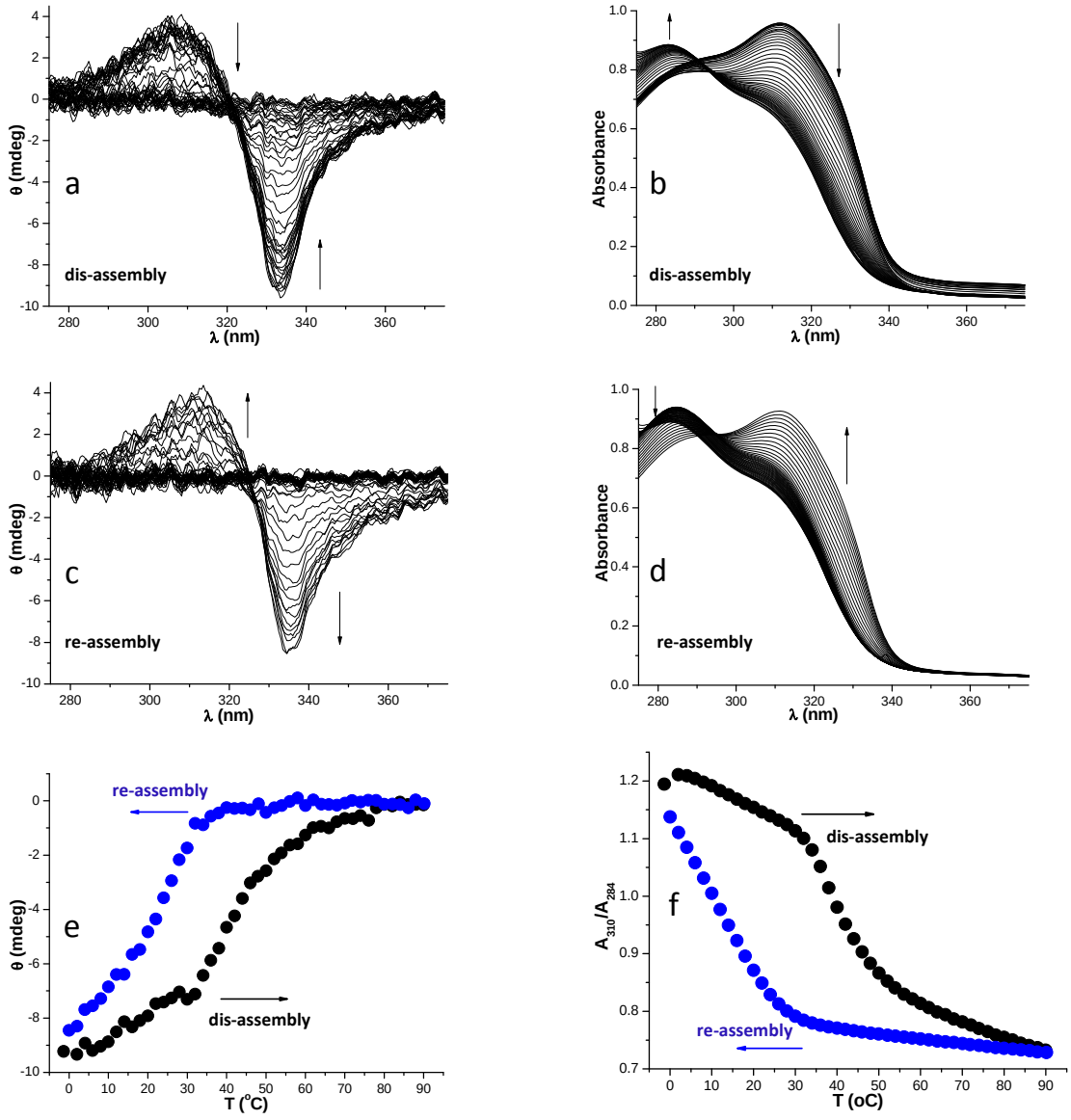

Figure 5.5. Dis-assembly and re-assembly of the self-assembled P(*p*-AT)-38 [7.50 µM]/PBLG template B [0.26 µM] complex studied by VT CD and VT UV-vis spectroscopy showing the decrease in CD activity with increasing temperature (a), the reverse increase in CD activity on cooling (c) and the resultant plot of the CD signals at 333 nm as a function of temperature (e). Figures 5.5b, d and f show the concomitant UV-vis spectra and the resultant absorbance ratios (A_{310}/A_{284}) plot respectively. A temperature gradient of 0.5 °C/minute was used between 0 and 90 °C.

Temperature dependent dis-assembly and re-assembly was monitored between 0 and 90 ^{o}C. CD signal intensity decreased with heating, Figure 5.5a, and recovered upon cooling, Figure 5.5c. A temperature gradient of 0.5 ^{o}C/min was used for both the heating and the cooling ramps. Initially a temperature gradient of 1 ^{o}C/min was used for both the heating and the cooling transitions. CD activity, however, was not fully recovered (only 50 % of original value) because the rate of cooling was too fast.

Figure 5.5a shows that receding CD signals went through an isodichroic point, indicating that the disassembly was a transition between two well-defined conformational states. Reassembly, on cooling, also went through an isodichroic point (Figure 5.5c) which also indicated that the process involved well defined states, *i.e*. the α-helical PBLG and helically folded P(*p*-AT)-**38**. These results indicate that the helical P(*p*-AT)-**38** foldamer threads off from the template and then unfolds, rather than unfolding whilst on the template. This is similar to the "threading off" of a rotaxane from its axle. In the same vein, during reassembly, the template threads into a folded P(*p*-AT) rather than the P(*p*-AT) folding onto the template, similar to "threading on" of rotaxanes.

The sigmoidal shape of the unfolding curve, Figure 5.5e, indicated that this process is cooperative.[11] This is expected since if the P(*p*-AT) foldamers at the ends of the template come off, it becomes progressively easier for the helical foldamer disks in the middle, which have better π – π stacking interactions between them, to thread off as well.

The concomitant UV-vis spectra were analyzed. In a stable helically folded P(*p*-AT)-**38**, the band at 310 nm is maximum whilst the band 284 nm is a shoulder. The reverse is true for the unfolded conformation. The band at 310 nm attenuated, with increasing temperature, whilst the band at 284 nm increased in intensity, Figure 5.5b. This evolution in band shape was reversed with cooling, Figure 5.5d. The plot of the subsequent absorbance ratios also exhibited a sigmoidal behavior for the disassembly step and a large hysteresis during the reassembly step, consistent with the findings from the VT-CD analysis, Figure 5.5e. The reassembly, upon cooling, also displayed hysteresis, in agreement with the CD analysis.

A comparison of Figures 5.5f and e, during the cooling step (blue curves), indicates that CD signal intensity and the absorbance ratio began to increase below 35 ^{o}C, which was

coincident with the appearance of CD activity. An increase in the absorbance ratio indicates strengthening of the helical folded conformation, which implies that as soon as a helically folded conformer became available it threaded onto the template polymer, as viewed from the CD experiment, and was stabilized, as evidenced by the UV-vis analysis. With further cooling more helically folded conformers become available for the self-assembly.

The reassembly process was not cooperative, which is expected since the helical P(*p*-AT)-**38** foldamers cannot physically assist each other during the assembly process. They cannot "queue up" one behind the other and "nudge"/push each other forward whilst the template threads through in the opposite direction. The increased stability of the templated foldamers (as indicated by the increasing absorbance ratio) indicates that once templated, there was a gain in stabilization from favorable interactions between foldamer helices in the stack and the template. This is further aided by the desire of the template to avoid unfavorable solvophobic interactions from solution.

Possible cause of the hysteresis

The observed hysteresis upon cooling probably emanated from an absence of helically folded conformers above 35 ^{o}C. It was rationalized that upon increasing the desire of the foldamer to fold, the hysteresis would be reduced or removed. The helical folded conformation can be stabilized by increasing the strength of the solvophobic driving force, *i.e*. by increasing the volume fraction of water in DMF. A series of VT CD and VT UV-vis spectroscopy experiments were carried out at various % H_2O in DMF. It was anticipated that increasing the % H_2O would stabilize the threaded off helical P(*p*-AT) foldamers more against thermal denaturation resulting in a smaller hysteresis loop.

Indeed when the temperature dependent dis-assembly and re-assembly experiments were carried out in higher % H_2O solutions, a marked change in the profiles of CD signal intensity, as a function of temperature, was observed (Figure 5.6). The hysteresis loop became smaller going from 18 % H_2O to 25 % H_2O; it was barely discernible at 30 % H_2O and was completely removed at 40 % H_2O. From a comparison of figures 5.6a and b, it is clear that the increase in % H_2O resulted in a better stabilization of the threaded-off folded helices, in solution. In

the cooling/re-assembly step this resulted in an earlier onset of threading-on/self-assembly as evidenced by smaller hysteresis loop in 25 % H_2O.

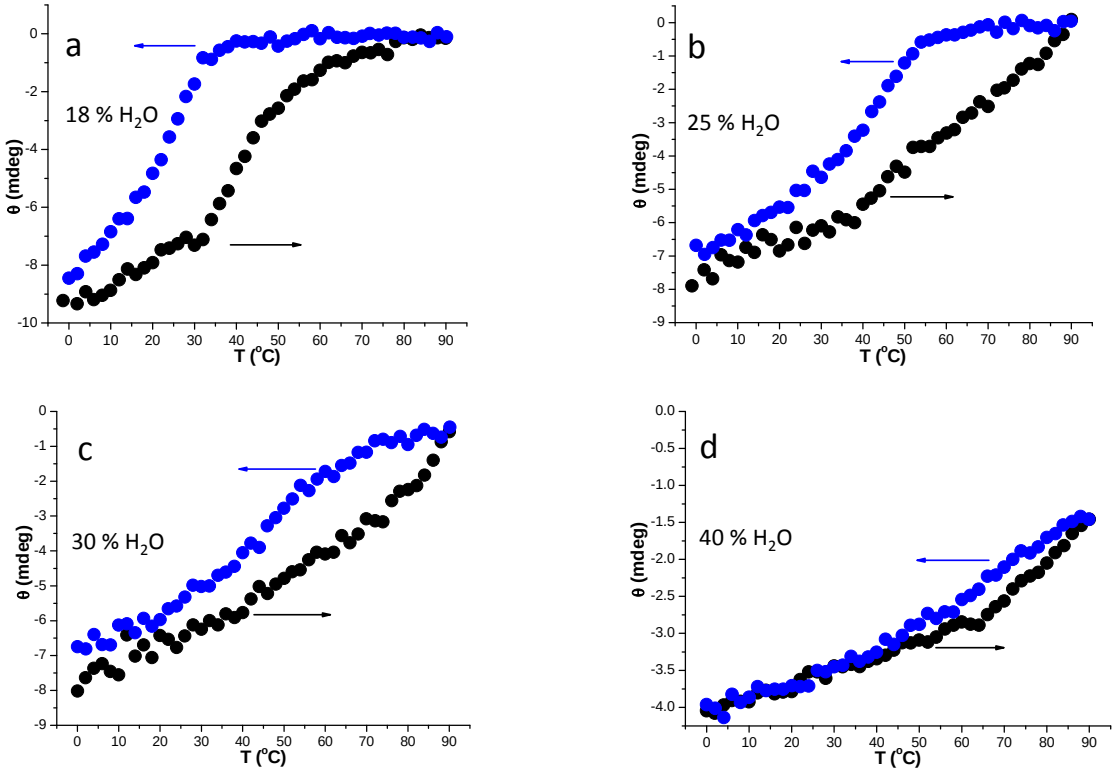

Figure 5.6. Disassembly and reassembly of the self-assembled P(*p*-AT)-38 [7.50 µM]/PBLG template B [0.26 µM] complex studied by VT-CD as a function of % H_2O in DMF, tracking the CD signal at 333 nm. Heating transitions are indicated by black curves and cooling transitions by blue curves. A temperature gradient of 0.5 °C/minute was used between 0 and 90 °C.

In 25 % water, Figure 5.5b, the temperature dependent disassembly profile is clearly not cooperative, but rather the CD signal intensity decreased gradually across the whole temperature range. A similar trend was observed in 30 % H_2O and in 40 % H_2O. It is likely that by increasing the solvophobic force, the threading off is also more unfavorable for the hydrophobic PBLG template, hence the loss of cooperativity in the threading off step. This conclusion was supported by the fact that in 40 % H_2O the CD signal intensity decreased by ~ 63 %, and not by 100 % as in 18 % H_2O and in 25 % H_2O. The apparent cause of this phenomenon will be addressed in the following section. The much greater solvophobic environment in 40 % H_20 prevented complete disassembly.

The absorbance ratio plots generated from the VT UV-vis spectra for the 18 % H_2O and the 25 % H_2O systems, Figures 5.7a and b, concurred with the findings in Figures 5.6a and b. The

hysteresis loop was clearly smaller in 25 % H_2O than in 18 % water. In the latter, the absorbance ratios, blue curves, began increasing below 40 ^oC, compared to 60 ^oC in the former. This confirmed that helical stability is higher in 25 % H_2O than in 18 % H_2O, as expected due to the increased volume fraction of water in the former solvent system. Therefore the interaction between the P(*p*-AT) and PBLG was observed at a higher temperature.

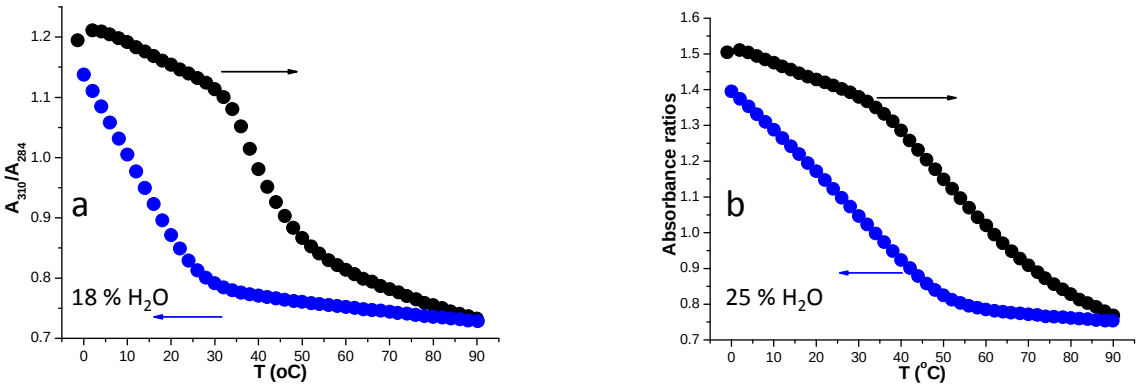

Figure 5.7. Disassembly and reassembly of the self-assembled P(*p*-AT)-38 [7.50 µM]/PBLG template B [0.26 µM] complex studied by VT UV-vis as a function of % H_2O in DMF, tracking the absorbance ratio (A_{310}/A_{284}). Heating transitions are indicated by black curves and cooling transitions by blue curves. A temperature gradient of 0.5 ^oC/minute was used between 0 and 90 ^oC.

Tenative evidence for interaction of the self-assembled complexes in higher water contents

In the preceding section, in Figure 5.6c and d, VT-CD analysis showed an incomplete loss of CD signal with increasing temperature in 40 % H_2O. On face value it would imply that the complex simply did not completely dissociate, *i.e*. not all helical P(*p*-AT)s threaded off and unfolded in solution with increasing temperature. Although this is probably true, there is also the possibility that the self-assembled P(*p*-AT)-PBLG complexes further interact either end-on end or bundled together, in higher % H_2O solvent ratio. At these solvent values the temperature increase is required first to disrupt the higher order assemblies and then disrupt the pseudo-rotaxane assemblies. This possibility was assessed by comparing the VT UV-vis spectra in 18, 25, 30 % and in 40 % H_2O in DMF, Figure 5.8a and b, for the dis-assembly step.

The UV-vis spectroscopic signature for a helically folded structure is the band at ~ 310 nm whilst the band at ~ 284 nm is a minor shoulder (Figure 3.11a, Chapter 3). The UV-vis curves in green are the initial curves at the beginning of the experiment at 0 °C whilst the curves in red are the final curves at 90 °C (Figure 5.8). In Figure 5.8a, the UV-vis absorption spectra evolved from a maximum at 310 nm and a shoulder at 284 nm to having the band at 284 nm as the maximum and the band at 310 nm as a minimum, with increasing temperature. This was consistent with a complete threading off first and then unfolding of the P(*p*-AT) helices.

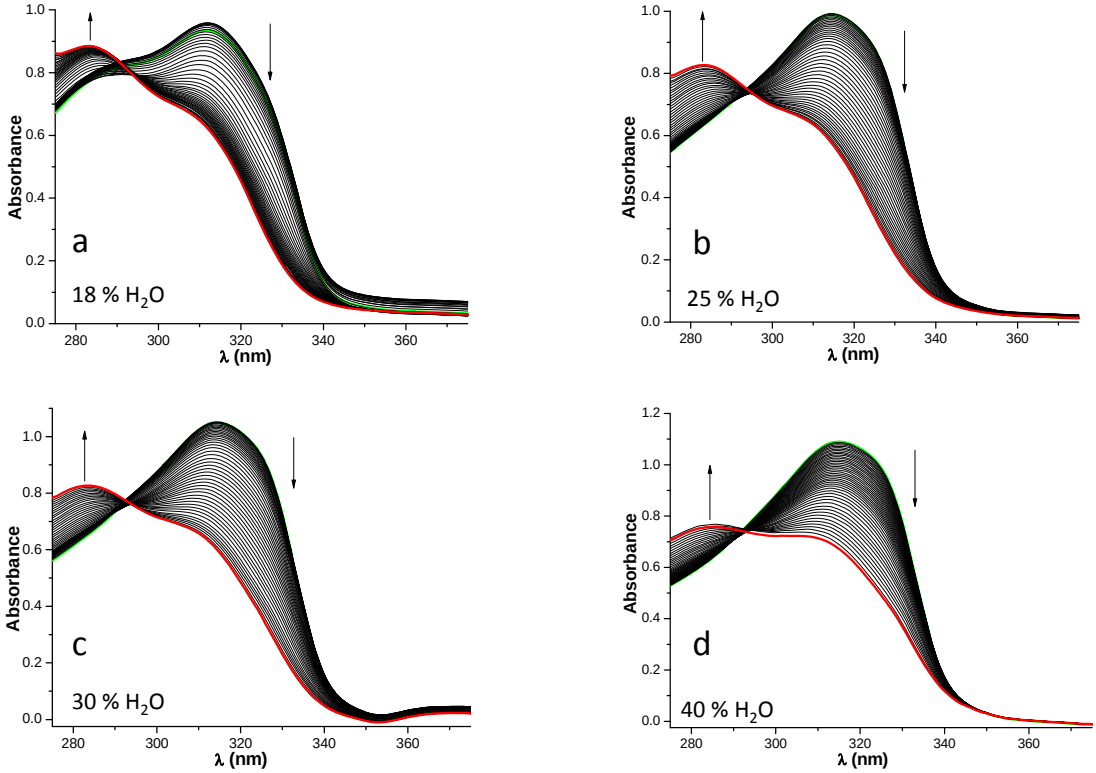

Figure 5.8: UV-vis spectra recorded during a VT UV-vis study as a function of % H_2O in DMF. The green curves are the initially recorded UV-vis spectra at 0 °C and the red curves were the final recorded spectra at 90 °C. A temperature gradient of 0.5 °C/minute was used between 0 and 90 °C.

This was also apparent for the sample in 25 % H_2O (Figure 5.8b). For the sample in 40 % H_2O (Figure 5.8c), however, the absorption band at 310 nm decreased less and was still present at 90 °C. This indicated an incomplete threading off and unfolding of the P(*p*-AT) helices. This was consistent with results in Figure 5.6d where it was shown that the CD signal was not completely lost with increasing temperature.

The observed incomplete decrease of the band at 310 nm in 40 % H_2O in DMF suggestively pointed to, firstly, a disruption of the higher order structures formed by the self-assembled construct and, secondly, a partial threading off of the foldamer helices (and unfolding), rather than a complete threading off and unfolding of the P(*p*-AT) helices. Since all the samples were at the same concentrations and the only variant was the volume fraction of water in DMF, it appears that the intensity of the band at 310 nm reflects the formation of higher order structures by the self-assembled complex. This is apparent, for example, by comparing the green curve in Figure 5.7a and any of the other green curves in Figures 5.8b, c and d.

Template concentration independence of the self-assembly

The dis-assembly and re-assembly processes were further studied as a function of template concentration, via VT-CD, by tracking the CD signal of the negative extremum at 333 nm.

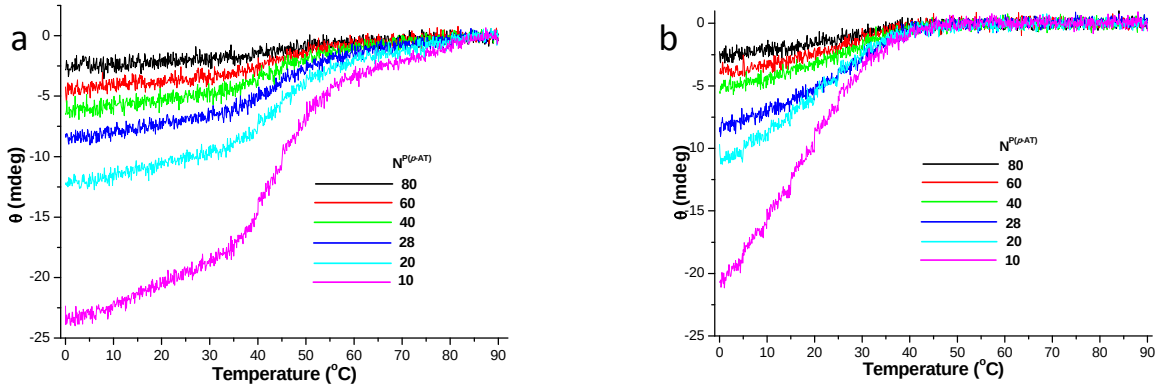

Figure 5.8: VT-CD disassembly (a) and reassembly (b) of the self-assembled complex, between P(*p*-AT)-38 [7.50 µM]/PBLG template B, as a function of template concentration, tracking the CD signal at 333 nm. A temperature gradient of 0.5 °C/minute was used between 0 – 90 °C. All samples were prepared in 18 % H_2O in DMF. The experimental $N^{P(p\text{-AT})}$ for template B is 26 (Chapter 4).

Figure 5.8 shows that disassembly and reassembly processes were independent of template concentration, because all the $CD_{333\ nm}$ curves had the same profile shapes. All the disassembly transition curves displayed sigmoidal behavior indicating a cooperative threading off mechanism. The reassembly curves displayed hysteresis. These findings are consistent with earlier results, since experiments were carried out with samples prepared in 18 % H_2O in DMF.

Conclusions

It was demonstrated, via time dependent studies, that the templated self–assembly process is very rapid. Then it was shown, by VT CD and UV-vis spectroscopy studies that templated self-assembly takes place between two distinct states, the helical foldamer and the α-helical template, the template threading into the cavity of the foldamer helix, contrary to having the foldamer helically wrapping around the template. This suggested to a self-assembled construct which can be considered to be a pseudo-rotaxane, with the template as the axle and the foldamer helices as the rotors.

When an achiral foldamer helix was used, optimum information transfer in the self-assembly, from guest to host was observed when carried out under the solvent regime at the coil to helix transition mid-point of the foldamer. These conditions allowed for a dynamic equilibrium in the self-assembly. When self-assembly was carried out with a chiral foldamer helix, with a screw sense matching that of the template, optimum self-assembly happened under the solvent regime in which the foldamer existed as stable (individual) helices. The ability of the template to discriminate against screw sense mismatches was estimated to be ~ 70 %.

It was shown, using the achiral foldamer helix, that when the templated self-assembly was carried out in solvents with high volume fractions of water, the dynamic equilibrium character of the system was lost because the foldamer helices were better stabilised. The balance between information transfer and the template's desire to avoid unfavourable solvent conditions was lost and the system fell into kinetic traps. This was reflected, firstly, by the leveling off of the induced CD activity and secondly by a decrease in the induced CD activity with as a function of volume fraction of water.

Under dynamic equilibrium conditions the helices threaded off the template in a cooperative fashion, however the threading was not cooperative and is characterized by a large hysteresis. In solvent systems with higher volume fractions of water, the cooperative nature of the disassembly process is lost and the foldamer helices gradually thread off, with increasing temperature. This loss of a cooperative character indicated the template's desire to avoid the unfavorable solvent conditions. Tentative evidence for the apparent formation

of higher order structures by the templated self-assembled constructs was also observed, via UV-vis spectroscopy experiments.

Experimental

All details concerning the P(*p*-AT) and the PBLG samples used are the same as in Chapter 4. The complexometric CD and UV-vis titrations were performed on a Jasco J-815 spectrophotometer equipped with a Jasco PTC348WI Peltier temperature controller. Spectrophotometric grade DMF and Milli-Q water were used. Stock solutions of the two the P(*p*-AT)s and another one of the PBLG, in DMF, were prepared. All titration samples were prepared volumetrically, by mixing a fixed volume of P(*p*-AT), from the same stock solution and then the appropriate volumes of PBLG, DMF and water were added to give a constant volume. The samples were shaken vigorously and allowed to sit for 2 h before measurements were taken. Titration measurements and time dependent measurements were carried out at 22 ^{o}C. Time constants, sensitivity and scan rates were chosen as deemed appropriate. Temperature gradients used are given in the main text. Samples for the time dependent studies were prepared as follows: the appropriate amounts of P(*p*-AT) and PBLG, dissolved in DMF, were added to a 1 cm quartz cuvette, then the appropriate volume of water was also added and the mixture was shaken vigorously for ~ 20 seconds. The cuvette was quickly transferred into the sample chamber care being taken to ensure readiness for measurement 60 seconds after adding water. In the other instance, the appropriate amounts of P(*p*-AT) and water were added to a 1 cm cuvette. The amount of water was calculated to ensure the desired final volume fraction of water in the fully constituted sample. Then the appropriate volume of PBLG solution was added, the mixture shaken vigorously for 30 seconds and quickly placed into the sample chamber so as to begin measuring 60 seconds after adding the PBLG.

References

(1) Tanatani, A.; Hughes, T. S.; Moore, J. S. *Angew. Chem. Int. Ed.* **2002**, *41*, 325.

(2) Star, A.; Steuerman, D. W.; Heath, J. R.; Stoddart, J. F. *Angew. Chem., Int. Ed.* **2002**, *41*, 2508.

(3) Amabilino, D. B.; Stoddart, J. F. *Chem. Rev.* **1995**, *95*, 2725.

(4) Wallace, B. A.; Janes, R. W. In *Modern Techniques for Circular Dichroism and Synchrotron Radiation Circular Dichroism Spectroscopy*; IOS Press: Amsterdam, 2009; Vol. 1, p 6.

(5) Simmons, N. S.; Cohen, C.; Szent-Gyorgyi, A. G.; Wetlaufer, D. B.; Blout, E. R. *J. Am. Chem. Soc.* **1961**, *83*, 4766.

(6) "Chapter 3, this work.."

(7) Harada, A.; Kamachi, M. *Macromolecules* **1990**, *23*, 2821.

(8) Harada, A.; Li, J.; Kamachi, M. *Nat. Protocols* **1992**, *356*, 325.

(9) Harada, A.; Hashidzume, A.; Yamaguchi, H.; Takashima, Y. *Chem. Rev.* **2009**, *109*, 5974.

(10) Harada, A.; Takashima, Y.; Yamaguchi, H. *Chem. Soc. Rev.* **2009**, *38*, 875.

(11) Pace, C. N.; Scholtz, J. M. In *Protein Structure: A Practical Approach*; Second ed.; Creighton, T. E., Ed.; IRL Press: Oxford, 1997, p 299.

Chapter 6. Summary, conclusions and recommendations for future work

General remarks

One of the prime challenges in supramolecular chemistry is to design self-assembling systems with precise control over size, shape and asymmetry. Equally important is the need to design host guest systems, encapsulating hydrophobic guests inside water soluble hosts in water, with predictable geometries.[1] Essentially this entails utilization off non-directional hydrophobic forces in water. The work detailed in this thesis scored a number of successes in this direction.

Firstly a facile synthetic procedure for making helices with large cavities was developed. The helical molecular programming entailed linking aryl and triazole rings, alternatingly, in a *para* fashion about the aryl ring, with a 1,4-disubstitution pattern about the triazole ring. The crescent was induced exclusively by the 1,4-disubstitution pattern on the triazole ring and helical bending was induced by forcing all the triazole units into a *cisoid* configuration. This linkage geometry reduces the bending, coding for a helix with a huge cavity, which can be considered as a cylindrical hollow with dimensions of 3 nm. In nature cavities of this size are encountered at the tertiary and quaternary levels of protein structure.[2,3] The backbones were appended with *o*EG side chains. The side chains have the dual roles of imparting solubility to the polymer system and imparting an amphiphilic character to the polymer molecules, necessary for instigating solvophobic effects. Additional stability for the folded conformation is realised from π-π-stacking interactions in the folded conformations.

The polymer synthesis protocol is not tedious unlike the iterative monomer by monomer then oligomer by oligomer coupling protocols reported in literature.[4] Therefore our protocol can rightfully be regarded as a true polymer synthesis approach in foldamer research. A challenge with the protocol, however, is the considerably high molecular weight dispersity (*Đ*) values of the subsequent polymers, which are typical of step growth polymerizations.

Coil to helix conformational transitions were subtly controlled using a DMF/H_2O good solvent/bad solvent composition. Spectroscopic signatures for the transitions from primary to secondary then to tertiary structure were observed. CD spectroscopy was successfully used to detect helical ordering, whilst UV-vis spectroscopy was used to track the stability of the helically ordered conformation. Both techniques gave extremely complimentary results. Reliable spectroscopic signatures for the conformational transitions, as a function of solvent quality were observed.

The aqueous solubility of the P(*p*-AT) foldamers could be tuned by the length of the *o*EG side chain. P(*p*-AT) oligomers appended with hexa-ethylene glycol side chains were completely soluble in water. This allowed the solution state tertiary conformation to be determined in water via cryoTEM experiments. To the best of our knowledge this is the most conclusive visual evidence for the formation of long stacks/fibers, with high aspect ratios, in solution, by helical foldamers. The helical stacks are, however, of indeterminate lengths, a recognised problem in the self-assembly of tubular objects.[5]

To overcome the lack of control over the lengths of the self-assembled helical stacks, we turned to the inspiring TMV self-assembly system found in nature. In TMV, the length (and the asymmetry) of the self-assembled construct is controlled by a RNA template embedded in the viral capsid. Templated self-assembly, of the helical P(*p*-AT) foldamers, was realised using the hydrophobic α-helical polypeptide polybenzyl glutamate. The self-assembly process is driven by solvophobic forces. The template mimicked the role of RNA in TMV by controlling the length and the asymmetry of the self-assembled complex. Mechanistic studies showed that a stable helical conformation is required for the templated self-assembly, with the template threading through the hollow of the helical foldamer, by a pseudo-rotaxane mechanism.

By carrying out the templated self-assembly under the solvent composition at the coil to helix transition mid-point of the foldamer helix, the assembly system operated under dynamic equilibrium conditions. Under these conditions, a balance between information transfer from the guest template to the assembled construct, in the form of chirality and length control, and the template's desire to avoid unfavourable solvent conditions, was achieved.

It was demonstrated that directional control of the non-directional hydrophobic forces, which are notoriously difficult to control in water was possible.[1] The directional control is illustrated by the fact that CD signal response increased with increasing templating effect clearly indicating that the screw sense of the self-assembled helices matched the chirality of the template.[1]

Future considerations

A number of potential functions of the hollow of the helical foldamers are often suggested in literature. These include possible functions as trans-membrane channels[6] or in preparing insulated nanowires[7] or even as catalysts.[8,9] All of these potential applications are viable with the helical foldamers prepared in this work.

The templated self-assembly system demonstrated in this work ensures length and asymmetric control of the hierarchical construct. In order to understand this system better, the dependency of the templated assembly on the size of the foldamer helix must be studied. The CuAAC catalysed step growth polymerization system used to prepare the P(*p*-AT)s in this work is successful at preparing high molecular weight in a facile nature. A drawback, however, is that the P(*p*-AT)s prepared this way have large molecular weight dispersities. Therefore stepwise divergent/convergent synthetic strategies must be used in order to accurately control the chain length of the P(*p*-AT)s and subsequently the number of turns of the foldamer helices.

The library of templates must be broadened to include, for example, other polypeptides, nucleic acids, and perhaps even synthetic vinyl polymers, and the efficiency of information transfer from the template to the assembled construct studied. It will be interesting also to design a system whereby the template can be covalently tethered to the foldamer helix, before threading analogous to the way the initiation region of the TMV RNA interacts with the disk proteins.

In order to design tubular nanostructures with control over the length and the chirality of the constructs it will be necessary to pursue post-assembly modification strategies to stabilise the assembled construct, for example by crosslinking the side chains on the outside, and then removing the template. Alternatively a more thorough investigation into

the solvent dependent self-assembly/polymerization of the foldamer helices, into long stacks, can be made, to see how uniformly the stacks grow. Then the use of end cappers, to regulate the growth of the helical stacks can be investigated.[10]

As remarked earlier, an interesting potential function is as a membrane channel. In this regards it will be interesting to reverse the polarity of the P(*p*-AT) foldamer helices, but tethering the backbone with long apolar alkyl chains and functionalizing the interior of the helices with polar groups. Putting long hydrophobic chains on the outside will enable the large hollow helices to better integrate with the lipid bilayers, whilst the polar interior can then function as an ion channel.

Work in all the directions suggested in this section is now on going.

References

(1) Menger, F. M. *Proc. Natl. Acad. Sci.* **2002**, *99*, 4818.

(2) Song, L.; Hobaugh, M. R.; Shustak, C.; Cheley, S.; Bayley, H.; Gouaux, J. E. *Science* **1996**, *274*, 1859.

(3) Nagano, N.; Gail Hutchinson, E.; Thornton, J. M. *Protein Science* **1999**, *8*, 2072.

(4) Gong, B. *Acc. Chem. Res.* **2008**, *41*, 1376.

(5) Balbo Block, M. A.; Hecht, S. *Angew. Chem., Int. Ed.* **2005**, *44*, 6986.

(6) Sanford, A. R.; Yamato, K.; Yang, X.; Yuan, L.; Han, Y.; Gong, B. *Eur. J. Biochem.* **2004**, *271*, 1416.

(7) Block, M. A. B.; Kaiser, C.; Khan, A.; Hecht, S. *Top. Curr. Chem.* **2005**, *245*, 89.

(8) Heemstra, J. M.; Moore, J. S. *J. Org. Chem.* **2004**, *69*, 9234.

(9) Heemstra, J. M.; Moore, J. S. *J. Am. Chem. Soc.* **2004**, *126*, 1648.

(10) Besenius, P.; Portale, G.; Bomans, P. H. H.; Janssen, H. M.; Palmans, A. R. A.; Meijer, E. W. *Proc. Natl. Acad. Sci.* **2010**, *107*, 17888.